



7th UHMWPE

INTERNATIONAL MEETING

OCTOBER 22-23, 2015

PHILADELPHIA, PA

UNION LEAGUE OF PHILADELPHIA

DREXEL UNIVERSITY & UNIVERSITY OF TORINO



THE PURPOSE OF THE MEETING is to bring together engineers, scientists, and clinicians from academia and industry and present leading edge research on advancements in medical grade UHMWPE technology and clinical applications. The focus of the 7th meeting is on clinical and retrieval studies of highly crosslinked UHMWPE (HXLPE), with a special emphasis on the performance of thin acetabular liners and knee arthroplasty; HXLPE performance in upper extremity, ankle, and spine; international registry outcomes for HXLPE in hip and knee; novel UHMWPE articulations with ceramic and PEEK bearing surfaces; advances in Vitamin E and new antioxidant technologies for UHMWPE; advances in thermal processing of HXLPE; structural composites and woven fiber applications of medical grade UHMWPE; as well as advances in biologic aspects of UHMWPE wear debris.

Scientific and clinical papers from the meeting will be submitted to a CORR Symposium that will appear in 2016.

**SCIENTIFIC AND ORGANIZING COMMITTEE
AND INVITED SPEAKERS:**

President: Steven Kurtz, PhD

Honorary President: Pierangiola Bracco, Ph.D.

President Emeritus: Luigi Costa, Ph.D.

José Antonio Puertolas, Ph.D.

Joanne Tipper, Ph.D.

Clare Rimnac, Ph.D.

Ebru Oral, Ph.D.

Orhun Muratoglu, Ph.D.

Stephen Graves, M.D.

Liz Paxton

Marco Regis

Henrik Malchau

Dan MacDonald

DAY ONE

UHMWPE Meeting Agenda Thursday, October 22, 2015

7:00 AM

On Site Registration Opens

8:00AM

Welcome, Opening Remarks

Steven Kurtz, Ph.D.

8:15 AM

Invited Talk 1: UHMWPE: Polymerization to Products

Presenter: Anthony Verrocchi

SESSION I: Oxidation and Stabilization of HXLPE

Session Co-Moderators: Luigi Costa, Ph.D., and Orhun Muratoglu, Ph.D.

8:45 AM

Podium Talk 1: The effects of oxidation on highly cross-linked UHMWPEs

Presenter: Jeremy Suhardi

9:00 AM

Podium Talk 2: Studies in Irradiated UHMWPE Oxidation

Presenter: Venkat Narayan, Ph.D.

9:15 AM

Podium Talk 3: Oxidation and Wear of Retrieved Long-Term, 1st Generation HXLPE Components in THA

Presenter: Steven Kurtz, Ph.D.

9:30 AM

Podium Talk 4: Chemical Nature of Vitamin E in UHMWPE after Irradiation: Investigations with Model Substances

Presenter: Reto Lerf, DSc

9:45 AM

Round Table Q/A and Discussion of Session 1

10:00 AM

How to Write for CORR

Presenter: Clare Rimnac, Ph.D.

10:15 AM

Morning Coffee Break

SESSION II: Sterilization and Crosslinking Technologies for UHMWPE

Session Co-Moderators: José Antonio Puertolas, Ph.D., and Ebru Oral, Ph.D.

10:30 AM

Podium Talk 5: Using Laser Optics to Construct the Phase Diagram of UHMWPE
Presenter: Leonid Pavlovsky, Ph.D.

10:45 AM

Podium Talk 6: The Properties of Highly Crosslinked UHMWPE Manufactured Using High Power X-Ray
Presenter: Mark Allen

11:00 AM

Podium Talk 7: Post Radiation Annealing Of UHMWPE Under Huge Pressure
Presenter: Anuj Bellare, Ph.D.

11:15 AM

Round Table Q/A and Discussion of Session 2A

11:30 AM

Podium Talk 8: Multiphase polymeric material for cushion-bearing orthopedic implants
Presenter: Bruce Carvalho, Ph.D.

11:45 AM

Podium Talk 9: A wear and highly oxidation resistant chemically cross-linked UHMWPE with improved toughness
Presenter: Ebru Oral, Ph.D.

12:00 PM

Podium Talk 10: Chemically cross-linked UHMWPE in the presence of an unsaturated additive
Presenter: Pierangiola Bracco, Ph.D.

12:15 PM

Round Table Q/A and Discussion of Session 2B

12:30 PM**Buffet Lunch and POSTER SESSION****SESSION III: Antioxidants in UHMWPE**

Session Co-Moderators: Pierangiola Bracco, Ph.D., and Orhun Muratoglu, Ph.D.

1:30 PM

Invited Talk 2: Anti-Oxidant Poly in the Hip & Knee
Presenter: Liz Paxton

2:00 PM

Podium Talk 11: Improved Crack Initiation Resistance from a Blunt Notch in a Hindered Phenol Antioxidant UHMWPE
Presenter: Clare Rimnac, Ph.D.

2:15 PM

Podium Talk 12: Non-Cemented Monoblock Hip Cup Made from vitamys®, Vitamin E Stabilised Highly Cross-linked UHMWPE
Presenter: Reto Lerf, DSc

2:30 PM

Round Table Q/A and Discussion of Session 3A

2:45 PM

Podium Talk 13: Measurement of Anti-Oxidant in Retrievals
Presenter: Barbara Currier

3:00 PM

Podium Talk 14: Highly Cross-linked Retrievals With and Without Vitamin E Stabilization
Presenter: Orhun Muratoglu, Ph.D.

3:15 PM

Round Table Q/A and Discussion of Session 3B

3:30 PM

Afternoon Coffee Break

DAY ONE

UHMWPE Meeting Agenda Thursday, October 22, 2015

SESSION IV: HXLPEs in the Knee

Session Co-Moderators: Steven Kurtz, Ph.D. and Clare Rimnac, Ph.D.

3:45 PM

Invited Talk 3: Crosslinked UHMWPE in the Knee: Australian Perspective

Presenter: Stephen Graves, M.D.

4:15 PM

Podium Talk 15: Biotribology of vitamin E stabilised polyethylene materials for total knee arthroplasty evaluated under highly demanding patient daily activities in vitro

Presenter: Thomas Grupp, Ph.D.

4:30 PM

Podium Talk 16: Surface Damage and Condyle Penetration of 1st Generation Remelted HXLPE in Total Knee Replacement

Presenter: Dan MacDonald

4:45 PM

Round Table Q/A and Discussion of Session 4

5:00 PM

Day 1 Meeting Adjourns

6:30 PM

Reception and Dinner Begins at the U.S. Constitution Center

DAY TWO

UHMWPE Meeting Agenda Friday, October 23, 2015

7:30 AM - On Site Registration Opens

SESSION V: Knee (III), Shoulder and Spine

Session Co-Moderators: Lisa Pruitt, Ph.D., and Joanne Tipper, Ph.D.

8:00 AM

Podium Talk 17: In Vitro Comparison of Conventional PE vs. Mechanically Annealed Vitamin E PE Unicompartmental Bearing Surfaces

Presenter: Brad Micheli

8:15 PM

Podium Talk 18: Characterization of Striated Pattern of Retrieved UHMWPE Tibial Liner by Raman Spectroscopy

Presenter: Elmira Moslemi-Rad

8:30 AM

Podium Talk 19: Layered UHMWPE as a Bearing Material for Use in Total Knee Arthroplasty

Presenter: Graham Buetler

8:45 AM

Round Table Q/A and Discussion of Session 5A

9:00 AM

Invited Talk 5: UHMWPE Choice for Total Shoulder Replacement: A Comparison between Conventional and Crosslinked Formulations

Presenter: Marco Regis

9:30 AM

Podium Talk 20: Bearing Surface Damage of Anatomical and Reverse Total Shoulder Replacements: Retrieval Analysis Across Fixation Designs and UHMWPE Composition

Presenter: Louis Malito

9:45 AM

Podium Talk 21: The Use of Highly Modified UHMWPE in Spinal Applications

Presenter: Mark Allen

10:00 AM

Podium Talk 22: Novel Radiopaque UHMWPE Wires for Spinal Deformity Correction: A Mechanical Assessment

Presenter: Alex Roth

DAY TWO

UHMWPE Meeting Agenda Friday, October 23, 2015

10:15 AM

Podium Talk 23: UHMWPE Wear Debris Induced Vascularization, Inflammation & Innervation after TDR
Presenter: Sai Veruva

10:30 AM

Round Table Q/A and Discussion of Session 5B

10:45 AM

Morning Coffee Break and POSTER SESSION

SESSION VI: New Frontiers in UHMWPE: Fibers and Beyond

Session Co-Moderators: Orhun Muratoglu, Ph.D., and Luigi Costa, Ph.D.

11:15 AM

Podium Talk 24: Advances in Medical-Grade UHMWPE Fiber Development: Additives for Visualization
Presenter: Harold Smelt, Ph.D.

11:30 AM

Podium Talk 25: Mechanical, tribological and chemical stability performance of a novel 1-2 layered graphene/UHMWPE composites
Presenter: Francisco Pascual, Ph.D.

11:45 AM

Podium Talk 26: Effect of Supercritical Fluid Sterilization on Microstructure and Properties of Porous UHMWPE
Presenter: Fedor Senatov, Ph.D.

12:00 PM

Podium Talk 27: Prevention of bacterial adherence and biofilm formation on implant surface by a highly hydrophilic and electrically neutral phospholipid polymer layer
Presenter: Masayuki Kyomoto, Ph.D.

12:15 PM

Podium Talk 28: Woven UHMWPE fibers for use in cardiovascular applications
Presenter: Karlien Boon-Ceelen, Ph.D.

12:30 PM

Round Table Q/A and Discussion of Session 6

12:45 PM

Closing Remarks
Presenter: Steven Kurtz, Ph.D.

1:00 PM

Meeting Adjourn

POSTER PRESENTATION DIRECTORY

7TH UHMWPE INTERNATIONAL MEETING

1. *Improvements in Efficiency of Oxidation Index and Trans-Vinyl Index Measurements by FTIR in UHMWPE*
2. *Dose Uniformity of Commercial High Power X-Ray, in the Manufacture of Highly Crosslinked UHMWPE*
3. *Notch Fatigue of UHMWPE: A Linear Elastic Fracture Mechanics Approach*
4. *Murine model of particle-induced osteolysis using a titanium tibial implant to test the influence of aging on bone turnover*
5. *Storage of UHMWPE Powder Blended with Peroxides*
6. *Effectiveness of AO Polyethylene: What early retrievals can tell us*
7. *An Alternative Vitamin E-Diffused UHMWPE with Improved Toughness*
8. *Nanoparticle reinforced UHMWPE for orthopaedic applications "parameters affecting the manufacturing process and mechanical properties"*
9. *Surface functionalisation of MWCNTs to Improve Behaviour of UHMWPE- Based Nanocomposites*
10. *Fatigue crack propagation testing in UHMWPE*
11. *Effect of Knee, Ankle and Hip Joint Replacements on Vitamin E Infused Highly Crosslinked UHMWPE Wear Particles Size, Shape and Morphologies Using a New Modified Base Digestion Method*
12. *Tribological Behaviour of the "Reverse" Inverse Shoulder Prosthesis: Shoulder Simulator Study with four Different Material Pairings*
13. *Hybrid Porous UHMWPE Scaffolds for Bone Defects Replacement*
14. *Oriented bulk nanocomposites based on UHMWPE/MWCNT*
15. *Finite Element Evaluation of the Newest ISO Testing Standard for Polyethylene TKR Liners*
16. *Quantification of the Cytokine Release from Macrophages Stimulated with Spherical Ultra-High Molecular Weight Polyethylene Particles of Varying Size Using Inverted Cell Culturing Process*
17. *Spatially cross-linked UHMWPEs using chemical cross-linking: Increased toughness for thinner implants*
18. *Peak Stress Dictates Fatigue Crack Growth in a Hindered Phenol Antioxidant UHMWPE*
19. *Toughness in High Temperature Treated UHMWPEs by Essential Work Fracture*
20. *3D Frictional Torque Results of HXLPE & Vitamin-E Infused UHMWPE against 28 mm Metal & 36 mm Metal & 36 mm Ceramic Heads*
21. *Biocompatibility Assessment of HALS Stabilized Highly Crosslinked UHMWPE*
22. *Effects of surface modification and bulk geometry on the biotribological behavior of cross-linked polyethylene*
23. *Effects of extra irradiation on surface and bulk properties of PMPC-grafted cross-linked polyethylene*
24. *Characterization of alginate modified UHMWPE; morphology and wear properties*

WITH
SPECIAL
THANKS
TO:



7th
UHMWPE



MATERIAL OF CHOICE FOR IMPROVED PATIENT COMFORT

For more than 50 years, GUR® UHMWPE has been the material of choice among orthopedic surgeons for joint replacements. Our durable and abrasion resistant UHMWPE improves patient comfort, and delivers excellent impact strength and lubricity. Contact us today and discover the benefits of GUR UHMWPE.

GUR UHMWPE benefits:

- Low wear
- Excellent lubricity
- Exceptional impact strength
- High energy absorption
- High purity
- Biocompatible
- ASTM F648, ISO 5834-1 approval
- FDA compliant
- Drug and device master file listed

GUR UHMWPE applications

- Hip, knee, and shoulder arthroplasty
- Other joint replacements
- Spine applications and replacements



CELANESE
222 West Las Colinas Boulevard
Suite 900N
Irving, TX 75039
(800) 833-4882

celanese.com/UHMWPE



SESSION
ONE:

Oxidation and
Stabilization of
HXLPE

The effects of oxidation on highly cross-linked UHMWPEs

Suhardi JV^{1,2,3}, Oral E^{1,2}, Muratoglu OK^{1,2}

¹Harris Orthopaedic Laboratory, Massachusetts General Hospital; ²Massachusetts Institute of Technology; ³Department of Orthopaedics, Harvard Medical School
eoral@mg.harvard.edu

Introduction: Radiation cross-linked ultrahigh molecular weight polyethylenes (UHMWPE) are preferred in total joint arthroplasty because they have decreased wear and decreased incidence of peri-prosthetic osteolysis. In addition to wear resistance, imparting oxidation resistance is important as oxidation decreases the mechanical and fatigue strength of UHMWPEs [1].

Recently, it was shown that IZOD impact strength correlated well with fatigue crack propagation resistance and could be used as a screening tool for comparatively assessing irradiated UHMWPEs [4]. In this study, we determined the effect of oxidation on the IZOD impact strength of three clinically relevant highly cross-linked UHMWPEs.

Methods and Materials: (1) GUR 1050 UHMWPE was e-beam irradiated to 100 kGy and then melted (CISM); (2) GUR 1050 UHMWPE was irradiated with 3 sequential doses of 30 kGy for a cumulative total of 90 kGy-with annealing at 130°C after each irradiation (SXL); (3) 100-kGy gamma irradiated, vitamin E-diffused and gamma sterilized (E1) tibial preforms were obtained from Biomet. All of these samples were then machined to 6.35 x 12.7 x 63.50 mm impact testing coupons according to ASTM F648-07. Accelerated aging: (a) Machined samples of each kind (n=4) were accelerated aged 'as is' at 70°C and 5 atm. of oxygen for 0, 2, 3 or 4 weeks. (b) Some samples (n=4) were accelerated aged after doping in a lipid emulsion comprising 0.0625 % wt cholesteryl linoleate, 0.0625 % wt cholesterol, 0.0625 % cholesteryl stearate, 0.0625 % wt squalene emulsified in 22.5 wt% Tween 20. Lipid doping was performed at 40°C for 3 weeks and accelerated aging at 5 atm of oxygen at 70°C for 0, 2, 3, or 4 weeks. Characterization IZOD impact testing was done according to ASTM F648. Oxidation was determined using FTIR on 150 um thin slices that were boiled in hexane for 16 hours. A carbonyl index was determined as the ratio of the peak area at 1740 cm⁻¹(1680-1780 cm⁻¹) to 1370 cm⁻¹(1330-1390 cm⁻¹). An average oxidation index was calculated. Crosslink density of the surface (0-1 mm) and bulk (4-6 mm) was determined according to ASTM F2214-02.

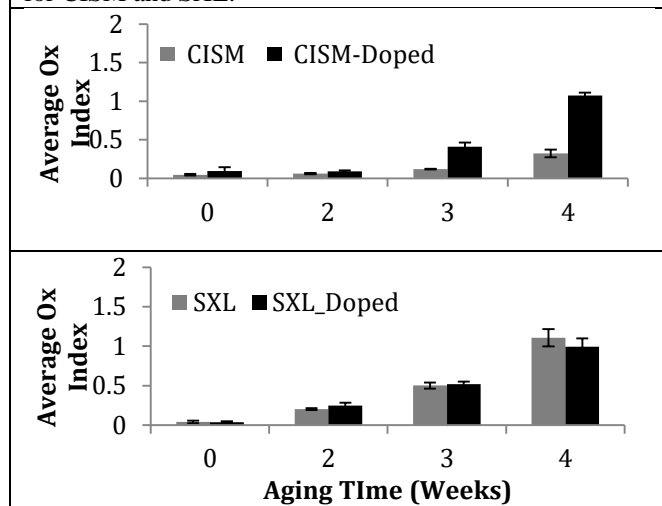
Results: The impact strength of CISM decreased after 3 weeks (p<0.01 for doped and p = 0.05 for undoped samples). After aging for 4 weeks, the impact strength of the lipid-doped samples was 82% less than the undoped.

SXL showed a decrease in impact strength after aging for 2, 3 or 4 weeks (p<0.01). There was no difference in impact strength between the lipid-doped and undoped samples after aging. Impact strength of E1 samples were not changed after aging for 4 weeks.

Oxidation of all samples except E1 increased with time (p<0.05; Fig 1). Lipid doping alone did not change oxidation except for CISM, for which it increased.

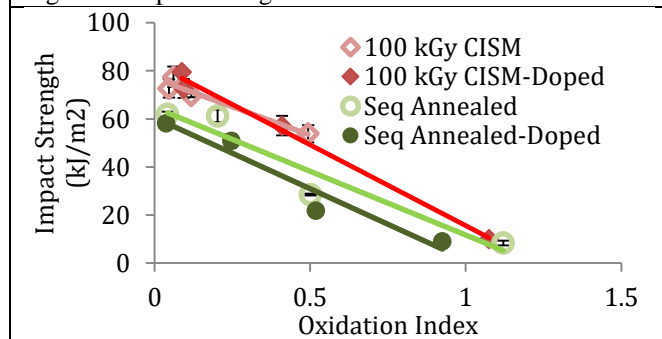
Cross-link density of both CISM and SXL decreased as aging length increased (not shown). There was no change in crosslink density for E1 with aging. Impact strength decreased linearly with increasing oxidation, which was not changed by lipid doping (Fig 2). **Discussion:** Post-irradiation melting of radiation cross-linked UHMWPE decreases free radicals to undetectable levels [2], whereas annealing below the melting point results in residual free radicals [3]. In irradiated and vitamin E-diffused UHMWPE, the vitamin E content is 0.7 wt% due to incorporation after cross-linking [4]. There are detectable residual free radicals at the time of implantation, the oxidative effects of which vitamin E can hinder throughout the lifetime of the implant.

Figure 1. The oxidation index as a function of aging time for CISM and SXL.



This study suggests that oxidation, even at low levels, can have detrimental effects on impact toughness, which correlated well with fatigue resistance.

Figure 2. Impact strength as a function of oxidation.



References: [1] Baker et al. Polymer 2000; 41: 795-808; [2] Muratoglu et al. J Arthroplasty 2001; 16: 149-160; [3] Wang et al. J Phys D 2006; 39:3213-3219; [4] Oral et al. Biomaterials 2007; 28: 5225-5237.

Studies in Irradiated UHMWPE Oxidation

+¹Narayan V.S.; ¹Ross, M.A.; ¹Warner, D; ¹Gupta, C.E.M.

+¹ DePuy Orthopaedics Inc., PO Box 988, 700 Orthopaedic Drive, Warsaw, IN 46581, USA.

Vnaraya5@its.jnj.com

Introduction

Oxidation of irradiated Ultra High Molecular Weight Polyethylene (UHMWPE) for orthopaedic implants both, on the shelf in the packaging as well as *in vivo* has been extensively reported to cause adverse effects on the mechanical properties [1]. Irradiation of UHMWPE using ionizing radiation sources such as gamma or electron beam generates free radicals which can trigger oxidation if left unaddressed. Clinical and *in vitro* test results have verified oxidative stability by remelting the irradiated UHMWPE materials used in orthopaedic devices [2,3]. This study characterizes the comparative response of UHMWPE materials to oxidation induced using an accelerated aging protocol. These UHMWPE materials are generated by either gamma or e-beam irradiation at various doses.

Materials and Methods

- * Non-irradiated GUR 1020 (Ticona), consolidated by ram extrusion at MediTECH Medical Polymers, hereafter referred to as **NI-1020**, has been employed in this study as control material.
- * Ram extruded and irradiated GUR 1020, hereafter referred to as **G-1020-50, G-1020-75, and G-1020-100**, are generated by gamma irradiation at doses of 50, 75 & 100 kGy respectively and subsequently remelted at or above 155°C.
- * Ram extruded and irradiated GUR 1020, hereafter referred to as **E-1020-50, E-1020-75, and E-1020-100**, are generated by e-beam irradiation at doses of 50, 75 & 100 kGy respectively and subsequently remelted at or above 155°C.

The accelerated aging was done as specified in ASTM F2003. The aging period was varied from 2 to 10 weeks. Characterization of the non-aged and aged materials involved:

- Oxidation Index by FTIR as described in ASTM F 2102
- Double Notched Impact per ASTM F 648
- Crystallinity by DSC per ASTM F 2625

Results and discussion

A. Oxidation Behavior:

The oxidation behavior has been monitored by FTIR as specified in ASTM F2102 and reported below in **Table 1**. All materials show little or no change in oxidation index up to 4 weeks aging. Any small differences in values noted up to this point are insignificant as, below an oxidation index of 0.1, there is considerable noise in the FTIR signal. However, the materials begin to separate out in oxidation response at the 6-week mark. Onset of oxidation is noted in all the materials. Statistically higher oxidation index values are noted for the e-beam irradiated materials relative to

their gamma-irradiated counterparts. The trend is confirmed at the 10-week mark wherein the e-beam materials are too brittle to measure. While there is progression in oxidation in the gamma materials, they are still ductile enough to be microtomed and characterized.

B. Double Notched Izod (DNI) Impact Toughness Response to Oxidation

The changes in DNI impact toughness were monitored as a function of aging and summarized in **Table 2**. While the remelted materials show good retention of properties at the end of 4 weeks, thereafter the trends noted in the FTIR measurements are replicated. The e-beam materials start showing loss in properties at 6 weeks aging. While the gamma materials, particularly at 50 and 75 kGy continue to remain stable. The 100 kGy gamma material shows some loss, though it is not statistically significant from the value at 4 weeks aging. At 10 weeks, all materials, including the non-irradiated UHMWPE show oxidative loss. The e-beam materials show consistently lower properties than the corresponding gamma materials beyond 6-weeks aging regardless of the radiation dose.

C. Response of Crystallinity to Oxidation:

The change in crystallinity in the materials in the present study has been summarized in **Table 3**. The trends seen here are consistent with that observed in FTIR and DNI measurements. While some small change is noted at 6 weeks, the gamma materials as well as the non-irradiated UHMWPE at 10 weeks aging show values at or about 70%. This has been associated with significant oxidation in a previous study [4]. The e-beam materials were highly oxidized and too brittle to measure.

Conclusion

- The materials upon irradiation and remelting show good stability for at least 4 weeks of ASTM aging on par with non-irradiated UHMWPE.
- The e-beam materials show greater scatter in response upon aging beyond 4 weeks than the corresponding gamma materials and tend to oxidize faster.
- The gamma materials show better stability than the e-beam materials in their properties and respond similar to non-irradiated UHMWPE, particularly at lower doses of 50 and 75 kGy.

References

- [1] C.M.Rimnac *et al.*, J. Bone Joint Surg., **76A**, pp 1052-56, (1994).
- [2] J.P.Collier *et al.*, CORR, **414**, pp. 289-304, (2003).
- [3] O.K.Muratoglu *et al.*, JOA, **16(2)**, pp 149-60, (2001).
- [4] V.S.Narayan *et al.*, Proceedings of the ORS, **2316**, (2010)

Table 1 – Oxidation Index with ASTM Aging

Aging Period	NI-1020	E-1020-50	G-1020-50	E-1020-75	G-1020-75	E-1020-100	G-1020-100
0	0.032±0.006	0.032±0.006	0.032±0.006	0.032±0.006	0.032±0.006	0.032±0.006	0.032±0.006
2W	0.032±0.012	0.051±0.014	0.069±0.018	0.054±0.007	0.077±0.013	0.027±0.013	0.057±0.011
4W	0.045±0.015	0.068±0.016	0.074±0.005	0.096±0.015	0.054±0.013	0.075±0.016	0.062±0.010
6W	*	0.225±0.012	0.086±0.011	0.253±0.084	0.114±0.028	0.223±0.029	0.142±0.019
10 W	0.220±0.015	**	0.600±0.059	**	0.513±0.253	**	0.704±0.059

* Sample not available for testing

** Sample too brittle to microtome

Table 2 – Double Notched Izod Impact with ASTM Aging

Aging Period	NI-1020	E-1020-50	G-1020-50	E-1020-75	G-1020-75	E-1020-100	G-1020-100
0		77.9±3.5	73.4±1.3	71.6±2.6	69.3±1.5	59.5±1.9	57.3±5.8
2W	139.4±2.3	88.8±9.6	74.5±0.8	72.5±2.7	68.7±1.8	58.3±2.0	58.9±2.0
4W	148.9±3.7	90.0±10.4	77.5±1.6	72.4±6.9	69.9±1.2	60.3±4.3	60.4±1.5
6W	*	32.3±9.4	79.1±2.6	50.6±11.8	69.7±4.6	27.4±5.6	43.8±14.1
10 W	27.4±5.1	1.4±0.7	23.0±1.8	2.4±0.7	23.1±7.0	1.2±0.3	10.4±2.4

* Sample not available for testing

Table 3 – % Crystallinity with ASTM Aging

Aging period	NI-1020	E-1020-50	G-1020-50	E-1020-75	G-1020-75	E-1020-100	G-1020-100
0	60.0±3.0	55.2±0.6	51.9±3.0	53.1±2.1	54.2±0.4	53.0±1.7	53.4±0.7
2W	59.1±1.8	55.6±2.3	54.2±3.6	55.8±0.4	53.6±3.0	54.1±2.1	55.6±2.3
4W	60.5±2.2	52.5±1.5	54.5±1.2	54.4±2.8	58.3±1.4	56.6±2.4	57.1±1.6
6W	60.0±3.0	65.9±2.4	58.2±2.8	66.5±1.3	59.0±2.3	62.9±1.2	60.6±0.8
10 W	71.2±3.0	**	74.0±0.8	**	68.7±4.0	**	73.6±1.8

** Sample too brittle to microtome

Wear and Oxidation of Retrieved, Long-Term, 1st Generation HXLPE Components in THA

Daniel W MacDonald, Jackie Schachtner, Antonia F Chen, Harold Cates, Gregg Klein, Michael Mont, Matthew Kraay, Arthur Malkani, Gwo-Chin Lee, Brian Hamlin, Clare Rinnac, and Steven M Kurtz
dm68@drexel.edu

Introduction: Highly crosslinked polyethylene (HXLPE) was clinically introduced approximately a decade and a half ago to reduce polyethylene wear rates and subsequent osteolysis. Clinical and radiographic studies have repeatedly shown increased wear resistance, however concerns of rim oxidation and fatigue fracture remain. Although short to intermediate term retrieval studies of these materials are available, the long-term behavior of these materials remains unclear.

Methods: Between 2000 and 2015, 115 1st generation HXLPE acetabular liners implanted for 5 or more years were collected and analyzed as part of an ongoing, multi-institutional orthopaedic implant retrieval program. There were two material cohorts based on thermal processing (annealed (n=45) and remelted (n=70)). Each cohort was stratified into two more cohorts based on implantation time (5 – 10 years and >10 years). For annealed components, the intermediate-term liners (n=30) were implanted on average (\pm SD) for 7.3 ± 1.7 years while the long-term liners (n=15) were implanted for 11.3 ± 1.8 years. For remelted components, the intermediate-term liners (n=59) were implanted on average (\pm SD) for 7.2 ± 1.3 years while the long-term liners (n=11) were implanted for 11.3 ± 1.2 years. For each cohort, the predominant revision reasons were loosening, instability, and infection (Figure 1). Short-term liners (in-vivo <5ys) from previous studies were analyzed using the same protocol for use as a reference.

For oxidation analysis, thin slices ($\sim 200 \mu\text{m}$) were taken from the superior/inferior axis and subsequently boiled in heptane for 6 hours to remove absorbed lipids that may interfere with the oxidation analysis. 3mm line profiles (in $100\mu\text{m}$ increments) were taken perpendicular to the surface at each region of interest. Oxidation indices were calculated according to ASTM 2102. Penetration was measured directly using a calibrated micrometer (accuracy=0.001mm).

Results: The penetration rates for both the annealed and remelted cohorts were low and similar between the two material cohorts (Figure 2). There were several cases of fractured zirconia heads associated with a manufacturer recall that resulted in higher penetration rates. At the bearing and rim surfaces, the annealed liners had higher oxidation indices than the remelted components ($p < 0.001$). For the remelted components, the intermediate-term liners had higher oxidation indices than the short-term liners ($p = 0.001$). For the annealed liners, both the long-term and intermediate-term liners had higher oxidation indices compared with the short-term liners ($p = 0.007$ and 0.001 , respectively).

Discussion: Thermally treated first generation HXLPEs were introduced to reduce polyethylene wear and prevent oxidative degradation. The results of this study suggest that both thermally treated HXLPEs demonstrate lower penetration rates than conventional polyethylene, however, the resistance to oxidation was formulation dependent. Specifically, the

remelted components were more effective at preventing oxidation than the annealed liners. However, despite the lack of measurable free radicals, we were able to observe temporal changes in the oxidation of the remelted liners. Future work will include analysis of long-term 1st generation annealed HXLPE to fully assess its performance in the second decade of service

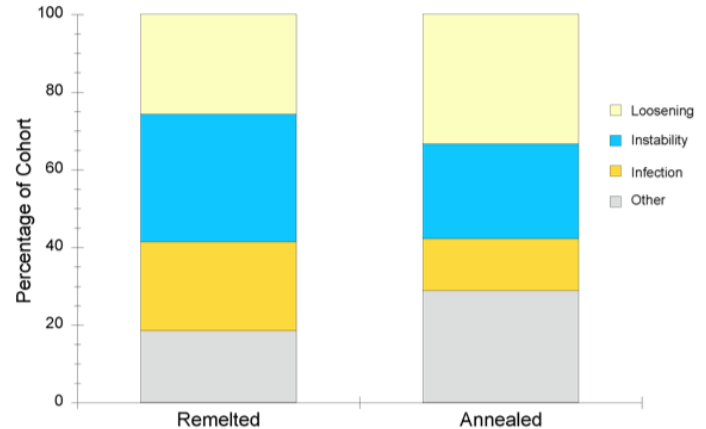


Figure 1: The predominant reasons for revision were loosening, instability, and infection for both cohorts.

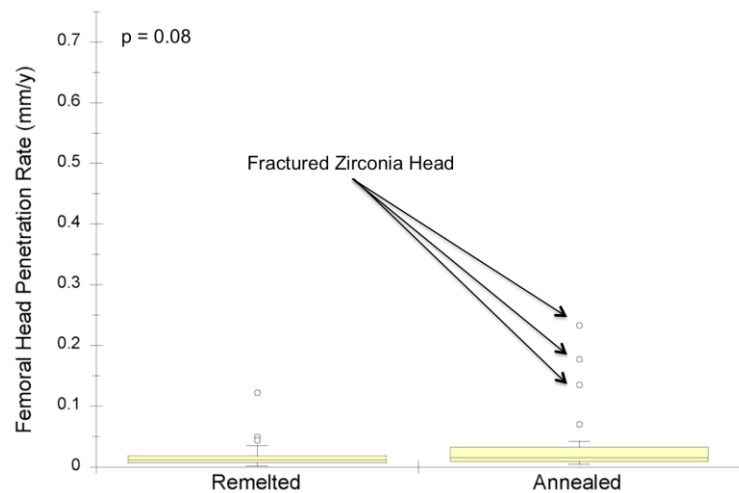


Figure 2: Penetration rates were low for both material cohorts.

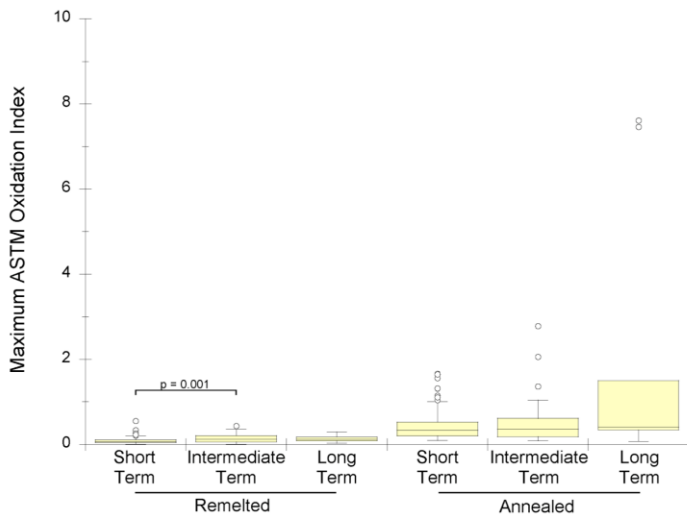


Figure 3: Oxidation indices for short, intermediate, and long-term cohorts for both remelted and annealed materials.

Chemical Nature of Vitamin E in UHMWPE after Irradiation: Investigations with Model Substances

Lerf R¹, Adlhart C², Delfosse D¹

¹Mathys Ltd Bettlach, Bettlach, Switzerland; ²Zurich University of Applied Sciences ZHAW, Waedenswil, Switzerland
reto.lerf@mathysmedical.com

Introduction: Several investigations have shown that during irradiation for cross-linking of UHMWPE with vitamin E (α -tocopherol, Figure 1) the latter is grafted to the PE macro-molecules (Lerf 2011, Badertscher 2012, Wolf 2011). In this context questions rise, about the chemical nature of this bond α -tocopherol – PE and whether the vitamin E molecule was changed upon binding? However, the determination of the particularities of chemical bonds by FTIR in a solid body is difficult. Liquid sample compounds with the same or similar characteristics may be used to elucidate the details of chemical bonds. Therefore, characterisation of substances extractable from UHMWPE after irradiation, irradiation and analyses of vitamin E dissolved in model hydrocarbons and analyses of UHMWPE blended with such compounds found in irradiated model hydrocarbons were performed.

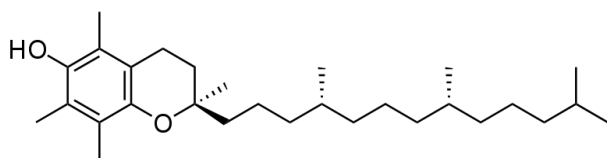


Figure 1: Chemical structure of the α -tocopherol molecule.

Methods and Materials: Dichloromethane extracts of sintered and γ -irradiated UHMWPE GUR 1020 samples containing 0.1 wt-% α -tocopherol at a dose of 29.5 kGy and 96.5 kGy as well as non-irradiated material were investigated by NMR and FTIR (GUR 1020 by Celanese, Oberhausen, Germany).

0.1% α -tocopherol was blended with the model hydrocarbons cyclohexane and *n*-octane (cf. Figure 2) and the blends were chemically characterised by means of GC-MS, HPLC, MALDI-TOF-MS and NMR before and after irradiation with dose levels corresponding to γ -sterilisation and cross-linking. Solutions of 100 ml cyclohexane or *n*-octane containing 0.1 wt-% α -tocopherol were γ -irradiated at a dose of 0.0 kGy (blank), 27.5 kGy, and 97.9 kGy at BBF Sterilisationsservice, Kernren-Rommelshausen, Germany. Experimental details are described by Badertscher (Badertscher 2012).

Based on the substances identified after γ -irradiation, 6-*O*-(4-heptyl)- α -tocopherolether, was synthetically produced, mixed to GUR 1020 powder at a concentration of 0.09 %, sintered and γ -irradiated at a dose of 104.4 kGy. Certain samples were artificially aged according ASTM F2003 for 14 and 60 days. Then, extraction of the heptyl-tocopherolether was done from the irradiated and non-irradiated samples using heptane. The extracts were

quantitatively analysed by GC-MS. Oxidation index (OI) of samples in the different ageing conditions were calculated from FTIR spectrum according ASTM F2102. Samples for IR analysis were slices of 0.2 mm cut by microtom.

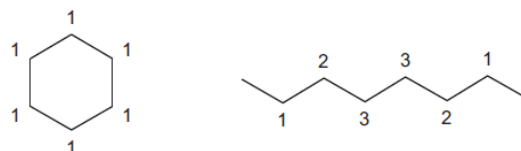


Figure 2: Chemical structure of cyclohexane (left) and *n*-octane (right).

Results, UHMWPE with α -tocopherol: As expected, almost no α -tocopherol or its degradation products were extracted after irradiation. 5-formyl- γ -tocopherol was identified as extractable degradation product (Figure 3). However, only partial conversion of α -tocopherol to formyltocopherol was observed.

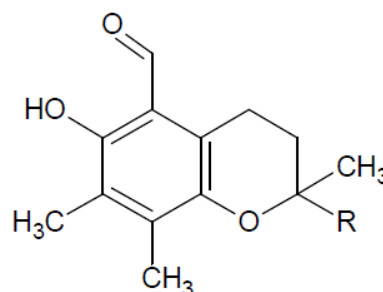


Figure 3: Chemical structure of 5-formyl- γ -tocopherol (phenol side shown only).

Model hydrocarbons with α -tocopherol: After irradiation of the model hydrocarbons blended with vitamin E, the different analysis show consistently that the α -tocopherol is chemically attached to the two hydrocarbons exclusively by a phenolic ether bond. The degree of ether formation was found to be strongly correlated with the irradiation dose. For the cyclohexane, 34%, resp. 68% of α -tocopherol was transformed into 6-*O*-cyclohexyl- α -tocopherol ether after irradiating with 27.5, resp. 97.9 kGy (cf. Figure 4). For *n*-octane, 31 % and 74 %, respectively, were transformed in three different but chemically equivalent ether products, as highlighted in Figure 5. These three equivalent compounds (2b, 2c and 2d in Figure 5) correspond to an ether bond α -tocopherol – *n*-octane at the three structurally different places in the octane molecule as indicated by numbers in Figure 2. The additional small peak labelled 2a corresponds to the non-

preferred chemical reaction with both end atoms of *n*-octane.

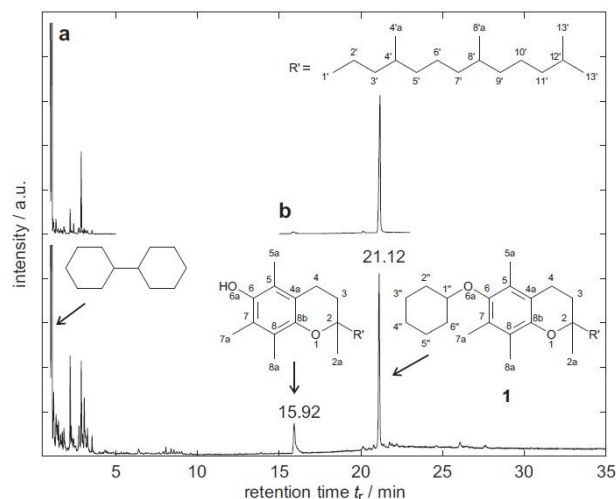


Figure 4: GC-MS chromatogram of the reaction products of 0.1% α -tocopherol in cyclohexane after γ -irradiation with a dose of 97.9 kGy

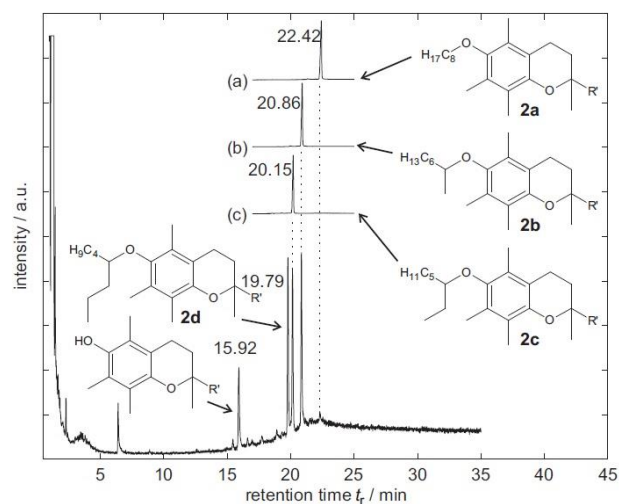


Figure 5: GC-MS chromatogram of the reaction products of 0.1% α -tocopherol in *n*-octane after γ -irradiation with a dose of 97.9 kGy

UHMWPE with 6-*O*-(4-heptyl)- α -tocopherol: The 6-*O*-(4-heptyl)- α -tocopherolether blended to UHMWPE could be extracted completely after sintering. Whereas after γ -irradiation, no heptyltocopherolether was detected in the extract any more, nor before nor after artificial ageing. In the “as sintered” sample, no oxidation was measured. After γ -irradiation, a slight oxidation in the outermost 0.6 mm was found with the maximum OI 0.046 in the 1st 0.2 mm section. After artificial ageing of 14 and 60 days, OI in the 0.2 mm increased to 0.173 and 0.118, respectively. A humble oxidation was found over the whole cross-section. For comparison: In UHMWPE γ -irradiated to 91 kGy, IO was not detectable after 60 days ASTM F2003 ageing with 0.05 wt-% α -tocopherol added

and was as high as 5.3 without vitamin E stabilisation (Lerf 2010).

Sample / condition	Heptyl- α -tocopherolether extracted [mass-%]	Maximum oxidation index
Powder mixture	0.089	--
As sintered	0.087	<0.025
Irradiated 104.4 kGy	<0.01	0.046
Irradiated + aged 14 days	<0.01	0.173
Irradiated + aged 60 days	<0.01	0.118

Table 1: UHMWPE samples blended with 6-*O*-(4-heptyl)- α -tocopherolether: amount of heptyltocopherolether extractable and oxidation indices.

Discussion: The degradation products of α -tocopherol extracted from γ -irradiated samples, 5-formyl- γ -tocopherol (Figure 3) has still its active HO-site of the phenolic group, albeit sterically hindered, and may still act as an anti-oxidant in PE.

The work with the hydrocarbons suggests that the grafting of vitamin E to PE after irradiation reported is an ether bond. However, it must be noted that these experiments were done with fluids, where kinetics and mobility of free radicals may differ from the solid UHMWPE. Analysis of the chemical nature of bonds in solid is difficult. Attempts doing it by FTIR failed. At least it seems plausible that such an ether bond is strong enough to prevent extraction of the 6-*O*- α -tocopherolether grafted to the PE chain.

Grafting of the synthetic 6-*O*-(4-heptyl)- α -tocopherolether (Figure 5, compound 2b) to UHMWPE due to γ -irradiation is surprising. The active HO-site does not exist in this molecule, i.e., it is replaced by the ether bond. A possible explanation could be the re-open of the ether bond upon irradiation followed by the statistically preferred reaction with the abundant PE molecule. Another surprise was the anti-oxidative effect of 6-*O*-(4-heptyl)- α -tocopherolether. Again, this effect in α -tocopherol is believed to depend on the HO group, which was not present in the tocopherolether. A possible explanation could be traces ($\leq 1\%$) of α -tocopherol in 6-*O*-(4-heptyl)- α -tocopherolether remaining from its synthesis. Alternatively we have to infer some antioxidant activity to the 6-*O*- α -tocopherolether, i.e. the α -tocopherol in its grafted condition, to prevent the oxidation cycle of UHMWPE.

References:

- Lerf R, 5th UHMWPE Conference, Philadelphia, 2011
- Badertscher RP et al., Polym Degrad Stab 2012;97:2255-61
- Wolf C et al., ORS annual meeting, 2011, Poster 1178
- Lerf R et al., Biomaterials 2010;31: 3643–3648



SESSION
TWO:

**Sterilization and
Crosslinking
Technologies
for UHMWPE**

Using Laser Optics to Construct the Phase Diagram of UHMWPE

Pavlovsky, L.¹; Le, K-P.¹; Bellare, A.²; Song, L.¹

¹Stryker Orthopaedics, Mahwah, New Jersey, USA; ²Brigham and Women's Hospital, Boston, Massachusetts, USA
Leonid.Pavlovsky@stryker.com

Introduction:

Ultra-high molecular weight polyethylene (UHMWPE) used in joint replacement prostheses is typically compression molded or ram extruded due to its high molecular weight. During the consolidation process, elevated temperature and pressure are used to fuse the powder in the melt state followed by recrystallization when the molded sheets, bars or components are cooled under pressure. Developing a Pressure-Temperature (P-T) phase diagram is of great interest to understand the effect of elevated pressure on thermal transitions and the lamellar morphology induced by heating or cooling UHMWPE under pressure. Few P-T phase diagrams have been reported in the literature for polyethylene, and none are specific toward medical-grade UHMWPE^{1,2}. The present study focused on designing and validating a bench-top optical system, the Laser Phase Diagram (LPD), to quantify and confirm the pressure dependency of the melting temperature (T_m) of GUR resins and consolidated forms. The current abstract describes the quantification based on consolidated forms only.

Methods and Materials:

Polyethylene: 3 different samples of compression molded virgin GUR1020 UHMWPE were cut into 1 mm thick sheets, from which 1 inch diameter specimens ($n \geq 5$) were punched.

Device setup: A Superpressure optical absorption cell (Newport Scientific; Jessup, MD) was used as a pressure vessel. This steel vessel had a 1 inch diameter shaft, enclosed on either side with sapphire windows, into which the UHMWPE sample was placed. Heaters and insulation were attached to the outside of the vessel to maintain temperature, which was measured internally at the approximate position of the specimen. Pressure was adjusted using a non-reactive fluid, Krytox GPL 107 oil (DuPont; Wilmington, DE), and monitored using an in-line pressure transducer. A 1.0 mW, 532 nm laser beam (Thorlabs, Inc.; Newton, NJ) was passed through the sapphire windows of the pressure vessel and the specimen. The power of the laser was monitored via detector (Edmund Optics; Barrington, NJ) on the opposite side of the pressure vessel. A schematic of the setup is shown in Figure 1:

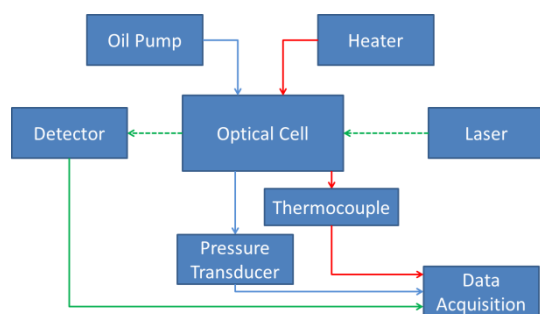


Figure 1: LPD setup schematic

LPD testing: Tests were conducted over a pressure range of 0-140 MPa. At each pressure, a defined temperature profile was incrementally applied to the sample using a custom-built, custom-programmed controller and data acquisition system. All signals (temperature, pressure, and laser power) were recorded and displayed in real-time.

Data analysis: An algorithm was used to determine when the instantaneous change in the detected laser power reached a maximum. The first derivative of laser power with respect to time was determined to confirm that this point corresponded to a local maximum. The temperature and pressure observed at this time were extracted to generate the phase diagram. A linear regression ($T_m = \text{Pressure} * \text{slope} + T_{m,a}$) was conducted to extrapolate the ambient melting temperature, $T_{m,a}$.

DSC: UHMWPE was analyzed via Diamond DSC (PerkinElmer; Waltham, MA) at ambient pressure to validate the results of the phase diagram testing as well as to determine the effect of Krytox oil on the observed properties. Testing was conducted in aluminum vented, crimped pans at a ramp rate of 10°C/min and the T_m was taken as the observed peaks.

Statistical analysis: Data were compared using a two-sample t-test in which $P < 0.05$ was considered significant. Linear regression was conducted using Minitab.

Results:

The plot of T_m vs. pressure generated a linear fit with $R^2 \geq 0.995$ for each specimen tested. The slopes and extrapolated ambient T_m are displayed below.

Specimen	Slope (°C/MPa)	$T_{m,a}$ (°C)
A	0.278	137.3
B	0.267	136.9
C	0.270	137.1

Combined, these results are used to create the phase diagram seen in Figure 2:

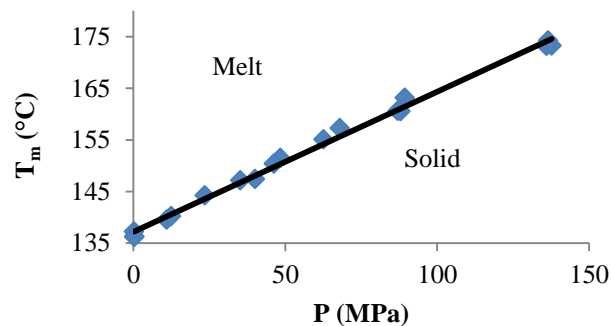


Figure 2: Phase Diagram of consolidated GUR. DSC tests found $T_{m,a} = 137.8 \pm 0.4$ °C, while no significant effect of Krytox oil on the T_m ($P = 0.332$) was observed.

Discussion:

The melting temperature of UHMWPE can be characterized by finding the greatest instantaneous change in the material's translucency to laser light. The extracted $T_{m,a}$ obtained from LPD testing was found to be in agreement with that observed via DSC. Future investigations into the various stages of UHMWPE processing are desired in order to understand the changes in material properties with respect to different methods of processing and consolidation.

References:

1. Corbeij-Kurelec, Lada. *Chain Mobility in Polymer Systems; On the Borderline between Solid and Melt*. Eindhoven: University Press, 2001. Print.
2. Bellare, Anuj. "High Pressure Crystallized UHMWPEs." *UHMWPE Biomaterials Handbook*. Ed. Kurtz, S. 2nd Ed. New York: Academic Press, 2009. 277 - 289. Print.

The Properties of Highly Crosslinked UHMWPE Manufactured Using High Power X-Ray

Allen M.D (mallen@orthoplastics.com)
Orthoplastics Ltd, Unit A, Beech Ind. Est, Bacup, Lancashire, OL13 9EL, UK.

Introduction

Commercial X-ray processing techniques have developed at Synergy healthcare (Daniken, Switzerland) utilising high energy electron beam accelerator. Previous studies have shown that dose distribution and attenuation are reduced significantly when compared to Gamma and e-Beam technologies. Highly crosslinked Ultra High Molecular Weight Polyethylene (UHMWPE) for orthopaedic applications, are characterised by physical/mechanical test methods outlined in both ISO and ASTM international standards.

The purpose of this study was to evaluate the physical mechanical characteristics of UHMWPE processed through X-ray and Gamma (Co₆₀) irradiation processes at different administered doses.

Materials and Methods

Compression moulded (Celanese GUR1020) was evaluated at five nominal irradiation doses (50, 75, 100, 125 and 150kGy). X-ray processing was also conducted on three polymer lots from Celanese.

Irradiation Method	Orthoplastics Batch Ref	Celanese Polymer Batch
X-Ray	20909M	CM0000415499
X-Ray	20994M	CM0000493126
X-Ray	21036M	CM0000508571
Gamma	21016M	CM0000508571

Processing was completed on a small scale development with product 84mm Ø x 500mm

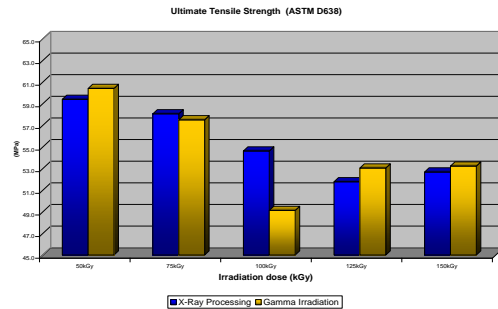
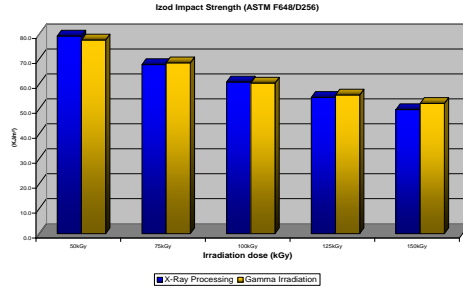
Analysis

Processed materials were analysed in accordance with the principle guidance of ASTM F2565, namely the characterisation of Extensively Irradiation-Crosslinked Ultra-High Molecular Weight Polyethylene Fabricated Forms for Surgical Implant Applications. Testing of the materials included;

Izod Impact Strength	ASTM D256/ F648
Tensile Testing	ASTM D638
In Situ determination of network parameters	ASTM F2214
Small Punch Testing	ASTM F2183
Thermal Properties (DSC)	ASTM F2625

Both Oxidation Index Analysis (ASTM F2103) and Trans-Vinylene Index Analysis (ASTM F2381) have been discussed in previous studies

Results and Discussion



Conclusions

One way ANOVA analysis of variance was completed on the data sets with a P<0.005 considered statistically significant. Limited statistical analysis indicated that the variation between X-Ray and Gamma processing on the properties of HXL UHMWPE was not significant.

Irradiation Dose	Ultimate Tensile Strength	Tensile Yield	Elongation @ Break	Izod Impact Strength
50	0.671	0.114	0.786	0.011
75	0.754	0.030	0.128	0.420
100	0.041	0.031	0.047	0.406
125	0.652	0.000	0.905	0.094
150	0.785	0.119	0.053	0.001

Any significant values could be attributed to the very small data sets for the Gamma products tested and the difference in Dose administered in the processes

X-Ray crosslinking is comparable to conventional Gamma processing

Further Studies

- Accelerated aging to evaluate low ozone environment in X-Ray processing.

	Irradiation Dose	Density	Izod Impact Strength	Ultimate Tensile Strength	Tensile Yield	Elongation @ Break	Swell Ratio	SMP Ultimate Load	Melting temperature at the peak of the melting endotherm	Percentage of crystallinity
		(D ²³ kg/m ³)	(KJ/m ²)	(MPa)	(MPa)	(%)	(q)	(N)	(°C)	(%)
20909M X-RAY	50kGy	931.2	79.7	56.4	21.66	352	3.33	91.57	136.4	55.3
20994M X-RAY		931.2	79.7	61.4	21.36	349	3.26	90.82	136.4	56.0
21036M X-RAY		931.0	78.3	60.3	21.88	336	3.21	95.04	137.0	54.2
21016M GAMMA		931.2	77.7	60.4	21.82	347	3.26	94.70	137.6	55.7
20909M X-RAY		931.8	67.3	61.1	21.52	318	3.17	93.21	137.7	56.3
20994M X-RAY	75kGy	931.6	69.0	57.2	21.38	303	3.18	96.83	136.0	56.1
21036M X-RAY		931.6	67.0	55.8	21.60	303	3.08	98.27	138.3	54.1
21016M GAMMA		931.5	68.5	57.5	21.20	301	3.02	95.95	137.5	54.1
20909M X-RAY		931.6	62.0	57.6	21.52	283	2.95	98.39	138.2	55.2
20994M X-RAY		931.4	60.7	54.2	21.52	272	2.93	100.46	138.7	55.4
21036M X-RAY	100kGy	931.8	59.7	52.0	21.30	264	2.85	103.09	138.9	54.5
21016M GAMMA		931.9	60.4	49.1	21.18	259	3.32	96.48	139.2	54.8
20909M X-RAY		932.1	55.8	55.7	21.50	261	3.35	96.61	137.8	56.2
20994M X-RAY		931.8	53.9	47.5	21.72	235	3.07	100.13	139.1	55.8
21036M X-RAY		931.8	54.2	52.2	21.34	244	2.74	100.13	138.8	55.7
21064M GAMMA	125kGy	932.0	55.6	53.0	22.28	248	3.45	102.50	138.8	55.1
20909M X-RAY		932.3	50.4	54.1	21.68	232	3.37	103.78	138.3	55.5
20994M X-RAY		932.2	50.3	53.7	22.66	231	3.32	103.55	138.7	55.3
21036M X-RAY		932.1	48.6	50.2	22.90	222	3.19	101.50	138.8	55.5
21064M GAMMA		932.0	52.2	53.2	21.96	238	3.29	102.94	138.7	54.5

Post Radiation Annealing Of UHMWPE Under High Pressure

Bellare, A¹, Rbiji, A^{1,2}, Bistolfi³, A, Matriciano, L⁴, Bracco, P²

¹Brigham & Women's Hospital, Harvard Medical School, Boston, MA, USA; ²University of Turin, Turin, Italy; ³CTO Hospital, Turin, Italy; ⁴Restoration Medical Polymers, Columbia City, IN
anuj@alum.mit.edu

Introduction: Ultra-high molecular weight polyethylene (UHMWPE) has been used to fabricate components of total joint replacements for several decades. In recent years, they have been used in a crosslinked form since highly crosslinked UHMWPE have shown a high resistance to wear compared to historic UHMWPE (1). It is well known that irradiation of UHMWPE using ionizing radiation introduces crosslinks in the amorphous regions but also introduces free radicals in the crystalline lamellae, leading to long term oxidative degradation (2). Radiation crosslinked UHMWPEs of the first generation in clinical use were remelted after radiation to quench free radicals in order to prevent oxidative degradation. In some cases, the irradiated UHMWPE was annealed at a temperature just below the melting temperature to preserve mechanical properties since it was shown that certain mechanical properties of irradiated and annealed UHMWPE were higher than the corresponding properties of irradiated and remelted UHMWPE (3). However, annealing at atmospheric pressure does not eliminate all free radicals and has been shown to result in some degree of oxidation in the long term (4). In this study, we hypothesized that post-radiation annealing would be more effective when conducted under pressure and at higher temperatures than at atmospheric pressure. The melting temperature of polyethylene increases with increase in pressure making it possible to anneal polyethylene at much higher temperatures than possible at atmospheric pressure (see Figure 1). We believed that annealing at the higher temperature would drive free radicals from lamellae more effectively, and thereby induce higher oxidation resistance in irradiated UHMWPE

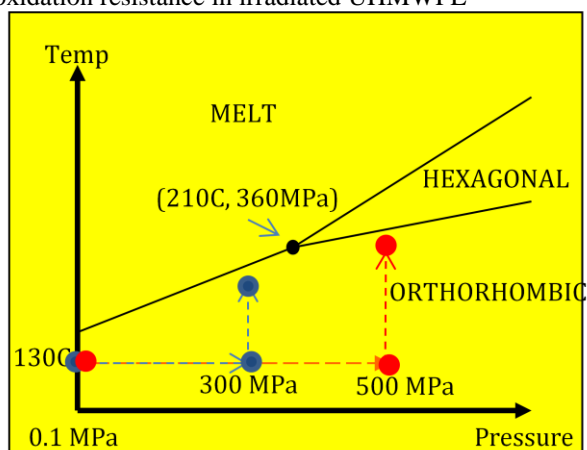


Figure 1. Phase diagram of Polyethylene showing the triple point at 210°C and 360 MPa pressure, as well as the Melt, Hexagonal and Orthorhombic crystal phases

Methods and Materials: Compression molded plaques of GUR 1020 (Mediatech Medical Polymers, Fort Wayne, IN) was the starting material (CTRL). The plaques were

radiation crosslinked using 100 kGy dose of gamma radiation (Group A). Some plaques were remelted and recrystallized prior to irradiation to introduce a different morphology to the plaques (Group B). Thereafter, cylinders of 3" height and 1/2" diameter were machined from the plaques and annealed in a custom built high pressure cell. Cylinders of crosslinked UHMWPE were (1) untreated (ACTR) and (BCTR) (2) annealed at 130°C for 4 hours at atmospheric pressure (A130At and B130At), (3) annealed at 130°C for 4 hours at 300 MPa (A130P1) and annealed at 130°C for 4 hours at 500 MPa (B130P2). (4) annealed at 190°C for 4 hours at 300 MPa (A190P1) and annealed at 210°C for 4 hours at 500 MPa (B130P2). Both these temperatures were carefully chosen to be just lower than the melting point of UHMWPE at those respective pressures. After treatment, selected cylinders were sectioned and aged for 14 days in an oxygen environment at 5 atmosphere pressure and 70°C in a Parr bomb reactor. Fourier transform Infrared Spectroscopy (FTIR) was conducted on thin sections of various cylinders using a Perkin-Elmer Spotlight FTIR instrument with a microscope attachment. The oxidation index, OI, was defined to be the ratio of the area under 1740cm⁻¹ carbonyl and 1370 cm⁻¹ methylene stretching absorbances. For each section, the maximum oxidation index, present at the first subsurface beam spot, was recorded at various locations. A Pyris 6 Differential scanning calorimeter (Perkin-Elmer, Waltham, MA) was used to measure the degree of crystallinity for each type of UHMWPE using heat of fusion of 293 J/g. A Rigaku Smax-300 small angle x-ray scattering (SAXS) instrument was used to obtain SAXS curves, which were inverse Fourier transformed using previous methods (5) to obtain the inter-lamellar spacing and converted to lamellar thickness by multiplying with the fraction crystallinity obtained by DSC. ASTM 638 type V specimens were punched from 1 mm thick sheets sectioned from the cylinders (n=5) and subjected to tensile testing using an Admet universal tensile tester. Tensile modulus, yield stress, maximum strain and ultimate tensile stress (UTS) were measured. Rectangular bars of 1/2" width, 1/4" thickness and 2 1/2" length were double notched and subjected to impact testing (n=5) to measure impact strength using a Ceast impact tester.

Results and Discussion: The crystallinity of various UHMWPEs ranged from 50.7 to 55.7%, which indicated that the annealing conditions, especially those under high pressure and elevated temperature, didn't result in melting and high pressure crystallization, which otherwise would have increased the crystallinity substantially (see Table 1). The lamellar thickness for Group A, crystallized under pressure during molding, was 23.9-25.5nm, whereas for Group B, which was remelted and crystallized at

atmospheric pressure, was only 19.6-20.7nm, since pressure induced crystallization leads to thicker lamellae. Table 1. Crystallinity and Lamellar thickness of various groups of polyethylene

Sample ID	Crystallinity [%]	Lamellar thickness [nm]
ACTR	53.0 ± 1.3	25.5 ± 0.6
A130At	53.3 ± 0.5	23.9 ± 0.2
A130P1	52.4 ± 0.4	23.9 ± 0.2
A190P1	55.7 ± 2.5	24.1 ± 1.1
BCTR	52.2 ± 0.5	20.7 ± 0.2
B130At	52.0 ± 1.1	20.6 ± 0.4
B130P2	50.7 ± 0.9	20.3 ± 0.4
B210P2	53.7 ± 0.6	19.6 ± 0.2

The oxidation index of accelerated aged, irradiated and untreated UHMWPEs (AACTR and ABCTR) was significantly higher than those of their un-aged counterparts (UACTR and UBCTR) ($p < 0.001$, ANOVA), (see Figure 2). While AA130At had a much lower oxidation index compared to AACTR, it were significantly higher ($p = 0.015$) than the oxidation index of UACTR. Pressure annealing at 130°C led to much higher oxidation index than annealing at atmospheric pressure, probably because at atmospheric pressure and 130°C, there is partial melting, resulting in a decrease in free radical content. However, at higher pressures, 130°C is much lower than the melting temperatures at those pressures and thus no partial melting can be expected.

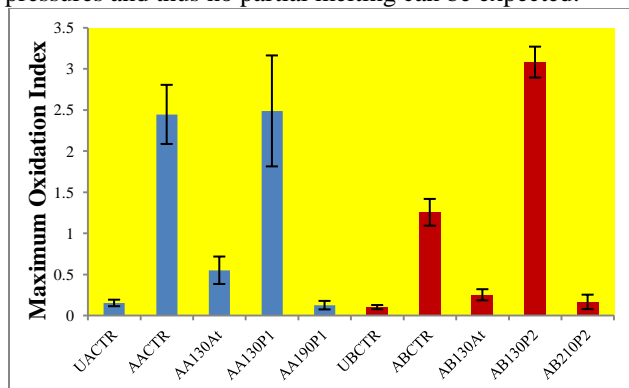


Figure 2. Maximum oxidation index of various groups of polyethylene (average ± standard deviation) (“U” and “A” preceding sample abbreviations refers to unaged and accelerated aged, respectively).

The most significant result of the accelerated aging study was that annealing at elevated pressure and at a higher temperature (190°C or 210°C) resulted in oxidation index that was statistically not different from their un-aged counterparts ($p = 0.866$ and 0.689 , respectively), indicating that post-radiation annealing under pressure is much more effective than annealing at atmospheric pressure in free radical removal, which makes the radiation crosslinked UHMWPE substantially more resistant to oxidation.

There was no remarkable trend in tensile properties with different annealing conditions (see Table 2). The untreated ACTR and BCTR had the highest modulus in

their groups probably since they retained the lamellar structure of the control. Although small but significant differences were noted, different annealing conditions did not greatly vary the yield stress, UTS and maximum strain compared to untreated, irradiated controls.

Table 2. Tensile Properties of various groups of polyethylenes

Sample ID	Modulus [MPa]	Yield Stress [MPa]	Max Strain	UTS [MPa]
ACTR	198 ± 12	22.7 ± 0.4	10.0 ± 0.9	51.5 ± 2.5
A130At	182 ± 6	22.8 ± 0.3	9.1 ± 0.5	53.6 ± 2.7
A130P1	168 ± 9	21.8 ± 0.1	9.2 ± 1.1	50.1 ± 6.0
A190P1	186 ± 5	22.4 ± 0.1	8.9 ± 0.9	47.7 ± 3.9
BCTR	151 ± 4	20.6 ± 0.1	7.2 ± 0.5	47.5 ± 2.9
B130At	137 ± 5	20.1 ± 0.4	7.6 ± 0.5	53.5 ± 2.7
B130P2	135 ± 14	19.8 ± 1.2	7.2 ± 0.4	46.9 ± 5.4
B210P2	141 ± 7	19.5 ± 0.4	7.7 ± 0.6	46.8 ± 3.9

The impact strength of unirradiated, GUR 1020 is substantially higher than the irradiated and annealed groups but there was no statistically significant difference between the irradiated Group A except for A190P1, which was significantly lower than A130At and A130P1 (see Figure 3). Group B behaved similarly in that B210P2 had the lowest impact strength. The lower impact strength in A190P1 and B210P2 is likely due to a slight increase in crosslinking since they were more effective in driving free radicals out of lamellae, which are expected to recombine in the amorphous regions to increase crosslinking.

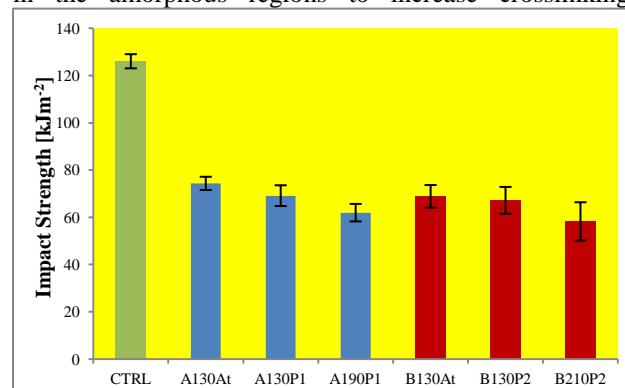


Figure 3. Impact strength of various groups of polyethylenes (average ± standard deviation).

In summary, post-radiation annealing at elevated pressure and at a temperature close to but below the melting temperature is more effective in inducing oxidation resistance than annealing at atmospheric pressure. Additionally, under the conditions investigated, pressure annealing did not affect the morphology, impact and tensile properties of irradiated UHMWPE to a great extent relative to atmospheric pressure annealing.

References: (1) Kurtz et al, CORR 2011, 469(8):2262-77 (2) Costa et al, Biomaterials 2002, 23(7):1613-24 (3) Medel et al JBMR: Appl Biomat 2007, 76(2):346-53 (4) Kurtz et al, J Arthroplasty 2010, 25(4):614-23 (5) George et al, J Mech Behav Biomed Matls 2014, 40:406-12

Multiphase polymeric material for cushion-bearing orthopedic implants

Bruce Carvalho¹ and Anuj Bellare²

¹Ceora, Boston, MA

²Brigham and Women's Hospital, Harvard Medical School, Boston, MA

bruce.carvalho@ceoratec.com

Introduction: We investigated a multiphase bearing material based on ultra-high molecular weight polyethylene (PE) and a polyethylene based elastomer (PLAST) as a compliant, cushion-bearing material. We hypothesized that blending in PLAST into UHMWPE would lower its density and decrease its modulus. We also hypothesized that melt-radiation of this multiphase polymeric blend would create a strong interface between the two phases and also further decrease the modulus of the blend, thereby creating a candidate material for cushion bearing implants. The advantage of such bearings is that it would reduce contact stress significantly and potentially decrease the incidence of stress related damage mechanisms in implants such as delamination wear in tibial inserts or rim fracture of acetabular cups.

Materials and Methods: GUR 1020 PE powder Celanese (Florence, KY) served as a Control (CTRL). Pellets of Attane™ 4404G (Dow Chemical, Midland, MI) (PLAST) were and cryogenically ground to reduce the pellet to powder and then added to GUR1020 powder in different weight fractions, mixed and molded using compression molding at a temperature of 200°C and an applied stress of 10 MPa. Following molding, the polymer plaques were subjected to 10 MeV electron beam irradiation at Iotron (Columbia City, IN). One set of plaques was subjected to irradiation and then remelted and slow cooled while the second set was irradiated in the melt state by preheating plaques to 180°C and then slow cooled after irradiation, providing various groups of PE (see Table 1).

Table 1. Various groups of PE and its blends

Specimen	Code
GUR1020 PE	CTRL
100% 4404G	PLAST
Irradiated, remelted PE	XR
Irradiated, remelted 95% PE + 5% 4404G	XR-5
Irradiated, remelted 90% PE + 10% 4404G	XR-10
Irradiated, remelted 80% PE + 20% 4404G	XR-20
Melt-irradiated PE	MR
Melt-irradiated 95% PE + 5% 4404G	MR-5
Melt-irradiated 90% PE + 10% 4404G	MR-10
Melt-irradiated 80% PE + 20% 4404G	MR-20

Differential scanning calorimeter (DSC) measurements were performed on all PE groups (n=3 per group) followed the ASTM F2625 standard. The degree of crystallinity was measured using a heat of fusion, Δh_f , of 289 J/g for 100% crystalline PE. Specimens consisted of small chards of polymer cut from the plaques (n = 3). ASTM D638 standard tensile tests were performed using a Series 1500 tensile tester (Oakland Instruments, Minneapolis, MN) operating at a crosshead speed of 10 mm/min and using D638-Type V dogbone specimens of 1

mm thickness (n = 6-10) to provide tensile modulus, yield stress, tensile strength and maximum strain for various groups of PE. Izod impact tests were conducted using the ASTM D256 protocol on double notched specimens of various groups of PE blends and PLAST (n = 5). Wear tests were performed on selected groups of specimens using a multidirectional pin-on-disk wear tester operating at 1 Hz for up to 1×10^6 cycles. Cylindrical pins of 9 mm diameter were machined from the following groups: CTRL, PLAST, MR and MR-10 (n = 6) and articulated against implant grade polished CoCr discs in a bovine serum medium maintained at 37°C. Prior to the testing, all specimens were presoaked for 30 days.

Results and Discussion: Control PE had the highest crystallinity whereas PLAST had the lowest crystallinity.

Table 2. Crystallinity [%] (mean \pm standard deviation) for Elastomer and various groups of UHMWPE

Sample ID	Crystallinity [%]
CTRL	57.4 \pm 1.3
PLAST	20.8 \pm 1.2
XR	53.4 \pm 0.5
XR-5	49.2 \pm 0.7
XR-10	49.2 \pm 2.0
XR-20	48.9 \pm 0.2
MR	47.5 \pm 1.3
MR-5	47.2 \pm 0.8
MR-10	46.8 \pm 1.7
MR-20	49.2 \pm 0.7

All crosslinked versions as well as the crosslinked blends had intermediate crystallinity (see Table 2) due to the presence of PLAST as well as due to the melting required to quench free radicals.

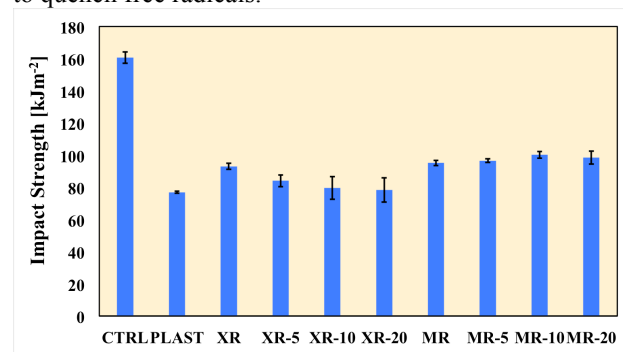


Figure 1. Izod impact strength [kJm⁻²] of various groups of PE (mean \pm standard deviation).

Izod impact strength of control unirradiated GUR 1020 was the highest compared to the rest of the groups ($p < 0.05$, ANOVA) (see Figure 1). The major result from these tests was that irradiation followed by remelting in the blends (XR-5, XR-10 and XR-20) had a significantly

lower impact strength compared to XR ($p < 0.05$, ANOVA) whereas all melt-irradiation (MR) groups were not significantly different from each other ($p > 0.05$, ANOVA). Thus, blending of PLAST into GUR 1020 followed by melt-irradiation did not significantly decrease the impact strength, demonstrating that under melt-irradiation there is a relatively strong interface due to crosslinking of the two phases across the interface.

Table 3. Tensile properties (mean \pm standard deviation) for Plastomer and various groups of UHMWPE

Sample ID	Tensile Modulus [MPa]	Yield Stress [MPa]	Max Stress [MPa]	Max Strain
CTRL	231 \pm 20	21.2 \pm 0.5	48.0 \pm 3.8	11.5 \pm 0.9
PLAST	35 \pm 3	3.8 \pm 0.3	9.5 \pm 0.6	7.9 \pm 1.0
XR	145 \pm 9	19.3 \pm 0.8	41.6 \pm 2.2	9.6 \pm 0.5
XR-5	123 \pm 7	18.1 \pm 0.8	21.4 \pm 2.5	3.9 \pm 0.9
XR-10	109 \pm 4	17.1 \pm 0.5	20.0 \pm 1.6	3.6 \pm 0.8
XR-20	55 \pm 4	14.7 \pm 0.2	17.2 \pm 0.9	3.7 \pm 0.5
MR	129 \pm 11	17.0 \pm 0.9	26.0 \pm 1.2	9.4 \pm 0.5
MR-5	117 \pm 7	16.6 \pm 0.5	23.6 \pm 2.4	8.5 \pm 1.3
MR-10	117 \pm 19	17.2 \pm 2.1	23.3 \pm 5.5	7.9 \pm 1.8
MR-20	84 \pm 10	15.0 \pm 0.3	16.8 \pm 0.3	5.8 \pm 0.5

Tensile tests demonstrated that the modulus of CTRL was the highest while PLAST had the lowest modulus and all other groups had intermediate tensile moduli (see Table 3). The main result is that with increasing volume fraction of PLAST, the modulus dropped monotonically, as expected, regardless of when the thermal treatment was performed. This indicates that incorporation of PLAST can make PE behave more like a cushion bearing rather than a conventional thermoplastic bearing due to its lower modulus. The yield stress of CTRL was the highest while that of PLAST was the lowest. With increasing volume fractions, the yield stress of the blend decreased regardless of whether it was irradiated and then remelted or melt-irradiated. The yield stress decreased due to both blending as well as crosslinking. The maximum stress (or ultimate tensile strength) of CTRL was the highest while that of PLAST was the lowest. Melt-irradiation had a much stronger effect on overall maximum stress than post-radiation remelting. Melt-irradiation substantially decreased the maximum stress of PE and its blends with PLAST but then post-radiation melted blends also had a similarly low maximum stress likely due to the weak interfaces present in them. The maximum strain, which is a measure of ductility, was the highest for CTRL. In this case, PLAST did not have the lowest ductility but instead the XR blends had the lowest ductility compared to PLAST and CTRL as well as the corresponding MR blends ($p < 0.05$, ANOVA). A decrease in maximum strain in the blends were exacerbated by the post-radiation melting, which is the clearest indication of weak interfaces present in them, likely due to PE matrix first crystallizing followed by crystallization of PLAST which crystallizes at a lower temperature. This is expected to

make the segregated domains of PLAST shrink away from the interface. Such an occurrence is avoided with melt-irradiation since there is potential for crosslinking of PLAST with PE across the interface due to both being in the melt state. This observation also confirms why impact strength was unaffected by increasing PLAST volume fractions in the melt-irradiation case unlike the case of post-radiation remelting.

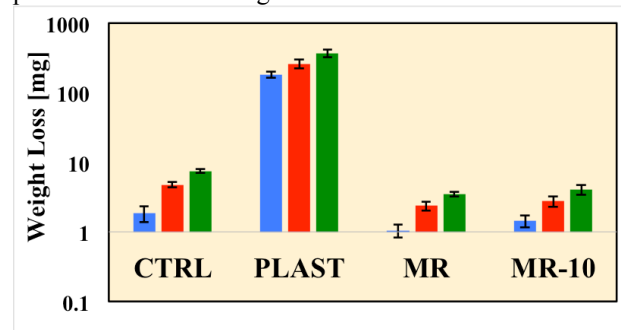


Figure 2. Weight loss [mg] after 330,000 (blue), 670,000 (red) and 1,000,000 cycles (green) for CTRL, PLAST, MR and MR-10 (mean \pm standard deviation).

Wear tests conducted on CTRL, PLAST, MR and MR-10 showed that PLAST had two orders of magnitude higher wear rate than all the UHMWPE groups (see Figure 2). Please note that the wear rate of PLAST was so high that in order to present the data, we had to present wear rate on a log scale on Figure 2. The cumulative wear rate of CTRL was higher than that of MR by a factor of 2.1 ($p < 0.001$, ANOVA) and higher than MR-10 by a factor of 1.84 ($p < 0.001$, ANOVA) whereas there was no statistically significant difference in the cumulative wear rates of MR and MR-10 ($p = 0.0747$). This result shows that there is no real penalty in terms of wear resistance when adding 10% PLAST to UHMWPE as long as they are melt-crosslinked, which makes their wear resistance much lower than that of UHMWPE. This is a key result that shows that one can significantly lower the modulus of PE by the addition of PLAST to prepare cushion bearings without significantly compromising wear resistance. It is all the more surprising that pure, uncrosslinked PLAST had two orders of magnitude higher wear rate than PE but when melt crosslinked at 10% in PE there was no significant difference in wear. In summary, this study provides a pathway to prepare cushion bearings which at the very least maintains wear resistance while decreasing the modulus by 50% over that of pure PE, thereby providing a more compliant, cushion bearing material by blending PE with a lower modulus plastomer to 10 weight percent. It must be noted that such compliant bearing surfaces are expected to have a higher propensity for creep deformation and further tests must be performed prior to application of such formulations of cushion bearings for clinical use.

Acknowledgements: Research reported here was supported by NIAMS of the National Institutes of Health under award number R43AR064626.

A wear and highly oxidation resistant chemically cross-linked UHMWPE with improved toughness

Oral E^{1,2}, Doshi BN¹, Neils AL¹, Lozynsky A¹, Muratoglu OK^{1,2}

¹Harris Orthopaedic Laboratory, Massachusetts General Hospital; ²Department of Orthopaedics, Harvard Medical School
eoral@mg.harvard.edu

Introduction: Radiation cross-linked UHMWPE is preferred in total hip replacements due to its wear resistance [1]. In total knees, where stresses are higher, there is concern of fatigue damage [2].

Antioxidant stabilization of radiation cross-linked UHMWPE by blending vitamin E into the polymer powder was recently introduced [3]. The concentration of vitamin E is limited to 0.2-0.3 wt% due to its ability to hinder radiation cross-linking in UHMWPE [4].

Cross-linking of UHMWPE by peroxides was less sensitive to the vitamin E concentration than radiation cross-linking, thus higher vitamin E concentration could be used with high cross-linking yield [5].

We have also shown that exposing UHMWPE to very high temperatures, around 300°C, increases the toughness by inducing controlled chain scission and enhanced intergranular diffusion of chains, simultaneously [6]. We present a chemically cross-linked UHMWPE with high vitamin E content and improved toughness by high temperature melting.

Methods and Materials: Medical grade GUR1050 UHMWPE was blended with vitamin E and with 2,5-Di(tert-butylperoxy)-2,5-dimethyl-3-hexyne or P130 (Sigma-Aldrich 544604). The mixed powder was consolidated into pucks (diameter 10 cm, thickness ~1 cm). The pucks were further melted for 5 hours in inert atmosphere at the desired temperature in a convection oven. The vitamin E concentration was 0.5 wt%, the peroxide concentration was 0.9 wt%. The temperatures used for melting were 300, 310 and 320°C.

One set of pucks melted at 310°C was accelerated aged at 70°C at 5 atm. oxygen for 2 weeks.

Tensile mechanical properties were determined using ASTM D638. Izod impact toughness was determined using ASTM D256 and F648. Wear rate was determined using a bidirectional pin-on-disc (POD) tester with cylindrical pins of UHMWPE (diameter 9 mm, length 13 mm) against polished CoCr discs in undiluted, preserved bovine serum. The wear rate was determined as the linear regression of weight loss from 0.5 to 1 MC.

Results: The vinyl index increased as a function of temperature (Fig 1a). Cross-link density steadily decreased and impact strength increased with increasing vinyl index (Fig 1b).

The ultimate tensile strength (UTS) was not affected by HTM (Table 2). Impact strength was significantly improved for all treatment temperatures ($P < 0.05$) and wear was significantly increased only for the sample melted at 320°C (Table 2).

Discussion: High temperature melting (HTM) was shown to increase toughness of UHMWPEs presumably due to controlled chain scissioning and increased intergranular diffusion of chains [6]. For radiation cross-linked UHMWPE, it was shown that an increase in elongation-

at-break and impact strength could be obtained without sacrificing wear resistance up to an elongation of about 500% [7].

Figure 1. Vinyl index (VI) as a function of high temperature (a) and cross-link density and impact strength as a function of VI (b).

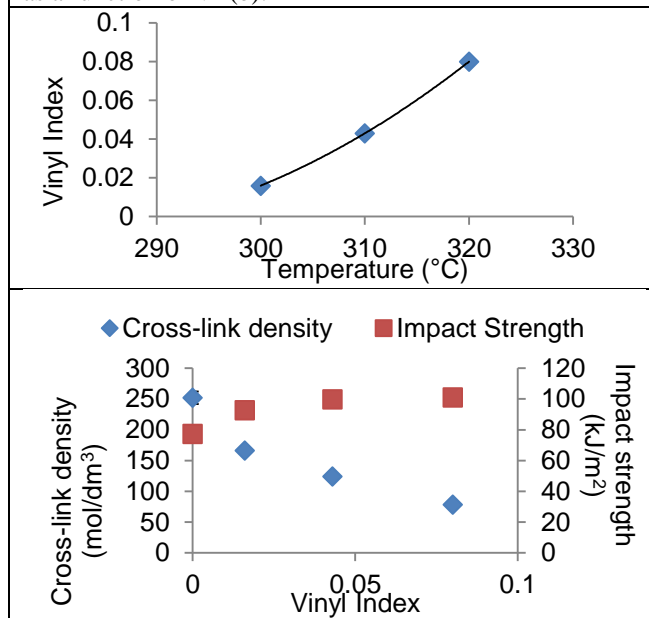


Table 2. Comparative properties of vitamin E-blended, chemically cross-linked high temperature melted UHMWPEs.

	UTS (MPa)	IZOD (kJ/m ²)	Wear (mg/MC)
No HTM	36.9±3.7	77.2±0.6	1.30±0.17
300	36.2±4.4	92.7±1.1	1.37±0.22
310	39.3±2.2	99.7±0.7	1.40±0.21
320	35.2±6.5	101 ±3.3	2.23±1.20

Here, we showed that the increase in impact strength was more effective for peroxide cross-linked UHMWPE than for radiation cross-linked UHMWPE with impact strengths similar to conventional, gamma sterilized UHMWPE (93 kJ/m²).

This vitamin E-blended, peroxide cross-linked, high temperature melted UHMWPE has very high oxidation resistance due to its high antioxidant content, high wear resistance due to cross-linking and much improved toughness, representing an optimum joint replacement surface.

References: [1] Kurtz et al. CORR (2011) 469:2262-77; [2] Rodriguez JOA (2008) 23:31-4; [3] Bracco et al. CORR (2011) 469:2286-93; [4] Oral et al. Biomaterials (2008) 29:3557-60; [5] Gul et al. ORS (2013) 1819; [6] Fu et al. Polymer (2010) 51:2721-31; [7] Doshi et al. ORS (2014) 9888.

Chemically cross-linked UHMWPE in the presence of an unsaturated additive

Bracco P, Costa L

¹Chemistry Department and NIS Center, University of Torino, ITALY

pierangiola.bracco@unito.it

Introduction:

Radiation cross-linking of UHMWPE has been widely employed to improve the wear resistance of UHMWPE and commercially produced highly crosslinked UHMWPE have been in clinical use for over 15 years.

Chemical cross-linking of UHMWPE with the addition of organic peroxides has recently known an upsurge of interest, due to the relative easiness and versatility of the process [1,2]. Nevertheless, concerns remain on the oxidative stability of the peroxide containing blends.

We have previously demonstrated that the addition of a double bonds-rich additive can enhance the cross-linking efficiency of irradiated UHMWPE [3]. In this study, we investigate the effect of an unsaturated, double bonds-rich additive on the peroxide cross-linking of UHMWPE. We choose a modified paraffin wax (MPW), with a high concentration of terminal double bonds, as a model additive.

Methods and materials:

Concentrations from 0.5 to 2% weight of 2,5-dimethyl-2,5-di(t-butylperoxy)hexane (POX: Luperox[®] 101, Sigma Aldrich, St. Louis, MO) were blended with GUR 1020 powder (Celanese, Germany) and immediately consolidated into discs (8 cm diameter, 1 cm height). A second set of samples was prepared by blending the GUR 1020 powder with 0.5% weight of POX and 0.5% or 2% weight of a modified paraffin wax (MPW).

The resulting samples were analyzed by FTIR (Perkin-Elmer, Waltham, MA), prior and after extraction with boiling cyclohexane for 8h, to monitor changes in the polymer structure. Oxidation index (OI) and trans-vinylene index (TVI) were determined according to ASTM F2102 and F2381, respectively. The cross-link density was determined gravimetrically, according to ASTM D2765. Crystallinity was assessed by DSC (Pyris 6, Perkin Elmer, Waltham, MA), using a heat of fusion of 293 J/g (n=3).

ASTM 638 type V specimens were punched from 0.2 mm thick sheets, sectioned from the discs (n=3) and subjected to tensile testing using an Adamel Lhomargy DY22 machine, with a crosshead speed of 10 mm/min.

After the analyses, the sample were stored in the dark, at room temperature.

Results:

FTIR examination of the peroxide containing samples evidenced no significant differences from the spectrum of pure UHMWPE, except for traces of an additional absorption at 965 cm⁻¹ (trans-vinylene) and at 1718 cm⁻¹ (ketones). The maximum oxidation index (OI=0.07±0.01) was measured in the 0.2%w POX sample.

The FTIR spectrum of the pure MPW showed strong absorption bands in the low wavenumber area, at 886

(vinylidene), 909 and 990 (vinyl) and 965 cm⁻¹ (trans-vinylene). The spectrum of the 2% MPW/0.5% POX sample showed significant absorption at the same wavenumbers, most of which were removed after cyclohexane extraction. None of these absorption bands, except for a weak trace at 886 cm⁻¹, was observed in the spectrum of the 0.5%MPW/0.5%POX.

The cross-link density of the POX containing samples increased with the POX content (Table 1). The cross-link density of the 0.5%MPW/0.5%POX sample was in between that of 0.5% and 1% POX, while that of 2% MPW/0.5% POX was below the applicability of the method.

The 2% MPW/0.5% POX sample showed the highest crystallinity, followed by 0.5% MPW/0.5% POX. The crystallinities of the POX containing samples were slightly decreasing with increasing the POX content.

The elongation at break (EB) and ultimate tensile strength (UTS) decreased with increasing the POX content and XLD. The 2% MPW/0.5% POX blend showed the highest EB and the lowest UTS.

	XLD, mol/dm ³	EB, %	UTS, MPa	Cryst, %
0.5%w POX	0.185 ± 0.005	245 ± 17	40.4 ± 3.0	46.0 ± 0.9
1%w POX	0.370 ± 0.004	204 ± 7	36.5 ± 1.8	43.2 ± 0.5
2%w POX	0.429 ± 0.007	141 ± 10	26.8 ± 1.7	42.6 ± 1.5
0.5%w POX + 0.5%w MPW	0.242 ± 0.006	202 ± 18	42.8 ± 3.5	47.1 ± 0.8
0.5%w POX + 2%w MPW	< 0.080	283 ± 7	26.5 ± 1.0	48.5 ± 1.1

Table 1: Cross-link density, tensile properties and DSC crystallinity of the POX and MPW/POX blends.

The FTIR and XLD measurements were repeated on the same samples, after 38 months of ageing. Again, the maximum OI (0.08 ± 0.02) was recorded on the 2%w POX blend. No significant differences were observed in the XLD of all blends.

Discussion:

The cross-link density of the POX containing samples increased with the POX content, indicating that the addition of POX during consolidation creates cross-links, as expected. The blends with a POX content ≥ 1%w showed higher XLD compared to a 100 kGy irradiated GUR 1020 (approx. 240 mol/dm³). Nevertheless, the TVI calculated from the FTIR spectra of the POX blends was very low (~0.01), suggesting differences in the chemical mechanism of cross-linking compared to that occurring during irradiation. OI of all blends were negligibly low. The crystallinity, UTS and EB decrease is in agreement with the XLD increase.

The MPW used in this study was chosen because it contains a large amount of vinylidene (FTIR absorption at

886 cm^{-1}), vinyl (909 and 990 cm^{-1}) and trans-vinylene (965 cm^{-1}) double bonds. The absence of these absorption in the spectra of the 0.5%MPW/0.5%POX, indicates that all the unsaturations have reacted during consolidation of the blend in the presence of POX. Accordingly, the 0.5%MPW/0.5%POX blend showed a higher XLD compared to that of the 0.5% POX sample, confirming that the reacted MPW has provided some additional cross-links. On the contrary, a significant amount of unreacted unsaturations was observed in the 2%MPW/0.5%POX sample. Their easy removal by cyclohexane extraction, indicates that a large fraction of the MPW was still present in the blend in a “free”, unbounded form. In addition, the XLD was no measurable in this sample, indicating that a MPW excess is detrimental to cross-linking.

The tensile properties of the two MPW/POX blends reflects the XLD trend: UTS and EB of the 0.5%MPW/0.5%POX blend are in the range expected for a highly cross-linked polyethylene, while a higher EB and a very low UTS for the 2%MPW/0.5%POX suggest that the free MPW might have acted as a plasticizer.

The results of the analyses after a quite long (38 months) real time ageing indicates that all the blends are reasonably stable and that no oxidation, neither chain scission have occurred during ageing. This is in contrast with what normally happens in unstabilized, radiation-cross-linked UHMWPE. Nevertheless, it must be kept in mind that most of the oxidative degradation developed in radiation cross-linked UHMWPE over time it is due to the free radicals that remain trapped in the crystalline and intermediate phase after irradiation and slowly migrate to the amorphous phase, where they react with oxygen [4]. On the contrary, peroxide cross-linking takes place during consolidation at high temperature, when the polymer is in the molten, fully amorphous state.

In summary, we have demonstrated how peroxide cross-linking of UHMWPE with or without the presence of an unsaturated additive can be used to obtain highly cross-linked UHMWPE, whose XLD and properties can be tuned by adjusting the amount of POX and by choosing the appropriate MPW/POX ratio.

References: [1] Gul, RM et al(2014) IOP Conf Series: Mat Sci Eng, 60 (1),012015 [2] Gul, RM (2008) J Mat Sci: Mat Med, 19 (6), 2427 [3] Bracco, P et al (2005) Polymer, 46 (24), 10648 [4] Carpentieri, I et al (2011) Polym Deg Stab, 96 (4), 624.



SESSION
THREE:

Antioxidants in
UHMWPE

Improved Crack Initiation Resistance from a Blunt Notch in a Hindered Phenol Antioxidant UHMWPE

Parran, K¹, Narayan V², Rinnac, C¹

¹Case Western Reserve University, Cleveland, OH; ²DePuy Synthes, Warsaw, IN
clare.rinnac@case.edu

Introduction: Fracture resistance is an important property of cross-linked ultra-high molecular weight polyethylene (UHMWPE) materials for use in total joint replacements. For example, *in vivo* crack initiation and fracture of crosslinked UHMWPE acetabular components has occurred, whereby the cracks have originated at notches in the components [1,2]. We found that crack initiation time and crack velocity in two generic crosslinked UHMWPE formulations (remelted 65 kGy and remelted 100 kGy) depended on the applied static load in a manner well-predicted from viscoelastic fracture theory [3]. In addition, the mechanism of crack initiation was found to be one that can occur as a single-layer or multi-layer process of coalescing decohesion sites and this process affects the time to crack initiation.

In this study we asked: 1) is there a difference in time to crack initiation and failure from a blunt notch between a first generation (XLKTM) and a second generation hindered phenol antioxidant (AOXTM) highly crosslinked UHMWPE; 2) does aging affect the time to crack in initiation and failure in a hindered phenol antioxidant UHMWPE; and, 3) what is the mechanism of crack initiation?

Methods and Materials: Crosslinked UHMWPE (XLKTM) (as a control material) and hindered phenol antioxidant UHMWPE (AOXTM) were received as ram extruded rods (DePuy Synthes, Warsaw, IN). Round compact tension specimens were machined according to ASTM 1820-01 with: notch depth, a=17mm; specimen length, w=40mm; thickness, b=20mm; and side groove depth of 2 mm on each side. A blunt notch root radius of 0.25mm was implemented to mimic the geometry of a UHMWPE joint replacement component design feature. Following machining, one half of the AOX specimens were aged for 40 days using a standard protocol based on ASTM F2003 of 5 atm. oxygen at 70°C.

For each of the three test groups (XLK, AOX, Aged AOX), specimens were loaded on an Instron servo-hydraulic test frame at three constant loads between 1000 N and 1400 N (n_≥3 specimens per load) until failure. A video microscope was focused on the face of the notch to visually obtain the crack initiation time (Ti video, Fig. 1). Crack initiation was defined as the time when multiple initiation decohesion sites coalesced across the thickness at the surface of the notch root. Crack initiation was also defined as the change in displacement of 0.5mm (i.e., 0.5mm of ligament reduction of the unfractured material ahead of the notch) collected from a travelling microscope (Ti disp, Fig. 1). The initiation and failure times as a function of load were determined using semi-log and log-log linear relationships to allow for comparison of linear regressions between material groups and between Ti video and Ti disp measurements.

The mechanism of crack initiation was qualitatively observed by way of the video microscope recording. The initiation region of the fracture surface was also examined via scanning electron microscopy from selected specimens from each test group.

Results: For all test groups, the time to initiation (Fig. 2) and the time to failure (Fig. 3) decreased with increased applied load. The time to crack initiation and to failure qualitatively appears to be longer in AOX versus XLK, though the regression lines were only significantly different (p > 0.05) between XLK and Aged AOX. The use of a definition of crack initiation as 0.5mm of displacement (Ti disp) appears to be a reasonable estimate of the time to crack initiation as compared with the video recording (Ti video). The mechanism of crack initiation was nucleation and coalescence of multiple decohesion sites in all three groups (Figs. 4,5).

Discussion: Understanding and ranking the relative fracture resistance from clinically relevant notch geometries of highly crosslinked UHMWPE materials can be useful in the design of joint replacement components. By necessity, these components will contain blunt notch features which can serve as stress risers. In this study, we demonstrate a potentially useful approach to evaluating fracture initiation resistance between UHMWPE formulations.

Limitations of this study include the lack of a physiologically-relevant environment in that the tests were conducted in ambient laboratory conditions.

The findings suggest that AOX is more resistant to crack initiation than XLK under a constant load. This is consistent with other studies that demonstrate somewhat better (fatigue) crack propagation resistance of AOX versus XLK [4]. AOX, because of its higher crystallinity due to avoidance of remelting, has previously been shown to have higher strength than XLK [5]. In addition, aging under a relatively severe aging protocol did not appear to reduce the time to crack initiation of AOX, supporting the effectiveness of the hindered phenol antioxidant against oxidative degradation and loss of mechanical and physical properties [6]. As with our observations of other crosslinked UHMWPE formulations [3], we found that crack initiation was a process of coalescence of decohesion sites and that the sites can be distributed on several planes. Multi-layer crack initiation may be due to consumed energy during deformation near the crack tip being distributed across multiple crack initiation layers on the notch surface, or neighboring nuclei shielding one another and relaxing the local stress severity. It may also be due to or promoted by machining defects or residual stresses on the surface of the notch.

The findings of this study may be more relevant and useful in the design of UHMWPE joint replacement components than the Paris fatigue crack propagation relationship. As we have previously suggested [3], such time-to-crack initiation data may be utilized in finite element analysis predictions of crack initiation from local stress concentrations in UHMWPE joint replacement components. Additionally, a ligament reduction criteria, such as the one proposed in this study (0.5mm) appears to be sufficient to reasonably estimate the time to initiation. If so, this may provide a relatively straightforward method by which to assess and compare crack initiation time between materials and notch root geometries (i.e., notch severity). In addition, the effect of notch manufacturing method (e.g., machined versus molded) could be explored with this approach.

Acknowledgements: This work was supported by a research agreement with DePuy Synthes. The Wilbert J. Austin Chair (CMR) is also gratefully acknowledged.

References: [1] Furmanski J, et al, Biomat, 2009; [2] Furmanski J, et al, JOA, 2011; [3] Sirimamilla P, et al., JMBBM, 2013; [4] Parran K et al, Trans ORS, 945:2015; [5] King R, et al, Trans Combined ORS, 2010; [6] Narayan V, et al, Trans ORS, 1058:2013.

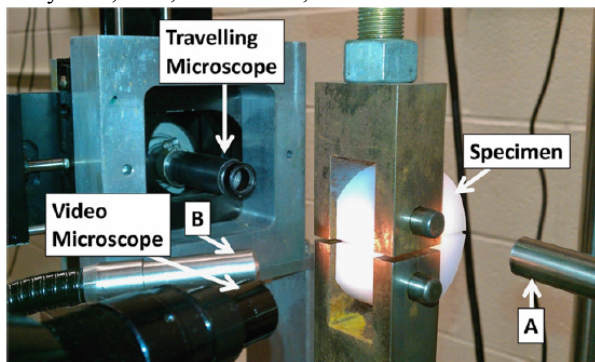


Figure 1. Test set-up showing video microscope trained on the blunt notch and travelling microscope trained on the side-view of the specimen [3].

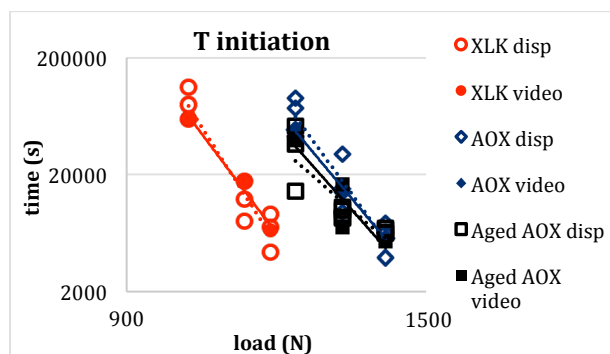


Figure 2. Plot of (log) Time to initiation (video, disp) versus (log) applied load for the three test groups.

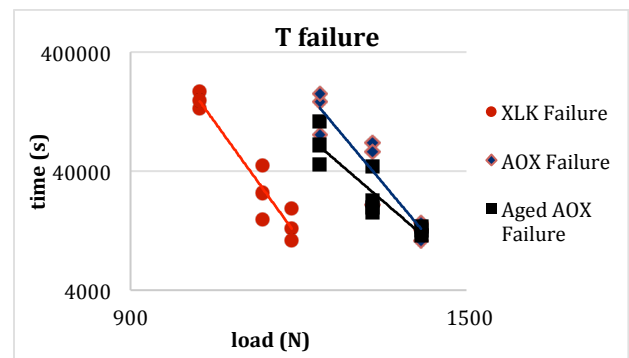


Figure 3. Plot of (log) Time to failure, determined from ligament reduction as measured from the travelling microscope, versus (log) applied load for the test groups.



Figure 4. Left: schema showing viewing orientation to observe the notch root. Right: Video image of an XLK specimen tested at 1400 N showing void coalescence along the plane of fracture initiation.

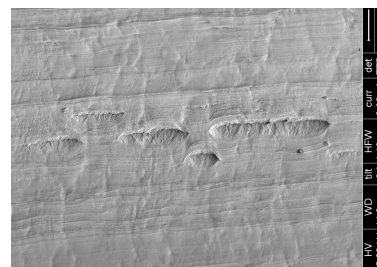


Figure 5. Scanning electron micrograph of an AOX specimen tested at 1400 N showing multiple decohesion sites in the notch root (not on the initiation plane).

Non-Cemented Monoblock Hip Cup Made from vitamys[®], Vitamin E Stabilised Highly Cross-linked UHMWPE: Overview of the Clinical Data Available per 2015

Halma JJ¹, de Gast A¹, Lurf R², Delfosse D²

¹Diakonissenhuis Hospital, Utrecht, The Netherlands; ²Mathys Ltd Bettlach, Bettlach, Switzerland
reto.lurf@mathysmedical.com

Introduction: The RM Pressfit vitamys[®] (cf. Figure 1) is a uncemented monoblock acetabular component by Mathys. Its concept, Ti particle coated all-poly cup, has a long history of success. The 1st generation of this cup RM Classic, was introduced in 1985. Its Kaplan-Meier survival rate is reported at 94.4 % after 19.8 years (Ihle 2008). The RM Pressfit vitamys[®] is the 3rd generation of RM cups. 1st implantation was in September 2009. At the same time, post market clinical follow-up studies (PMCF) started. 11 clinics in Switzerland, Netherlands, United Kingdom, Austria, Germany, and New Zealand take part in this on-going, multi-centre study. Until now, more than 40'000 RM Pressfit vitamys[®] were sold worldwide (except US).



Figure 1: The RM Pressfit vitamys[®] by Mathys. The monoblock is made from vitamin E stabilised, highly cross-linked PE (vitamys[®]).

Methods and Materials: Two of the centres mentioned above include the measurement of head penetration in the study. In the Netherlands, 112 patients (117 hips) were prospectively enrolled between September 2009 and May 2011. 95.5 % of the patients could be followed up for 2 years. Visual analogue scale (VAS) score and Harris Hip Score (HHS) were obtained pre-operatively and followed up after 3, 12 and 24 months. At these points in time, radiographs were taken for the assessment of cup position, radiolucency and head penetration (Halma 2015).

In France, there is a prospective RSA study running which follows up 28 patients with RM Pressfit vitamys[®] and 27 bearers of conventional RM Pressfit, all with articulation Ø 28 mm and CoCr heads. RSA X-rays were taken postoperatively and at 6, 12, 24 and 36 months after surgery (Vielpeau 2014).

Data from the Mathys Post Market Surveillance system for the RM Pressfit vitamys[®] as per March 2015 were

analysed. Finally, the RM Pressfit vitamys[®] registry data from Switzerland (Siris) per end of 2014 were evaluated and discussed. Until now, Siris is the only registry presenting RM Pressfit vitamys[®] as a separate implant family and not combined with the conventional RM Pressfit.

Results: The mean VAS score for patient satisfaction increased from a mean of 3.09 at baseline to 8.64 at 3 months follow-up and ended with 8.82 at 24 months. The values for the mean HHS were 61.1 before surgery, increased to 91.4, 93.8 and 94.2 at 3, 12 and 24 months of follow-up, respectively. Two cups had to be revised due to infection. Of the total of 108 hips (103 patients) with complete radiographic follow-up, the mean two-dimensional linear femoral head penetration rate was 0.055 mm/year (95% CI 0.050–0.057; SD 0.017). The mean total femoral head penetration was 0.073 mm in the first year of follow-up and decreased to 0.035 mm in the second year of follow-up. Figure 2 illustrates this non-linearity (Halma 2015).

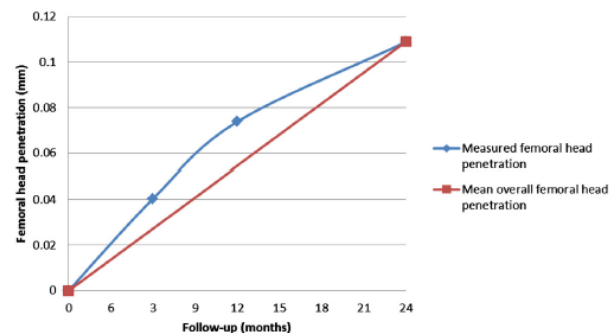


Figure 2: Two-dimensional linear femoral head penetration rate of RM Pressfit vitamys[®] made from vitamin E blended HXLPE at 2 year follow-up (Halma 2015).

In the 1st half year of the RSA study, head penetration was similar for both cups, with a mean of 0.13 mm for RM Pressfit vitamys[®] and of 0.15 mm for the conventional RM Pressfit. After one year, head penetration into the vitamys[®] cup is markedly reduced compared to the standard cup. After 3 years of follow-up, the heads seated 0.20 mm into vitamys[®] and 0.32 mm into conventional UHMWPE (mean values). Table 1 gives an overview of all the RSA results. Prof Vielpeau argues that during the 1st year head penetration is mainly due to creep. He calculates a steady-state wear rate as the difference between one and 3 years after implantation, i.e. 0.02 mm/y for the vitamys[®] implant and 0.06 mm/y for standard UHMWPE. Hence, head penetration is 67 % less in favour of RM Pressfit vitamys[®].

Follow-up [months]	Hips assessed vitamys®	Head penetration vitamys® [mm]	Hips assessed UHMWPE	Head penetration UHMWPE [mm]
6	26	0.13 ± 0.03	26	0.15 ± 0.04
12	21	0.16 ± 0.03	25	0.20 ± 0.05
24	26	0.18 ± 0.03	23	0.26 ± 0.06
36	17	0.20 ± 0.03	18	0.32 ± 0.08

Table 1: Head penetration measured by RSA of the prospective study comparing RM Pressfit vitamys® and conventional RM Pressfit.

The Mathys Post Market report by March 2015 is based on 36'889 RM Pressfit vitamys® cups sold since September 2009 until February 2015. The total number of revisions reported is 12. This yields an overall revision rate of 0.03 % an estimated revision rate per 100 component years (CY) of 0.025. From these 12 revisions, one was attributed to aseptic loosening and two to tilting of the cup. All other revisions were due to reasons not related to the implant, such as luxation, infection, acetabulum penetration and trauma. In one case the reason for revision was not reported.

By end of 2014, the Swiss Siris Registry collected a total of 37833 hip implants, of which 3025 were RM Pressfit vitamys®. The number of all revisions performed on hips including a RM Pressfit vitamys® cup was 49, giving a revision rate of 1.62 % or 1.489 revisions/100 CY. The most frequent reasons for revision were periprosthetic fracture, luxation, femoral loosening and early infection. The average revision rate per 100 CY of all 37833 implants was 1.785. From these 49 revisions in 16 cases the cup was revised, only. This yields 0.53 % revision rate and 0.486 revisions/100 CY with end point cup replacement. Table 2 provides an overview of the revision data provided by Siris.

Component	Primaries	Revisions	CY	Revisions/100 CY
All revisions				
vitamys®	3025	49	3291	1.489
Total	37833	846	47384	1.785
Revisions acetabular component				
vitamys®	3025	16	3291	0.486
Total	37833	276	47384	0.582

Table 2: Siris data of RM Pressfit vitamys® acetabular component and comparison with all hip implants registered.

Discussion: Both measurements of head penetration show an embedding phase during the 1st year after implantation and reduced penetration after the initial 12 months. The

penetration assessment by analysis of radiographs results in a head penetration of 0.035 mm in the 2nd year, where steady state is assumed. This value is well in the range of 2-D linear head penetration of first generation HXLPE found in literature (Kurtz 2011). The RSA study yields a penetration rate of 0.02 mm/y for the vitamys® cup. Again, this value corresponds to RSA penetration rates published for first generation HXLPE (Bragdon 2006, Glyn-Jones 2008). Most likely the gap in head penetration found between the two present studies is due to the differing method of assessment. However, both penetration rates are low and promising for a future with low rates of aseptic loosening.

Post market surveillance data show a very small number of early revisions and these cases are due to divers reasons. The two cases of tilting of the cup could have been avoided by using additional screw fixation of the RM Pressfit vitamys®.

The only registry data available for RM Pressfit vitamys® attest rates of revision per 100 component years lower than the average of all hip implants surveyed.

As a conclusion, the first years of clinical surveillance show a save implant, save meaning reproducible OP technique and initial low wear. The stabilisation of the UHMWPE by vitamin E promises a wear and oxidation resistant acetabular implant for a long-term future.

References:

- Bragdon CR et al., Clin Orthop Relat Res 2011;448: 52-57
- Glyn-Jones S et al., J Bone Joint Surg (Br) 2008;90-B: 556-61
- Halma JJ et al, J Arthroplasty 2015;30: 615-21
- Ihle M et al., J Bone Joint Surg (Br) 2008;90-B: 1284-90
- Kurtz SM et al., Clin Orthop Relat Res 2011;469: 2262-77
- Vielpeau C, EFORT Congress, London 2014

Measurement of anti-oxidant in retrievals

Currier, BH,¹ Currier, JH,¹ Levine RAC,¹ Van Citters, DW¹

¹Dartmouth College, Hanover, NH USA
barbara.h.currier@dartmouth.edu

Introduction: Assessing anti-oxidant (AO) concentration in retrieved polyethylene inserts is important to determine how much of the anti-oxidant remains in place and active. Absorbed species from the in vivo environment have been shown to artificially raise the ASTM OI. Extraction of retrievals is necessary for the ASTM OI to correctly report actual polyethylene oxidation. Absorbed species also impact the low wave numbers of the FTIR spectra, where the anti-oxidant peaks are found, by increasing peaks or elevating the baseline. The hypotheses explored in this study are: 1. Due to absorbed species near the articular and nonarticular surfaces (a) retrieved non-Vitamin E tibial inserts will exhibit artificially higher anti-oxidant concentration; and (b) Vitamin E tibial inserts will exhibit artificially lower anti-oxidant concentration. 2. Anti-oxidant index will correlate with ASTM OI, allowing actual anti-oxidant to be estimated.

Methods and Materials: An IRB-approved retrieval laboratory received 20 AO polyethylene tibial insert retrievals from three manufacturers with in vivo time of 0-3 years. The retrievals were sectioned with a microtome through the medial condyle in the A-P plane. These vertical cross-sections were analyzed for oxidation and anti-oxidant index using a Thermo Scientific iN-10 FTIR microscope.

Oxidation was reported as ASTM OI in the scan from the articular surface to the backside of the bearing. Anti-oxidants were characterized as Vitamin E Index (VEI, wave numbers 1245-1275 cm^{-1}) or antioxidant index (AOI, wave numbers 1125-1150 cm^{-1}), depending on the anti-oxidant used. Each anti-oxidant peak was normalized to a thickness proxy.

Results: AO polyethylene retrievals exhibited minimal oxidation, except near the articular surfaces where absorption of in vivo fluids is expected (Figure 1). No AO polyethylene insert was retrieved for oxidation-related cracking or delamination. The AOI near the articular and nonarticular surfaces was elevated in the case of non-Vitamin E antioxidant and VEI was lowered in the case of Vitamin E antioxidant (Figure 2). The lower Vitamin E index was seen in both infused and grafted Vitamin E polyethylene. Antioxidant concentration was found to correlate with ASTM OI, positively for non-Vitamin E materials (Figure 3a) and negatively for Vitamin E materials (Figure 3b). Hexane extraction of non-Vitamin E materials retrievals removed measurable oxidation and resulted in articular and nonarticular anti-oxidant concentrations consistent with the average concentration found in the bulk of the insert (Figure 2a). In Vitamin E infused polyethylene, extraction removed both the absorbed species and the Vitamin E (Figure 2b).

Discussion: AO polyethylene was developed to address the problem of free radicals in polyethylene resulting

from irradiation used in cross-linking or sterilization. Each manufacturer uses a different antioxidant or method of incorporating the antioxidant. However, all of the antioxidant materials appear to be effective at minimizing oxidation over the in vivo period of this study. Retrieved tibial inserts show elevated ASTM OI near the articular and nonarticular surfaces, shown to be absorbed species by the extraction of the non-Vitamin E antioxidant polyethylene. Extraction allowed measurement of actual antioxidant concentration, rather than the artificially higher concentration measured in as retrieved inserts. However, in the case of Vitamin E infused polyethylene, extraction removes both the absorbed species and the Vitamin E. Correlation of VEI with unextracted ASTM OI allows the actual Vitamin E index to be estimated without the use of extraction.

Figure 1: Maximum ASTM OI by material before extraction.

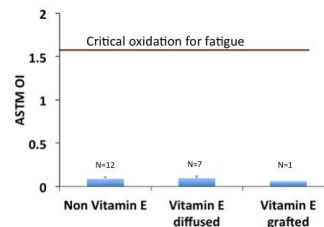


Figure 2: (a) AOI versus depth through the retrieved insert, as-retrieved and after hexane extraction. (b) VEI versus depth through the retrieved insert, as-retrieved and after hexane extraction.

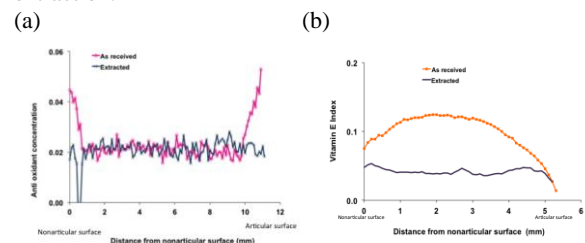
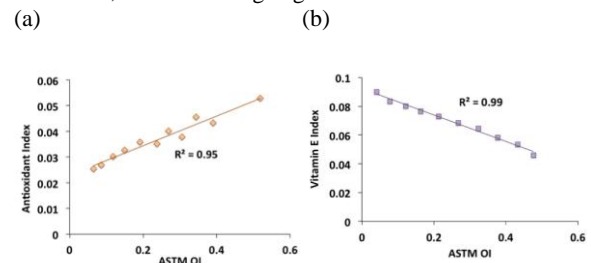


Figure 3: (a) AOI versus ASTM OI, before extraction, shows a strong linear correlation. (b) VEI versus ASTM OI, before extraction, shows a strong negative linear correlation.



Highly Cross-linked Retrievals With and Without Vitamin E Stabilization

Rowell, SL¹; Reyes, CR¹; Chan D¹; Estok, D²; Malchau, H¹; Muratoglu, OK¹

¹Harris Orthopaedics Laboratory, Massachusetts General Hospital, Boston, MA

²Dept of Orthopaedics, Brigham and Women's Hospital, Boston, MA

slrowell@mgh.harvard.edu

Introduction: Radiation cross-linking, used to improve wear resistance of ultra-high molecular weight polyethylene (UHMWPE) bearings in total joint arthroplasty, generates residual free radicals which are the precursors to oxidative embrittlement. First generation materials adopted thermal treatments such as post-irradiation remelting to eliminate radiation crosslinking-induced free radical content, but these came with compromises in reduced mechanical properties¹. In their second decade of use, new concerns have also arisen over unexpected *in vivo* oxidation influenced by lipid absorption and cyclic loading in irradiated and melted materials with no initial free radicals²⁻⁴. High levels of oxidation have historically been associated with loss of mechanical properties and wear resistance, but clinical outcomes have not yet validating these concerns nor shown an impact on clinical performance⁵⁻⁷. On-going studies, both retrieval and clinical, continue to monitor performance.

Many second generation highly cross-linked materials address first generation concerns through the use of antioxidant-stabilization, including irradiated and vitamin E-diffused UHMWPE which was clinically introduced 8 years ago in hips and 7 years ago in knees. *In vitro* studies predict excellent oxidation and wear resistance in vitamin E-stabilized bearings⁸, but the long-term *in vivo* oxidation behavior remains largely unknown.

In this update to our ongoing investigation, we report on *in vivo* material property changes seen in both first generation irradiated and melted UHMWPE and second generation vitamin E-stabilized UHMWPE surgically-retrieved implants.

Methods and Materials: 145 highly cross-linked hip and knee retrievals were collected with IRB approval (Table 1). All components were disinfected in ethanol upon receipt; subsequently the components were stored under vacuum in a -20°C environment to minimize ex vivo oxidation. Sections were removed from the rim or non-

loaded eminence and the articular surface of each explanted component. Thin films (150 µm; n=3 from each component) were analyzed using Fourier Transform Infrared Spectroscopy (FTIR) as a function of depth from the surface across the thickness of the component. FTIR analyses took place both before and after films were refluxed in boiling hexane for 16 hours to extract absorbed esterified fatty acids, then dried for 24 hours under vacuum. Additional thin sections were also extracted with hexane and reacted with nitric oxide to measure the hydroperoxide content using FTIR [8]. Carbonyl index values both before and after hexane extraction were calculated by normalizing the carbonyl absorbance area over 1680 cm⁻¹ - 1780 cm⁻¹ to the absorbance area over 1330 cm⁻¹ - 1390 cm⁻¹, per ASTM F2102-01⁶¹. Oxidation potential, or hydroperoxide index, was calculated by normalizing the nitrate peak height at 1630 cm⁻¹ to the absorbance peak height from the polymer backbone at 1895 cm⁻¹. Cross-link density was calculated as per ASTM F2214 through gravimetric swelling analysis using xylene at 130°C for 2 hours on samples from each region of the liners. Crystallinity measurements were performed using differential scanning calorimetry (DSC) by integrating the enthalpy between 20 and 160°C and normalizing that with the heat of fusion of 100% crystalline polyethylene (291 J/g). Material property data was compared using a Mann-Whitney U-test to determine statistical differences between the material types. Wilcoxon Signed Ranks Test was used to compare material properties between loading regions.

Results: Irradiated and Melted UHMWPE Retrievals

First generation irradiated and melted UHMWPE retrievals in both hips and knees all showed detectable (OI>0.1) low level oxidation in the form of sub-surface peaks (Figure 1-2). All material types, in both hips and knees, showed significantly higher oxidation levels in the loaded articular surface than in the unloaded rim or eminence (p<0.001). Tibial inserts were observed to have

Table 1. 1st and 2nd generation highly cross-linked UHMWPEs

Material	Resin Type	Irradiation + Free radical stabilization Method	Sterilization	Sample Size	Time In Vivo (years)			
					Mean	Median	Range	
Marathon™ Acetabular Liners	GUR 1050	50kGy gamma-irradiation at room temperature, followed by remelting	Gas plasma	33	4.3 ± 3.0	3.7	0.1 - 10.2	
AltrX™ Acetabular Liners	GUR 1020	75kGy gamma-irradiation at room temperature, followed by remelting	Gas plasma	5	3.4 ± 2.0	2.7	1.4 - 6.1	
Longevity™ Acetabular Liners	GUR 1050	100kGy e-beam irradiation at 40°C, followed by remelting	Gas plasma	14	4.3 ± 3.9	3.9	0.1 - 13.0	
Durasul™ Tibial Inserts	GUR 1050	95kGy e-beam irradiation at 125°C, followed by remelting	EtO	55	8.8 ± 1.9	9.1	5.8 - 10.5	
Prolong™ Tibial Inserts	GUR 1050	65kGy e-beam irradiation at 125°C, followed by remelting	Gas plasma	5	3.1 ± 2.3	3.5	0.1 - 7.1	
X-LK™ Tibial Inserts	GUR 1020	50kGy gamma-irradiation at room temperature, followed by remelting	Gas plasma	12	5.6 ± 1.9	5.6	3.3 - 9.0	
E1™ Acetabular and Tibial Inserts	THA: GUR 1050	100kGy gamma-irradiation, followed by vitamin E diffusion and homogenization	25-30kGy gamma	THA	17	0.7 ± 0.7	0.6	0.1 - 2.2
	TKA: GUR 1020			TKA	4	1.9 ± 1.2	2.0	0.5 - 3.1

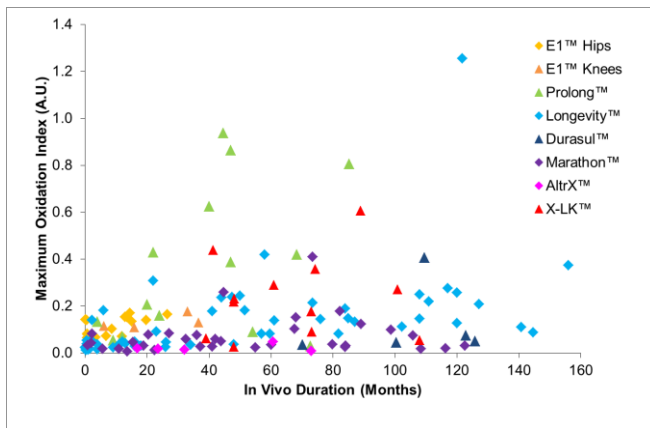


Figure 1. Box plot showing overall maximum oxidation indices per retrieved component for each retrieved (a) THA and (b) TKA material type.

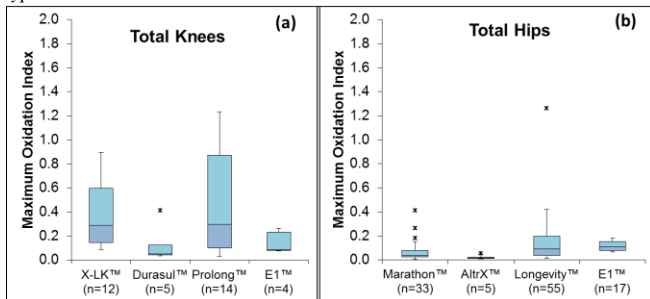


Figure 2. Box plot showing overall maximum oxidation indices for retrieved (a) TKA and (b) THA implants.

a greater variability and higher oxidation at earlier *in vivo* durations than their acetabular counterparts (Figure 2), with one Prolong insert displaying observable white banding (OI=0.86). Additionally, a ten year Longevity acetabular liner, revised for subsidence and femoral impingement, had an oxidation peak that exceeded an OI of 1.0 (OI=1.26) located below the articular surface (Figure 3). This liner showed a 46% decrease in cross-link density at the articular surface (0.183 ± 0.006) compared to the bulk, backside and rim (0.341 ± 0.005). Similarly crystallinity had a measurable increase at the articular surface, measuring 61% crystallinity, compared to the bulk, backside and rim values at 55% crystallinity.

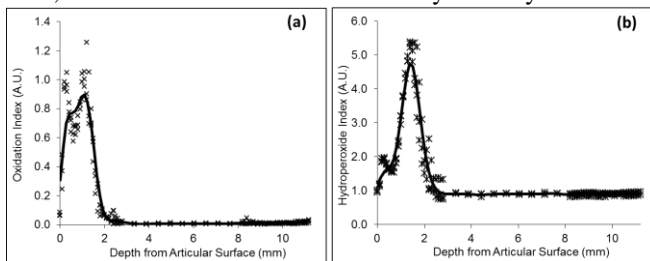


Figure 3. Oxidation and hydroperoxide profiles across the articular surface to backside of a ten year retrieved Longevity acetabular liner.

With the exception of the one retrieval described above, no change was observed in the cross-link density or crystallinity at these regions of oxidative activity in first generation irradiated and melted materials. However, hydroperoxide levels in the same subsurface regions

where oxidation was detected were elevated with up to a 130% increase from bulk levels.

Vitamin E-Stabilized UHMWPE Retrievals

Twenty-one irradiated and vitamin E diffused retrievals showed no substantial oxidation at the time of surgical removal, with oxidation indices remaining below 0.2 with maximum values located at the surface rather than subsurface. There was no increase in hydroperoxide index and no change to cross-link density or crystallinity.

Discussion: *In vivo* oxidation was observed in all six types of irradiated and melted polyethylenes. Maximum oxidation values remained below an OI of 1.0, except in the case of a twelve year Longevity acetabular liner. Historically, conventional UHMWPE studies concluded that an ASTM OI of less than 1.0 reflected early oxidative changes but were unable to correlate these levels to loss of mechanical properties⁹⁻¹⁰. The same studies showed that OI greater than 3.0 demonstrated a loss of mechanical integrity. By these standards, very few of these irradiated and melted retrievals have reached a critical level of oxidation, (although one has exceeded an OI of 1.0), and none reported in this study have been revised due to an oxidation-related failure of the material. It should also be noted that the critical level of oxidation leading to long-term clinical failures may differ in this generation of highly cross-linked polyethylenes. However increased subsurface hydroperoxide peaks, even with low oxidation levels, suggest an on-going oxidative chain reaction. With one example of high oxidation after ten years *in vivo*, it has been demonstrated that this type of oxidation can also progress to a loss of material properties. This is particularly important to monitor in tibial inserts, which are showing higher oxidation at earlier time points, due to their greater clinical susceptibility to oxidation-derived delamination and fracture.

In contrast, while vitamin E-stabilized retrievals showed low but detectable OI values after 0 to 3 years *in vivo*, there were no observed subsurface oxidation peaks or increases in hydroperoxides. These early results suggest that the scavenging activity of the vitamin E is preventing radiation-induced free radicals from initiating oxidation.

Limitations of this study include small samples sizes for the majority of materials as well as high variability in average *in vivo* duration, limiting our ability to perform direct comparisons of material properties between material types. Continued monitoring should reduce these limitations and provide greater insight into the clinical significance of *in vivo* oxidation observed in first generation UHMWPE and the long-term performance of vitamin E-stabilized UHMWPEs.

Acknowledgements: Partially funded by Biomet Inc. and DePuy Inc.

Reference: [1] Muratoglu. JOA, 2001; 16(2):149-160. [2] Muratoglu. JBJS Am 2010;92(17):2809-16 [3]Currier. JBJS:Am 92A: 2409-2418, 2010[4]Currier. JBMR:B, 101(3):441-8, 2013. [5]Engh. JOA, 27(8 Suppl): 2-7 e1. [6]MaCalden JBJS:Am 91(4): 773-82, 2009. [7] Jacobs. JBJS:Am 89-A(12): 2779-2786, 2007. [8] [9] Currier. JOA 22(5): 721-31, 2007. [10]Kurtz. JOA. 18(7 Supp. 1): 68-78, 2003.



SESSION
FOUR:

HXLPEs in the
Knee

Biotribology of vitamin E stabilised polyethylene materials for total knee arthroplasty evaluated under highly demanding patient daily activities in vitro

T.M. Grupp^{1,2}, B. Fritz¹, I. Kutzner³, Georg Bergmann³, J. Schwiesau¹

¹*Aesculap AG, Research & Development Tuttlingen, Germany,*

²*Ludwig Maximilian University, Clinic for Orthopaedic Surgery, Campus Grosshadern Munich, Germany*

³*Julius Wolff Institut, Charité Universitätsmedizin Berlin, Germany*
thomas.grupp@aesculap.de

Introduction: Highly cross-linked polyethylene (XLPE) inserts have shown significant improvements in decreasing wear and osteolysis in total hip arthroplasty [1]. In contrast to that, XLPE has not shown to reduce wear or aseptic loosening in total knee arthroplasty [2,3,4]. The analysis of the wear behaviour of XLPE materials for knee arthroplasty today is difficult, due to the fact that current ISO 14243 series wear testing is not able to produce demanding wear conditions as required in patients service under in vivo loading conditions.

One major limitation is that current wear testing in vitro is mainly focused on abrasive-adhesive wear due to level walking test conditions and does not reflect “delamination” as an essential clinical failure mode [5,6].

The objective of the current study was to use a highly demanding daily activities wear simulation to evaluate the delamination risk of polyethylene materials with and without vitamin E stabilisation.

Methods and Materials: A cruciate retaining fixed bearing TKA design (Columbus® CR) with artificially aged polyethylene knee bearings (irradiation 30 & 50 kGy) blended with and without 0.1% vitamin E was used under medio-lateral load distribution and soft tissue restrain simulation. The polyethylene gliding surfaces were packed under nitrogen atmosphere and sterilised by γ -irradiation (30 ± 2 kGy). All tibial inserts were used after artificial ageing according to ASTM F2003-02 (parameters: 70 °C, pure oxygen at 5 bar, duration 14 days) and soaked prior to wear simulation in serum-based test medium for 30 days to allow for saturated fluid absorption. Oxidation index measurements were performed by Fourier transform infrared spectroscopy (FTIR) and the oxidation index was calculated in accordance with ISO 5834-4:2005 from the area ratio of the carbonyl peak (between 1650 and 1850 cm^{-1}) to the reference peak for polyethylene (1370 cm^{-1}). Daily patient activities measured by Bergmann et al. [7] in vivo, were applied for 5 million knee wear cycles in a combination of 40% stairs up, 40 % stairs down, 10% level walking, 8% chair raising and 2% deep squatting with up to 100° flexion [8,9].

The specimens were evaluated for gravimetric wear and analysed for abrasive-adhesive and delamination wear modes.

Results: There was a substantial difference in the oxidation index between the vitamin E stabilised polyethylenes irradiated with 30 kGy and 50 kGy and the standard material (Fig. 1).

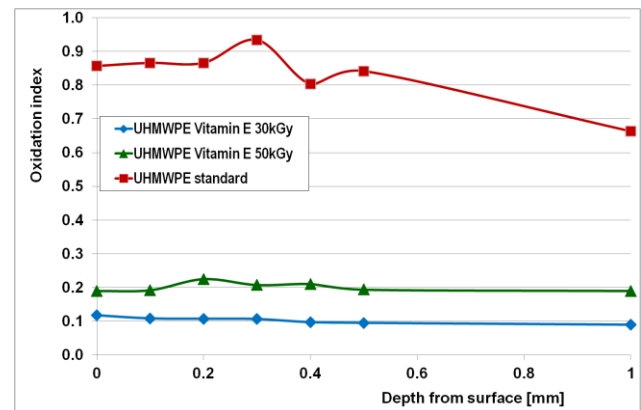


Fig. 1: Oxidation index of stabilised and unstabilised polyethylene gliding surfaces after 14 days of artificial ageing

The combination of artificial ageing and high demanding knee wear simulation leads for unstabilised standard polyethylene to visible signs of delamination in the articulating standard polyethylene bearing areas in vitro. Delamination began after 2 million test cycles for the standard polyethylene, indicated by the transition between linear and exponential slope in Fig. 2. Delamination was not found in the Vitamin E blended gliding surfaces.

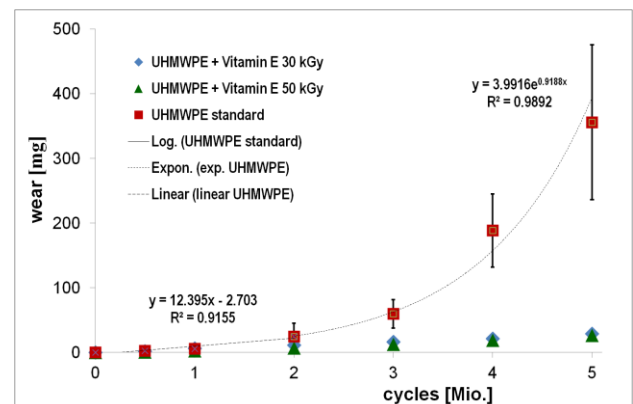


Fig. 2: Wear behaviour of stabilised and unstabilised polyethylene gliding surfaces during daily activities knee wear simulation

The total amount of gliding surface wear was 28.7 ± 1.9 mg for the vitamin E stabilised polyethylene irradiated with 30 kGy and 26.5 ± 5.7 mg with 50 kGy irradiation, compared to 355.9 ± 119.8 mg for the standard material.

Discussion: To evaluate moderately or highly cross-linked polyethylenes for total knee arthroplasty in regard to ageing and wear behaviour in vitro, conditions are simulated to create clinical relevant failure modes given in vivo. With the applied test protocol it is possible to discriminate between the polyethylene bearing materials with and without Vitamin E stabilisation.

References:

- ¹ Kurtz et al. 2011
- ² Hinarejos et al. 2013
- ³ Hodrick et al. 2008
- ⁴ Minoda et al. 2009
- ⁵ Grupp et al. 2009, 2013
- ⁶ Walker et al. 2000
- ⁷ Bergmann et al. 2014
- ⁸ Schwiesau et al. 2013
- ⁹ Schwiesau et al. 2014

Surface Damage and Condyle Penetration of 1st Generation Remelted HXLPE in Total Knee Replacement

Daniel W. MacDonald, Judd S. Day, Gregg Klein, Matthew Kraay, Clare Rinnac, Steven M. Kurtz
dm68@drexel.edu

Introduction: Highly crosslinked polyethylene (HXLPE) was clinically introduced approximately a decade and a half ago to reduce polyethylene wear rates and subsequent osteolysis. Clinical and radiographic studies have repeatedly shown increased wear resistance in total hip arthroplasty. However, due its slower adoption and the increased difficulty to perform radiographic studies, the performance of remelted HXLPE in total knee arthroplasty has not been widely reported.

Methods: Between 2002 and 2015, 169 1st generation remelted HXLPE tibial inserts were collected and analyzed as part of an ongoing, multi-institutional orthopaedic implant retrieval program. Of these, 23 components were identified as being of the same size as available unimplanted controls. The inserts were revised primarily for loosening, instability, and infection. None of the inserts were revised for osteolysis or fracture of the HXLPE. The components were implanted for a mean of 3.2 years (Range: 1.0 – 7.3 years; Table 1).

Surface damage mechanisms were assessed using a semi-quantitative scoring method similar to the method described by Hood et al. Penetration of the remelted HXLPE inserts was assessed using micro-computed tomography (microCT). The retrieved and control components were scanned at 74-micron isotropic resolution using a commercial microCT scanner (μ CT 80, Scanco Medical, Switzerland). The retrieved component datasets were manually registered with the unimplanted control datasets using unworn areas as landmarks. Penetration maps were produced by calculating the difference in thickness between the two components across the entire implant. To determine the contribution that of plastic deformation (creep) on the penetration into the tibial inserts, a melt-recovery procedure was used. The lateral condyles of 20 components were melted at 150°C for approximately 30 minutes to initiate melt-recovery.

Results: The predominant surface damage mechanisms observed were pitting, burnishing, and scratching. Two of the inserts had evidence of embedded debris in within the articulating surfaces. Penetration rates of the retrieved HXLPE inserts varied greatly within this cohort (Figure 1; Mean Volumetric Penetration Rate = 86.6 ± 71.1 mm³/yr). This corresponded to maximum linear penetration rates of 0.19 ± 0.14 mm/yr (Range: 0.05-0.47 mm/yr; Figure 2). The volumetric and linear penetration rates were negatively correlated with implantation time (Spearman's Rho = -0.42 and -0.59; $p=0.045$ and 0.0032, respectively). Penetration rates were not correlated to individual or cumulative damage mechanism scores. Seven of the inserts exhibited near-full recovery, while 11 exhibited partial recovery of the original surface during melt-recovery. Two implants displayed little or no melt recovery. In several cases, the apparent damage completely disappeared after the melt experiments (Figure 3).

Discussion: Thermally treated first generation HXLPEs were introduced to reduce polyethylene wear and subsequent wear-debris induced osteolysis. Although visual damage scores can qualitatively describe surface damage, these scores were not correlated with penetration volumes or depths and could not identify recoverable pitting. Moreover, the melt-recovery experiments suggest that creep is a contributor to the penetration rates, particularly in the first 2 years of use. Therefore, researchers should use caution when interpreting these metrics, as they may not indicate the amount of material released from the implant. More research is necessary to understand these phenomena in sub-melt annealed and anti-oxidant stabilized HXLPEs.

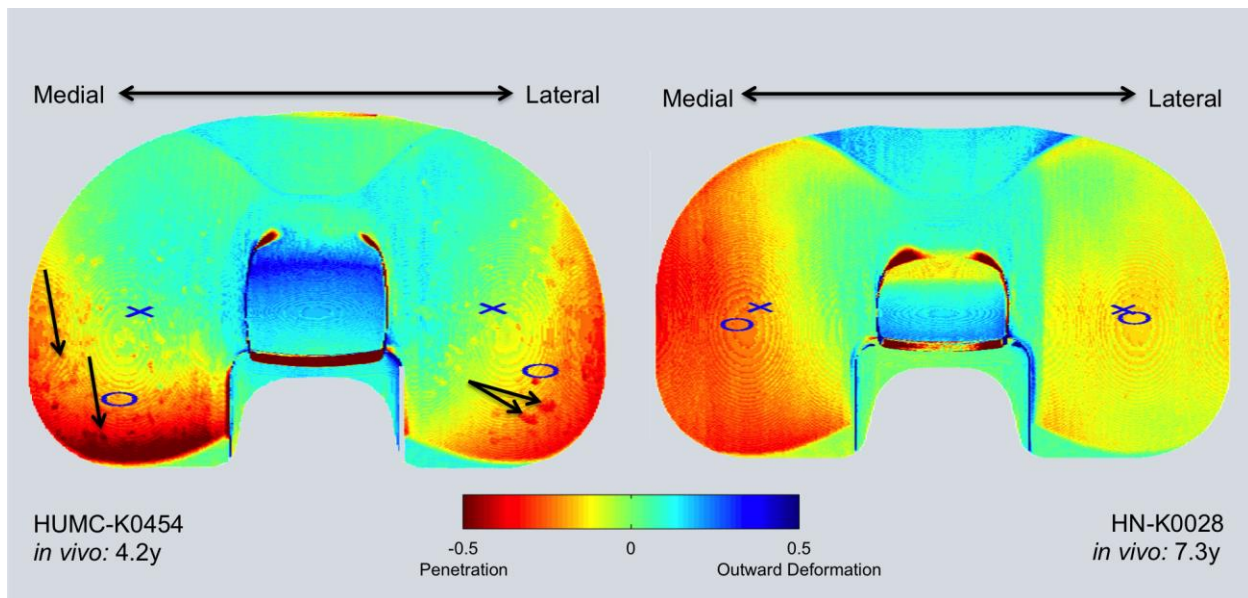


Figure 1: Example penetration maps constructed from registered microCT data of exemplar and retrieved tibial inserts for two patients.

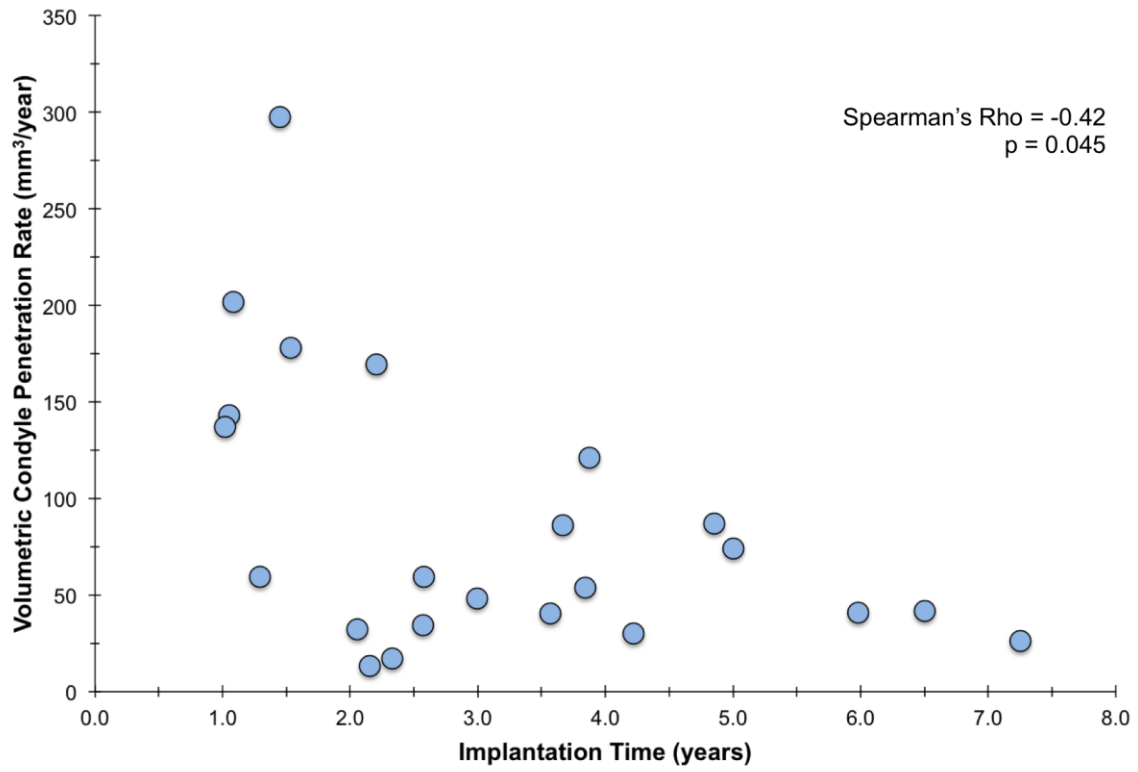


Figure 2: The volumetric condyle penetration was negatively correlated with implantation time (Spearman's Rho = -0.42; p = 0.045).

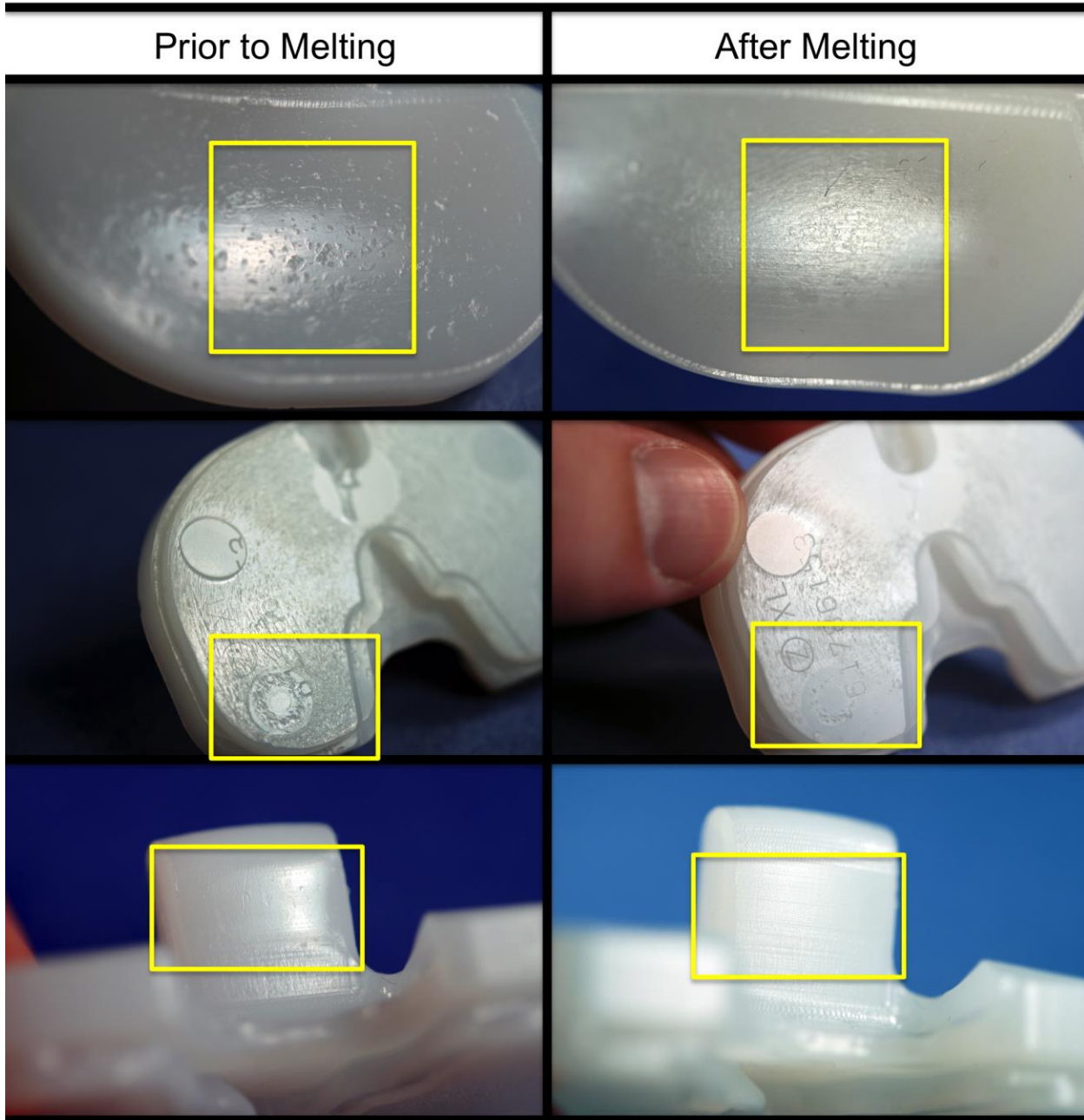


Figure 3: Tibial insert prior to and post melt-recovery experiments. The insert was implanted for 1.25 years. Note the near full recovery of the insert after melting, particularly on the posterior post.



SESSION
FIVE:

**Knee (II),
Shoulder and
Spine**

IN VITRO COMPARISON OF CONVENTIONAL PE vs. MECHANICALLY ANNEALED VITAMIN E PE UNICOMPARTMENTAL BEARING SURFACES

*Micheli BR, *Lozynsky AJ, *Wannomae KK, +*Muratoglu OK

+ * Harris Orthopaedic Laboratory, Massachusetts General Hospital, Boston, MA 617-726-3869 Fax: 617-643-2521

omuratoglu@partners.org

Introduction: Irradiated and melted, highly cross-linked ultra-high molecular weight polyethylene (UHMWPE) has been in clinical use in total knee arthroplasty for almost a decade. Recently introduced, second generation highly cross-linked polyethylenes avoided the post-irradiation melting step and therefore have better mechanical properties [1]. The addition of vitamin E is one of the alternative methods used in second generation materials to improve the oxidative stability of irradiated polymer. In addition, mechanical annealing had been shown to eliminate residual free radicals [2]. We propose that the combined benefits of vitamin E stabilization and mechanical annealing would yield a good candidate load bearing material for unicompartmental knee arthroplasty, where failures due to periprosthetic osteolysis secondary to UHMWPE wear debris and oxidative damage are common.

Knee simulator wear testing has been the standard method of determining wear resistance of tibial inserts. In this report, we present the details of a simulated normal gait knee simulator wear study of conventional PE tibial inserts and vitamin E blended and mechanically annealed PE (VitE-PE) tibial inserts used in unicompartmental knee arthroplasty.

Methods and Materials: The tested UHMWPE tibial bearings were MAKO MCK Implant System tibial onlay inserts, size 8 (MAKO Surgical, Ft. Lauderdale, FL). Each tibial bearing construct consisted of a medial and lateral UKA-style insert. The conventional PE components were machined from GUR1050 UHMWPE stock and subsequently gamma sterilized in an inert atmosphere. The VitE-PE components were machined from a 0.1 wt. % vitamin E stock that had been irradiated to 100 kGy, mechanically annealed to a compression ratio of 2, and then thermally annealed to activate the shape memory property of UHMWPE. The VitE-PE components were then EtO sterilized.

Prior to testing, all samples were accelerated aged in a pressure vessel under 5 atm of pure oxygen at 70°C for 3 weeks. Microtomed thin films (~150 µm,) from sacrificed samples were analyzed by Fourier Transform Infrared Spectroscopy (FTIR) to quantify oxidation per ASTM F2102.

Knee simulator testing was carried out to a total of 5×10^6 cycles of simulated gait on an AMTI 6-station displacement controlled knee simulator using ISO 14243-3 gait waveforms. Load waveform used in conjunction

with the kinematics was scaled to increase the peak load to 3200N. Three aged conventional PE and three aged VitE-PE tibial constructs were tested under both load and motion while two of each were subjected to only load as load-soak constructs. The simulator was interrupted in 0.5×10^6 cycle intervals between 0 – 3×10^6 cycles and in 1.0×10^6 cycle intervals thereafter where samples were cleaned and weighed to assess wear gravimetrically. The weight loss of each component was corrected for fluid absorption by subtracting the average weight gain of the load-soak components from the weight change of the motion components of the same material. A wear rate was calculated by applying a linear regression on the corrected weight loss of each component from 0.5×10^6 to 5×10^6 cycles. The slope of the linear regression was the wear rate in milligrams per million cycles (mg/MC). At every simulator interruption, an overall picture was taken with a Canon Powershot G10 digital camera to document the wear scar.

Results: The conventional components showed oxidation, while there was no detectable oxidation with VitE-PE after accelerated aging (Fig.1).

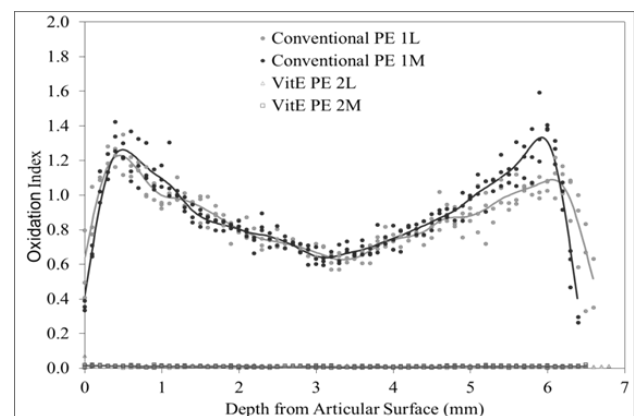


Fig. 1: Oxidation profiles after ASTM F2003 aging. Actual data from all samples in a group is represented by the individual data points; the splined average of the three profiles in each sample group is shown as the solid line.

The combined linear wear rate for the aged VitE-PE components was 12.9 ± 1.4 mg/MC, with a range of 12.9 to 14.4 mg/MC. The combined linear wear rate for the conventional PE components was 34.5 ± 6.7 mg/MC, with a range of 28.5 to 41.7 mg/MC for the first 3×10^6 cycles of simulated gait. At that point in study the conventional PE components exhibited a sharp increase in weight loss and the combined linear wear rate for the final 2×10^6 cycles

of simulated gait was 147 ± 51 mg/MC, with a range of 94 to 196 mg/MC (Fig. 2).

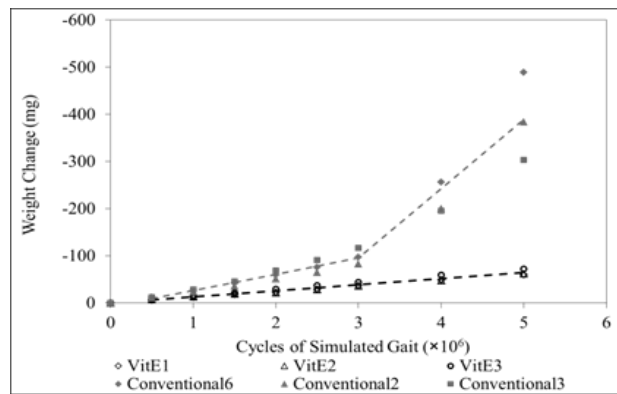


Fig. 2: Wear profiles after 5×10^6 cycles of simulated gait. Actual data from all samples in a group is represented by the individual data points; linear wear rate is shown as the dotted line.

Discussion:

Accelerated aging yielded a high subsurface oxidation peak as well as high oxidation throughout the bulk of the conventional PE tibial bearings, due to the unquenched residual free radicals. As expected the VitE-PE components showed no oxidation.

For the first 3×10^6 cycles of simulated gait the aged VitE-PE constructs exhibited a 62.8% reduction in total construct wear as compared to the aged conventional PE constructs. After the 3.0×10^6 cycles of simulated gait, all of the aged conventional PE components exhibited delamination and pitting, this dramatically increased the weight loss of these components. For the final 2.0×10^6 cycles of simulated gait the aged VitE-PE constructs exhibited a 91.2% reduction in total construct wear as compared to the aged conventional PE constructs. The aged VitE-PE components showed no damage due to oxidation and retained their polished wear scar even after the full 5×10^6 cycles of simulated gait (Fig 3).

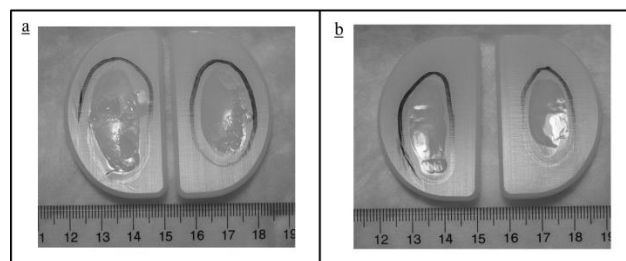


Fig 3: photos of a representative (a) conventional GUR1050 PE and (b) Esyntal PE tibial construct after 5×10^6 cycles of simulated gait.

The reduced free radical content imparted by mechanical annealing coupled with the active protection of vitamin E yielded a material with excellent resistance to adhesive wear and oxidation damage in unicompartmental knee components.

Acknowledgements:

This Study was funded by MAKO Surgical, Ft. Lauderdale, FL

References:

- [1] Oral E, et. al. J Arthroplasty 2006 Jun; 21 (4): 580-91
- [2] Muratoglu OK, et. al. ORS 2005: Poster 1661

Characterization of Striated Pattern of Retrieved UHMWPE Tibial Liner by Raman Spectroscopy

Rad E^{1,2}, Pourzal R¹, Laurent MP¹, Liao Y³, Wimmer MA^{1,2}

¹Rush University Medical Center, Chicago, Illinois, ²University of Illinois at Chicago, Chicago, Illinois

³Northwestern University, Evanston, Illinois

elmira_moslemi-rad@rush.edu

Introduction: Failure of total knee replacements (TKR) due to wear remains a significant issue. Therefore, it is important to understand the occurrence of specific wear features. We have observed a characteristic striation pattern on the articular surfaces of explanted polyethylene tibial liners that is absent in hip liner articular surfaces. The pattern consists of submillimeter hills and troughs aligned approximately in the anterior-posterior direction. The pattern may play an important role in understanding the evolution of surface disruption on the tibial articulation. In this study, the morphological features of the striated pattern were examined with Raman spectroscopy to determine changes in crystallinity. It was hypothesized that the hills have a higher crystalline content than the troughs, so wear less and stand proud of the articular surface.

Methods and Materials: The Raman spectra in the 950-1600 cm^{-1} range were obtained using an Acton TriVista CRS Confocal Raman system with excitation radiation of an Ar-Kr 514.5 nm gas laser at ~ 10 mW with a microscope of 50X magnification and spectral resolution of 1.2 cm^{-1} . In order to validate the method of crystallinity calculation by Raman spectroscopy, four control samples with variable but known crystallinity (47.91%-53.98%) were made by Orthoplastics, Ltd (UK). A representative explanted tibial liner (NexGenTM, CR, Zimmer, Inc.), exhibiting striations on both the medial and the lateral articulating surfaces, was chosen for analysis. Five spectra per hill and trough were obtained on the medial and lateral sides. In addition, five spectra were obtained for each control sample. The relative content of three different interphases α_o , the fraction of orthorhombic crystalline phase, α_a , the amorphous phase, and α_b , intermediate anisotropic disorder was estimated from the relative intensities of specific Raman bands using the Strobl and Hagedorn method [1]. To determine the integrated band areas at 1416 cm^{-1} and 1080 cm^{-1} , as well as the area of the internal standard at 1295 cm^{-1} and 1305 cm^{-1} , curve fitting was performed (Origin 9.1) on the original spectra after baseline correction by using the linear combination of Gaussian and Lorentzian function (PsdVoigt1).

Results: The estimated values for three out of four control samples were approximately 10% higher than the values measured by DSC; however, the relative ranking and the relative differences were preserved. The Raman spectra on the tibial plateau exhibited qualitative differences between hills and troughs: the band at 1416 cm^{-1} , assigned to the crystalline phase, was greater in intensity on the hills compared with the troughs. In contrast, the bands at 1440 and 1460 cm^{-1} , which are

assigned to the amorphous phase, were slightly weaker on the hills than the troughs, suggesting a higher crystallinity of the hill compared with the trough.

The mean (\pm SD) values of α_o , α_a and α_b were calculated from the spectra (Figure 1). The orthorhombic content (α_o) on the hills was significantly ($p=0.001$) greater than that of the troughs (0.67 ± 0.08 and 0.54 ± 0.04 , respectively). The amorphous content (α_a) was lower for the hills (0.18 ± 0.04) than for the troughs (0.22 ± 0.02 ; $p=0.03$). The intermediate phase content (α_b) was also significantly ($p=0.01$) lower for the hills (0.13 ± 0.09) than for the troughs (0.22 ± 0.05), an indication of partial transformation from intermediate to the orthorhombic phase.

Discussion: Based on these results, the hills of the striated pattern have a higher degree of crystallinity than the troughs, as hypothesized. Since the striated pattern has only been reported for tibial liners and not for hip liners, and it is known that mechanical stress can lead to changes in crystallinity [2], it is likely that tractive rolling of the knee joint has caused a reorganization of the microstructure into alternating crystalline and amorphous areas. Once this reorganization has taken place, wear occurs preferentially in the amorphous zones, explaining the height difference between hill and trough ($R_z= 5.5 \mu\text{m}$ [3]). Although Raman spectroscopy proved valuable to determine relative local crystallinity on a wear surface, further work is needed to obtain absolute crystallinity values consistent with DSC measurements.

In conclusion, this is another example where the nature of the mechanical stresses acting on the surface, not just the load, appears to play an important role in the wear mechanism of polyethylene through chain re-alignment processes.

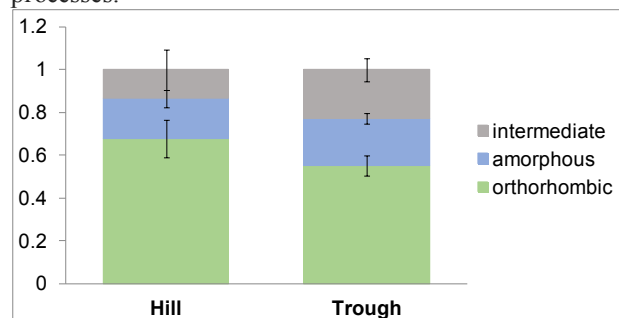


Figure 1. Mean values of α_o , α_a and α_b contents from the Raman spectra recorded on the hill and trough of the striated pattern.

References:

- [1] Strobl GR et al (1978)
- [2] Edidin AA et al (1999)
- [3] Wimmer MA et al (1998)

Layered UHMWPE as a Bearing Material for Use in Total Knee Arthroplasty

Beutler, GB¹, Chan, DS¹, Konsin, ZB¹, Oral, E¹, Muratoglu, OK¹

¹Harris Orthopaedic Laboratory, Massachusetts General Hospital, USA

gbeutler@mgh.harvard.edu

Introduction: Ultra high molecular weight polyethylene (UHMWPE) has been used successfully in total joint arthroplasty for multiple decades. Currently, the vast majority of UHMWPE acetabular liners and tibial bearings are manufactured from a homogeneous material – that is, the material at the articular surface of an implant is the same as the material in the bulk and at the locking mechanism. By instead creating a layer of highly crosslinked UHMWPE only on the articular surface of an implant, wear resistance can be improved while the bulk of the material retains its high fatigue resistance and impact strength to prevent component fractures. Utilizing a chemical crosslinking agent, such as peroxide, and an antioxidant, such as vitamin E, we hypothesize that a layered tibial bearing, with a highly crosslinked, wear resistant articular surface and a non-crosslinked, mechanically strong bulk, that is oxidatively stable, can be reproducibly fabricated.

Methods and Materials: First, the recipe of peroxide and vitamin E in UHMWPE was investigated to optimize the wear, mechanical, and oxidation-resistant properties of the material to be used as the highly crosslinked articular surface layer. Concentrations of vitamin E from 0.2 to 0.7 weight percent (DSM Nutritional, Belvidere, NJ) in GUR1020 UHMWPE were blended with concentrations of 2,5-di(tert-butylperoxy)-2,5-dimethyl-3-hexyne (P130, Sigma-Aldrich, St. Louis, MO) between 0.5 and 1.1 weight percent and immediately compression molded into pucks. Pucks were then machined and stamped into 3.2 mm thick Type V dog-bone specimens for tensile testing per ASTM D638. Gravimetric crosslink density was measured per ASTM D2765. Pin-on-disk (POD) wear testing was then conducted on samples with the best mechanical properties.

Next, a technique was investigated for creating a repeatable layer on a contoured surface that was a rough approximation of a tibial bearing. The geometry of the consolidated contoured sample is shown in **Figure 1** and **Figure 2**.

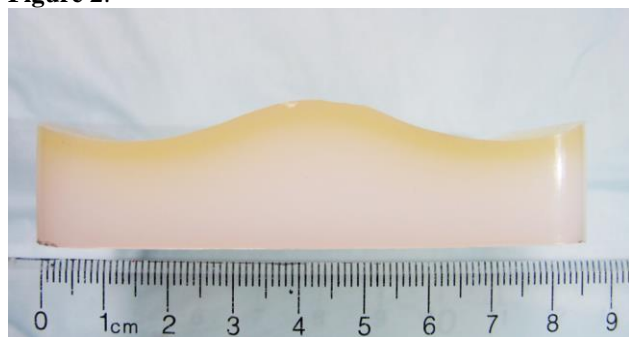


Figure 1. Side view of the consolidated contoured sample, 85 mm in length and 50 mm in width.



Figure 2. Side view of the consolidated contoured sample, condyle height 14 mm and eminence height 19 mm.

Material for the bulk of the component was first pressed at 10 MPa for 3 minutes at room temperature. The material for the highly crosslinked articular surface layer was then added on top of the bulk pellet. The desired layer thickness was 2-3 mm. A 3D-printed plunger, the geometry of which was the negative of the contoured surface of the sample, was used to ensure even distribution of the layer material across the contoured surface of the bulk pellet. The material was then compression molded into a single layered construct.

The consolidated layered material was analyzed using Fourier transform infrared spectroscopy (FTIR) to determine the thickness and uniformity of the layer. FTIR was used to calculate the trans-vinyl index (TVI) of the material at different depths, per ASTM F2381. Four locations were analyzed using FTIR: one at the eminence, one in the middle of each condyle, and one towards the posterior edge of the left condyle.

Flat samples were molded using the same parameters to analyze the mechanical properties of the consolidated layered material. Crosslink density at the surface of the layered sample was measured per ASTM D2765. Tensile mechanical properties were determined per ASTM D638 with samples prepared such that the cross-section was half layer material and half bulk material. Izod impact testing was performed per ASTM F648 with samples cut from the layered material that included both crosslinked material and bulk material. Pin-on-disc wear testing was performed. Oxidative induction time (OIT) was performed per ISO 11357 to measure the relative oxidative stability of the material.

Results: Table 1 shows the effect of vitamin E in a 0.5 wt.% P130 blend and Table 2 shows the effects of P130 in a 0.5 wt.% vitamin E blend.

As measured using FTIR, TVI versus depth of the layered material at four locations is shown in **Figure 3**.

The mechanical properties of the layered sample, as well as of the bulk material and of the layer material, are shown in **Table 3**.

	XLD (mol/m ³)	Wear Rate (mg/10 ⁶ Cycles)	UTS (MPa)	EAB (%)	DSC XLT (%)
GUR 1020 CISM 75	247±3	2.5±0.1	45.3±1.5	241±9	54.0±0.3
GUR 1050 CISM 75	201±3	2.7±0.4	50.0±1.4	286±4	56.2±0.3
0.2 wt% VitE	194±4	-----	36.5±0.8	332±4	49.9±0.5
0.5 wt% VitE	169±2	6.1±2.2	43.5±1.8	348±12	51.4±0.2
0.7 wt% VitE	158±4	-----	46.1±2.6	272±96	-----

Table 1: Table of Mechanical Properties displaying the effects of Vitamin E concentrations in GUR1020 UHMWPE blends with 0.5 weight percent P130.

	XLD (mol/m ³)	Wear Rate (mg/10 ⁶ Cycles)	UTS (MPa)	EAB (%)	DSC XLT (%)
GUR 1020 CISM 75	247±3	2.5±0.1	45.3±1.5	241±9	54.0±0.3
GUR 1050 CISM 75	201±3	2.7±0.4	50.0±1.4	286±4	56.2±0.3
0.5 wt% P130	169±2	6.1±2.2	43.5±1.8	348±12	51.4±0.2
0.9 wt% P130	220±8	1.7±0.1	34.8±0.6	287±8	49.2±0.1
1.1 wt% P130	233±2	1.2±0.3	35.0±3.0	297±11	48.1±0.1

Table 2: Table of Mechanical Properties displaying the effects of P130 concentrations with 0.5 weight percent Vitamin E GUR1020 blend.

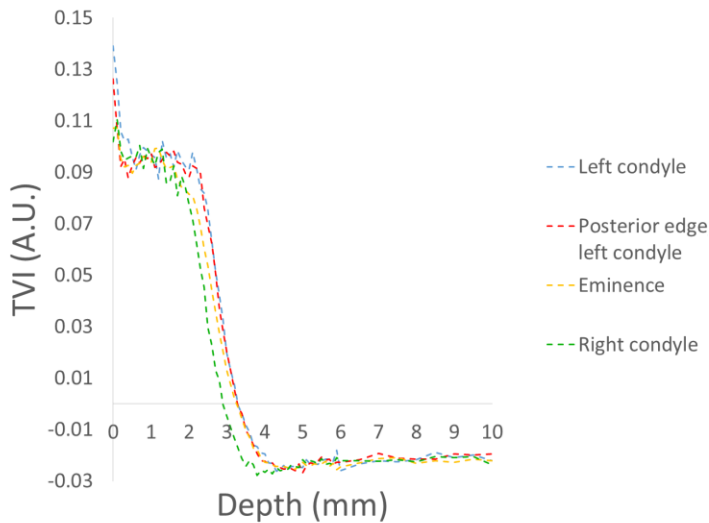


Figure 3. TVI versus depth of layered crosslinked GUR 1020.

	Layered sample	Bulk material	Layer material
Material	0.5 wt% VE bulk + 0.2 wt% VE - 0.9 wt% P130 layer	0.5 wt% VE	0.2 wt% VE - 0.9 wt% P130
XLD (mole/m ³)	253 ± 5	N/A*	252 ± 5
Wear rate (mg/million cycles)	2.0 ± 0.2	N/A*	1.4 ± 0.5
Izod impact strength (kJ/m ²)	96.9 ± 2.6	123.8 ± 6.5	76.4 ± 4.1
UTS (MPa)	35 ± 2	59 ± 3	36 ± 4
EAB (%)	260 ± 13	414 ± 38	284 ± 20
OIT (min)	-	> 60	13.1 ± 0.3

Table 3. Mechanical properties of 0.5 wt% VE GUR 1020, 0.2 wt% VE - 0.9 wt% P130 GUR 1020, and layered 0.5 wt% VE GUR 1020 bulk + 0.2 wt% VE - 0.9 wt% P130 GUR 1020 layer. The wear rate and crosslink density was not measured on the bulk material since it would not be on the articular surface of any construct.

Discussion: By fixing the concentration for P130 blends, we saw that with increasing vitamin E concentration there was an increase in the ultimate tensile strength (UTS). However, with increasing vitamin E concentrations, there was also a decrease in crosslink density. In order to maximize the UTS without compromising the crosslink density, 0.5 weight percent vitamin E was the designated optimum value. Using this value, we compared how P130 was affecting the blends. Increasing the P130 content in blends caused an increase in both cross link density but however caused a decrease in the UTS. A blend of 0.9 wt.% P130 was chosen as it exhibits the excellent wear resistance necessary for use in an articular surface layer. We decreased the vitamin E content slightly (to 0.2 wt.%) for the highly crosslinked surface layer to further improve its wear resistance; the bulk of the material was kept at 0.5 wt.% vitamin E with no P130.

The goal of creating a localized layer of crosslinked UHMWPE on a contoured surface was achieved. Moreover, the thickness of this crosslinked layer was uniform across the contoured surface, with the TVI measurement indicating a 2 mm crosslinked layer with an additional 1 mm boundary layer of less crosslinked material.

The layered construct was able to maintain an excellent wear rate, comparable to that of the homogenous crosslinked material, while improving its overall impact strength by nearly 28%, from 76 to 97 kJ/m². The mechanical properties as measured by tensile testing was not improved, most likely because, when the highly crosslinked layer failed, it dramatically increased the stress on the stronger bulk material in the layered sample, causing it to fail at the lesser load. The OIT of the layered construct was not measured but is expected to be somewhere in between the OIT measurements of its constituent materials.

Homogeneous materials currently used in hip and knee implants are limited by a tradeoff between the wear resistance necessary at the articular surface and the mechanical strength needed elsewhere. This layered material may provide a versatile alternative to homogeneous materials for fabricating implants with decreased wear *in vivo*, further improving the long-term success rate for total knee arthroplasty.

Bearing Surface Damage of Anatomical and Reverse Total Shoulder Replacements: Retrieval Analysis Across Fixation Designs and UHMWPE Composition

Bonnheim, N¹; Malito, L¹; Ansari, F¹; Chou, S¹; Gunther, S²; Norris, T³; Ries, M⁴; Pruitt, L¹

¹University of California at Berkeley, Berkeley, CA; ²Martha Jefferson Hospital, Charlottesville, VA; ³San Francisco Shoulder, Elbow & Hand Clinic, San Francisco, CA; ⁴Tahoe Fracture & Orthopedic Medical Clinic, Carson City, NV
noah.bonnheim@berkeley.edu

Introduction: Osteolysis due to ultrahigh molecular weight polyethylene (UHMWPE) wear debris has been well documented across total joint replacements (TJR) [1-3]. Retrieval studies examining the surface damage of polymeric bearings have focused on knee and hip components, while comparatively little attention has been given to devices used in the shoulder [4,5]. This work presents an analysis of the mode and geometric extent of surface damage for anatomical total shoulder arthroplasty (TSA) and reverse shoulder arthroplasty (RSA) retrievals. The cohort of retrievals spans more than 20 years of device designs with different fixation types and UHMWPE formulations. A better understanding of the relationship between material behavior and damage mechanics can inform implant designs which better resist *in vivo* damage.

Methods and Materials: *TSA:* Twenty-four retrieved glenoid components with different fixation designs and UHMWPE formulations were analyzed. Fixation designs were categorized as either all-polyethylene-backed or metal-backed. The UHMWPE glenoids were of Hylamer, 2.5-4 Mrad gamma-air sterilized, and 2.5-5 Mrad irradiated (gamma-inert or gas-plasma sterilized) cross-linked formulations. The gas-plasma sterilized glenoids (n=2) were re-melted post irradiation. Glenoids used in this study were implanted between 1987 and 2011, with an average patient age at implantation of 61 years and an average time *in vivo* of 6.1 years. Each glenoid bearing surface was divided into 17 regions of equal area via a grid, and all regions were photographed at 249 dpi using a Nikon 1 J1 camera and an Infinivar Video Microscope lens under an AMScope LED ring light. The presence and extent of 11 damage modes (**Figure 1**) were noted using Image J (Bethesda, MD, v1.48) image processing software. The 11 damage modes used were based on an implant classification methodology described by the Hood technique and expanded upon by other investigators [4,5,6,7,8]. Each implant was scored by at least two observers, and inter-observer agreement was evaluated by calculating the average percent agreement for damage mode identification, geometric extent, and severity.

TABLE 1. SUMMARY OF CLINICAL INFORMATION.

Clinical Information	All (n=42)	Glenoids (n=24)				Humeral Cups (n=18)	
		Poly-Backed (n=18)	Metal-Backed (n=6)	Hylamer (n=8)	X-Linked (n=9)	Gamma-air (n=3)	X-Linked (n=15)
Age at surgery	60±9 years	62±9 years	58±11 years	64±10 years	58±6 years	70±4 years	57±7 years
<i>In vivo</i> duration	5±5 years	4±3 years	15±5 years	7±3 years	2±1 years	4±3 years	3±3 years

RSA: Eighteen retrieved UHMWPE humeral cups were analyzed for mode and geometric extent of surface damage. UHMWPE components were of 2.5-4 Mrad gamma-air sterilized and 2.5-4 Mrad gamma-inert sterilized (cross-linked) formulations. The humeral cups used in this study were implanted between 2004 and 2014, with an average patient age at implantation of 60 years and an average time *in vivo* of 3.2 years. The bearing surfaces of the humeral cups were divided into four regions of equal area, similar to the method reported by Nam [9]. Six observers noted damage modes through visual inspection of each quadrant.

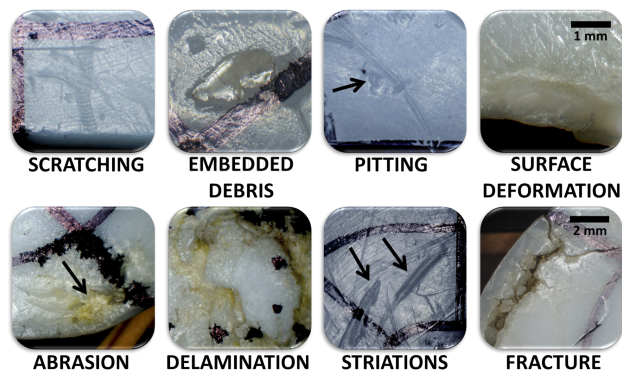


FIGURE 1. EIGHT OF THE ELEVEN PRIMARY DAMAGE MODES OBSERVED ON UHMWPE SHOULDER IMPLANTS. WEAR THROUGH, SUBSURFACE CREAKING, AND BURNISHING ARE NOT SHOWN.

Results: Damage mode data is presented in **Table 2**. All TSA components demonstrated instances of scratching, striation, pitting, and surfaced deformation regardless of fixation design or UHMWPE formulation. Only 4 (22%) RSA components demonstrated concurrent existence of all four of these damage modes. At least one glenoid for each material formulation and fixation type had fractured. The group of cross-linked glenoids had the shortest time *in vivo* and exhibited scratching, striation, pitting, surface deformation, and abrasion in all samples, in line with damage modes in components made from non cross-linked UHMWPE formulations. Metal-backed glenoids had the longest time *in vivo* and exhibited the highest instance of embedded debris.

For RSA devices, subsurface cracking was the only damage mode category that was not observed. Twelve samples (67%) demonstrated abrasion on the rim of the humeral cup in the inferior quadrant (**Figure 2**). Approximately half of the rim material was missing for 5

samples (20%). The most common damage modes in the reverse TSR cohort were scratching and striations, which in occurred in all quadrants on 10 (56%) of the samples. One sample contained significant metal debris embedded in the surface of the humeral cup.

TABLE 2. SUMMARY OF DAMAGE MODES. *METAL-BACKED GLENOIDS WERE 2.5 MRAD GAMMA-AIR STERILIZED. **CROSS-LINKED GLENOIDS WERE EITHER GAMMA-INERT STERILIZED (2.5-4 MRAD) (N=7) OR IRRADIATED (5 MRAD) REMELTED AND GAS-PLASMA STERILIZED (N=2).

Damage Mode	All (n=42)	Poly-Backed (n=18)	Metal-Backed* (n=6)	Hylamer (n=8)	X-Linked (2.5-5 Mrad)** (n=9)	Gamma-air (2.5-4 Mrad) (n=3)	X-Linked (2.5-4 Mrad) (n=15)
Scratching	86%	100%	100%	100%	100%	67%	67%
Striations	86%	100%	100%	100%	100%	33%	73%
Surface Def.	81%	100%	100%	100%	100%	66%	53%
Pitting	76%	100%	100%	100%	100%	33%	47%
Abrasion	57%	72%	100%	75%	78%	100%	13%
Delam.	57%	67%	83%	88%	44%	100%	33%
Fracture	38%	56%	83%	88%	44%	0%	7%
Embedded Deb.	26%	22%	67%	25%	11%	66%	7%

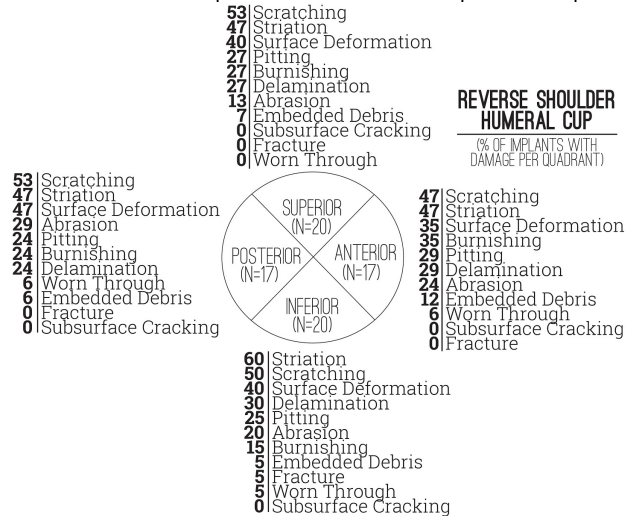


FIGURE 2. FREQUENCY AND LOCATION OF DAMAGE FOR UHMWPE HUMERAL CUPS. ALL VALUES ARE EXPRESSED AS PERCENTAGES.

Discussion: To the authors' knowledge, this is the only study that assesses the presence of damage modes on shoulder components for both conventional and reverse designs across fixations types and UHMWPE compositions. The study encompasses more than 20

years of implant evolution, from gamma-air sterilized metal-backed glenoids to lightly cross-linked reverse humeral cups. The degree of damage seen in this broad range of shoulder devices evokes questions about the extent of progress of shoulder implant designs and materials with respect to surface damage resistance. The introduction of low-to-moderately cross-linked UHMWPE in the shoulder to reduce wear has not fundamentally changed the damage modes observed compared to older polymer formulations. The reduction in fatigue crack growth resistance for cross-linked UHMWPE may have contributed to the early incidence of significant fracture observed in one of the cross-linked glenoids (less than three years *in vivo*). Some lightly cross-linked glenoids exhibited less severe fracture at shorter *in vivo* times (1.8 years). The observed damage on these implants is likely associated with some degree of oxidative embrittlement, as there was no post-sterilization heat treatment for the gamma-inert sterilized samples. Damage (including fracture) on the re-melted implants indicate that surface damage is not solely attributable to oxidative embrittlement and that cross-linked implants generally show damage at short *in vivo* times.

The high frequency and severity of inferior rim damage observed in the RSA cohort likely indicates a high prevalence of scapular notching; a finding in line with other investigations [10]. Damage modes including scratching, striations, pitting, and surface deformation are present on implants with short *in vivo* durations, suggesting that damage can occur shortly after implantation. While the clinical relevance remains uncertain, changes in shoulder component design and UHMWPE formulation (including modern RSA designs and cross-linked UHMWPE) have not prevented against certain damage modes in shoulder arthroplasty.

Acknowledgments: We would like to thank Isabel Yang, Lulu Li, Taylor Lee, and Helen Park for their contributions to this study.

References:

[1] Raiss et al. *J Bone Joint Surg Am.* 2014; 96(e54): 1-9.
 [2] Alidousti et al. *J Mech Behav Biomed Mater.* 2014; 32: 225-244.
 [3] Naudie et al. *J Am Acad Orthop Surg.* 2007; 15(1): 53-64.
 [4] Hood. *J Bio Mat Res.* 1983; 17: 829-42.
 [5] McKellop. *Biomater.* 2007; 28: 5049-57.
 [6] Harman et al. *J Mat Sci-Mater M.* 2011; 22(5): 1137-1146.
 [7] Gunther et al. *J Athroplasty.* 2002; 17(1): 95-100
 [8] Scarlat et al. *J Athroplasty.* 2001; 16(6): 795-801
 [9] Nam, et al. *J Shoulder Elb Surg.* 2010; 19(7): 1003-1012.
 [10] Le'vigne, et al. *Clin Orthop Relat Res.* 2011; 469: 2512-2520.

THE USE OF HIGHLY MODIFIED UHMWPE IN SPINAL APPLICATIONS

Allen M.D (mallen@orthoplastics.com)

Orthoplastics Ltd, Unit A, Beech Ind. Estate, Bacup, Lancashire, OL13 9EL, UK.

INTRODUCTION

Historically spinal devices have been manufactured from PEEK, Titanium or composites structures. This has been due primarily to the limited availability of creep resistant biomaterials.

The use of Ultra High Molecular Weight Polyethylene (UHMWPE) in spinal implants has been somewhat limited to high wear applications in composite structures (i.e lumbar disc replacement). The use of this material in spinal cages and other applications has been restricted by the poor creep resistance. This study aims to show that the manufacturing a highly modified UHMWPE can significantly improve creep resistance, yielding greater stability of a material in this application whilst possessing more synergies with actual bone properties.

MATERIALS AND METHODS

Three formulations of compression moulded UHMWPE were evaluated in the study, an initial screening study was undertaken using a simple long term deformation under load prior to selected materials progressing.

Samples were prepared for the following ASTM F2077 Creep-recovery testing following axial compression testing and compressive-shear testing

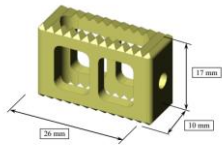


Figure 2: Representative spinal device specimen for shear testing is presented.

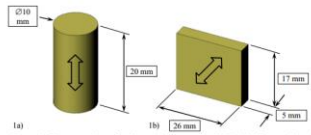
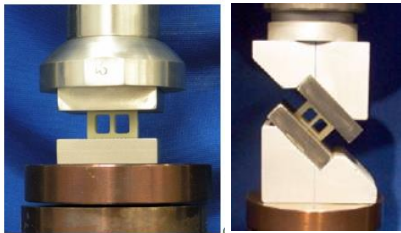
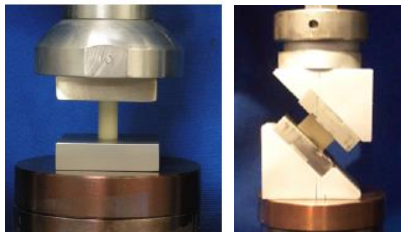


Figure 1: Coupon specimens for shear testing are presented. (a) Axial Compression and (b) Axial Compression-Shear testing. Arrows mark the direction of applied loading.



During testing, the applied loading and attained creep displacement was recorded at 1 Hz capturing the viscoelastic response of the material. The creep load phase involved ramping the set compressive loading to a pre-set peak level within 3 second span and held at this force over a 2-hour period.

The procedure for axial compressive-shear testing followed the same procedure as the axial compressive testing. A 10 lbf (2.25 N) compressive pre-load was used to align the fixture assembly train while aligning the specimen with the loading axis. Static ramp testing utilized the same 6 mm/min. (0.1 sec./min.) loading rate while capturing data at 20 Hz. Creep-recovery testing also used the same three-phase procedure using load-control for conducting testing.

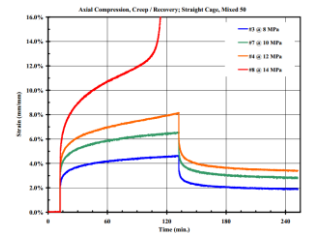
RESULTS AND DISCUSSION

Material creep was observed using set stress levels within the elastic linear region at 8 MPa of compressive stress during axial compressive loading with the creep rate increasing with increasing

compressive stresses.

Creep failure was observed within the 2-hour period at 12 MPa with the Mixed 100 material and at 14 MPa for the Standard 100 and Mixed 50 materials when testing with the straight PLIF cages. With testing with solid cylindrical test pin coupons, creep failure was still not observed at 14 MPa for all three materials.

Compression-shear testing at 0.8 MPa of shear stress and above induced material creep within the straight PLIF cages. Creep failure within the 2-hour period used for testing was observed at 1.1MPa for the Mixed 100 and Mixed 50 materials. The standard 100 material was near failure, but still intact at the end of the 2 hours at 1.1 MPa. With testing solid rectangular shape coupons, creep failure was observed at stress levels above 4 MPa.

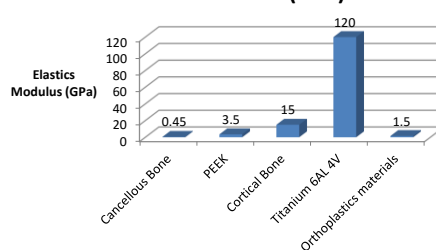


Static Compression: (Ramp Test Data)

	Compression Modulus (MPa)	Ultimate Stress (MPa)	Yield Stress (MPa)
PEEK	1,230 ± 112	178.5 ± 9.4	127.3 ± 1.8
Orthoplastics Std 100	404 ± 8	19.4 ± 0.5	14 ± 0.04
Orthoplastics Mixed 100	589 ± 92	22.1 ± 0.5	12.2 ± 0.3
Orthoplastics Mixed 50	513.9 ± 68	21 ± 2	13.1 ± 1.0

	Stiffness (N/mm)	Ultimate Load (N)	Yield Load (N)
PEEK	8,566 ± 92	12,953 ± 747	9,248 ± 51
Orthoplastics Std 100	1457 ± 31	1405 ± 37	1010 ± 3
Orthoplastics Mixed 100	2125 ± 333	1597 ± 36	885 ± 23
Orthoplastics Mixed 50	1853 ± 248	1521 ± 155	945 ± 74

Elastic Modulus (GPa)



Elastic Modulus of implantable materials is often compared to the mechanical performance of Cancellous and Cortical bone, thus assessing the bio integration of the materials.

CONCLUSIONS

- The CREEP resistance of the modified UHMWPE was significantly higher than conventional orthopaedic polyethylene materials.
- Compression Data within the public domain is limited and predominantly design dependant, the following data can be considered although there was a significant difference in the design of the larger PEEK ALIF cage compared to the PLIF cage tested in the Orthoplastics study.
- Impact strength of the Orthoplastics materials is significantly higher to PEEK, although values are confounded by different test methods data indicates PEEK at 7-10 kJ/m² and Orthoplastics materials at 40-70 kJ/m²
- Studies show that the compressive fracture load for the lumbar vertebra is 7-9KN, with design changes modified UHMWPE may offer a solution to what is commonly an over engineered solution to spinal devices due to availability of biomaterials.

Novel Radiopaque UHMWPE Wires for Spinal Deformity Correction: A Mechanical Assessment

Roth, AK¹ Boon-Ceelen, K², Smelt, H² van Rhijn, LW¹, Arts, JJ¹

¹Maastricht University Medical Center, Maastricht, the Netherlands ²DSM, Geleen, the Netherlands

alex.roth@maastrichtuniversity.nl

Introduction: Although pedicle screw usage has become increasingly widespread in the surgical treatment of thoracolumbar spine disease, sublaminar wiring remains a valuable technique, especially in technically demanding cases such as neuromuscular scoliosis or osteoporotic/osteopenic patients. Wide-profile woven polymeric sublaminar wires increase bone contact area, thereby distributing load and allowing for higher correction forces. The use of a soft and pliable wire is also expected to decrease the risk of dural injury in case of the need for removal during revision surgery¹. Currently available high-strength polymeric wires lack radiopacity and therefore the possibility for adequate postoperative radiological assessment. For this reason, novel radiopaque ultra-high molecular weight polyethylene (UHMWPE) sublaminar wires have been developed. Low friction between the UHMWPE wire and a metal spinal rod could facilitate sliding of the wire along the rod. Radiopacity, enabling radiological follow-up, and unconstrained longitudinal growth through free sliding allow for potential application in a growth-guidance type of construct for the treatment of early onset scoliosis².

In this study, novel radiopaque UHMWPE wires were mechanically tested and their tensile strength, tensile stiffness, fatigue strength, and creep were compared to a control UHMWPE counterpart without radiopaque additive and experimentally determined values or literature values for a titanium sublaminar wire (Atlas® cable system) and a SecureStrand™ UHMWPE sublaminar wire. The goal was to assess the novel radiopaque UHMWPE sublaminar wire in a setting relevant for the intended purpose; therefore all tests were performed on looped and secured wires.

Methods and Materials: The novel radiopaque wire is a 4 mm wide woven UHMWPE sublaminar wire made from radiopaque Dyneema Purity® fibers (DSM, The Netherlands). Radiopacity is attained through the integration of bismuth oxide particles (Bi₂O₃) particles within each fiber. In all cases, UHMWPE sublaminar wires were ethylene oxide sterilized prior to testing. A sliding double racket hitch was used to create a double-stranded loop. The racket hitch was secured using a single square knot throw, tensioned using a custom tensioning device to 500 N, and finally tied-off using 5 additional square knot throws for all tests (Figure 1). A titanium sublaminar cable (Atlas® cable system, Medtronic Sofamor Danek, Memphis, USA) was used as a comparison for tensile strength and stiffness testing. Creep and fatigue strength values for the titanium cable as well as for the SecureStrand™ UHMWPE wire (Smith & Nephew) were taken from Dickman et al³.

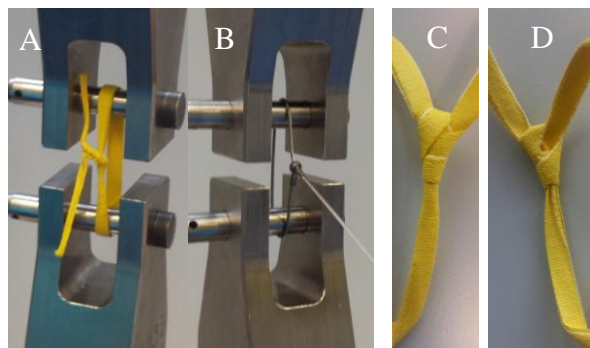


Figure 1. The test setup and the knotted double-stranded UHMWPE sublaminar wire (A) and the crimped titanium Atlas® cable (B). The double racket hatch knot is shown in more detail (C and D).

Tensile strength, tensile stiffness, and creep were determined in accordance with ISO 527 on a tensile testing machine (Zwick GmbH, Ulm, Germany) fitted with Clevis grips. The diameter of the pins was 10 mm and the distance between the longitudinal axes of the two parallel pins was 40 mm. Tensile strength and stiffness were determined at an actuator displacement speed of 1 mm/s. The stiffness was determined from the initial (linear) slope of the load-displacement curve between 100 and 500 N. Fatigue strength was determined using the same setup on a servo-hydraulic material testing machine (MTS Bionix 858, MTS, Eden Prairie, MN, USA) running at 5 Hz and minimum cycle load of 10 % of the maximum load. The fatigue strength was defined as the load at which 3 samples survived 5 million cycles.

Results: Results of the mechanical tests are summarized in Table 1. Tensile strength and fatigue strength of the novel radiopaque UHMWPE wire are superior to the compared wires⁷. The tensile stiffness of the tested standard and radiopaque UHMWPE wires are comparable to the crimped titanium Atlas® cable. A comparison to the SecureStrand™ is difficult as experimental and literature stiffness values for the Atlas® cable are different. As is to be expected, creep is negligible for the titanium Atlas® cable, while the novel radiopaque UHMWPE wire shows similar creep behavior as the SecureStrand™ wire. Yarn-on-yarn slip is slightly higher for the standard UHMWPE wires in comparison to the radiopaque UHMWPE wires, which results in a slightly higher tensile strength, but also in slightly increased creep.

	Radiopaque UHMWPE wire	Standard UHMWPE wire	Titanium Atlas® cable	SecureStrand™ UHMWPE cable
Tensile Strength	2232 ± 105 N (n=5)	2493 ± 143 N (n=5)	1129 ± 28 N (n=5)	1565 ± 71 N*
Tensile Stiffness	979 ± 80 N/mm (n=5)	965 ± 97 N/mm (n=5)	872±25 N/mm (497±32 N/mm)*	322±51 N/mm*
Fatigue Strength	1559 N (n=3)	Yet to be determined	<45 N*	578 N* (3million cycles)
Creep (24h)	2.58±0.20% (475 N, n=5)	2.12±0.18% (475 N, n=5)	0.74%* (902 N)	3.27%* (471 N)

Table 1. Summary of experimental results and comparison to literature values. * Denotes a value taken from Dickman et al³.

Discussion: The use of a knotted double-loop woven UHMWPE sublaminar wire has significant advantages in comparison to metal or other commercially available polymeric wires; tensile strength and fatigue strength are substantially increased. Slight creep behavior is to be expected from a knotted UHMWPE wire in comparison to a metal wire due to their intrinsic properties, but the novel radiopaque UHMWPE wire shows superior or at least equivalent performance to the SecureStrand™ UHMWPE cable. The novel radiopaque UHMWPE wire may find wider application in the field of orthopedic surgery, like in the design of a cerclage cable to fixate periprosthetic fractures in trauma surgery. This is the first study to assess the mechanical properties of a novel radiopaque woven UHMWPE sublaminar wire, which has potential for widespread application in the field of orthopedic surgery.

References

1. Albert MC, LaFleur BC. Hybrid fixation with sublaminar polyester bands in the treatment of neuromuscular scoliosis: a comparative analysis. *J Pediatr Orthop* 2015;35:172-7.
2. Bogie R, Roth A, Faber S, et al. Novel Radiopaque UHMWPE Sublaminar Wires in a Growth-Guidance System for the Treatment of Early Onset Scoliosis: Feasibility in a Large Animal Study. *Spine (Phila Pa 1976)* 2014.
3. Dickman CA, Papadopoulos SM, Crawford NR, et al. Comparative mechanical properties of spinal cable and wire fixation systems. *Spine (Phila Pa 1976)* 1997;22:596-604.

UHMWPE Wear Debris Induced Vascularization, Inflammation & Innervation after TDR

Veruva SY,¹ Lanman TH,² Isaza JE,³ Freeman TA,⁴ Kurtz SM,^{1,5} Steinbeck MJ¹

¹School of Biomedical Engineering, Science and Health Systems, Drexel University, Philadelphia, PA

²Department of Surgery, University of California Los Angeles, Los Angeles, CA, USA

³Tulane University, Baton Rouge, LA, USA

⁴Department of Orthopaedic Surgery, Thomas Jefferson University, Philadelphia, PA

⁵Exponent, Inc. Philadelphia, PA

syy23@drexel.edu

Introduction

The pathophysiology of low back pain remains poorly understood [1], and even less is known about mechanism(s) involved in the generation of unintended pain after metal-on-UHMWPE total disc replacement (TDR). The normal human lumbar disc consists of an avascular/aneural nucleous pulposus, and a surrounding annulus fibrosus that is not highly vascularized or innervated [2]. Painful disc degeneration has been associated with innervation by sensory nerve fibers, which follow the path of ingrowing blood vessels into disc tissue [3, 4]. This process can be further exacerbated by inflammatory cell infiltration and the release of factors that ultimately lead to pain sensitization. In a previous study, we reported an increase in vascularization and inflammation in TDR revision tissues [5]. Thus, it was hypothesized that biological reactions to UHMWPE wear debris in the lumbar spine result in the production and interplay between key biochemical mediators that contribute to neurovascular and neuroinflammatory invasion, and the development of pain. In this study, we evaluated periprosthetic tissues collected at the time of TDR revision surgery using immunohistochemistry (IHC) to quantify the levels of select vascularization, inflammation, and innervation factors that are known to play a direct role in the mediation of pain. Understanding the biological responses and factors present in TDR periprosthetic tissues will enable us to discover the mechanistic pathways that link UHMWPE wear debris to pain, and allow us to identify potential diagnostic biomarkers that can serve as quantifiable measures of pain. It will also provide information needed to identify therapeutic targets and treatment strategies to mitigate chronic pain after TDR.

Materials & Methods

Patients and Tissue Collection

Tissues were evaluated from three patient groups: periprosthetic tissue samples (n=30) obtained at revision of contemporary metal-on-UHMWPE TDRs from 11 patients (implantation time 1.2-6.0 yr, average 3.3 yr); painful degenerative disc disease (DDD) tissue samples (n=3) obtained from patients exhibiting pain at the time of initial TDR surgery; and normal disc tissue samples (n=2) obtained at autopsy from patients with no clinical history of back surgery. Periprosthetic revision and initial TDR surgical tissues were collected by Dr. Todd H. Lanman, Beverly Hills, CA or by Dr. Jorge E. Isaza, Baton Rouge, LA, as part of a public, multi-center retrieval research program initiated in 2004 [6]. Normal disc tissues samples were obtained from the Cooperative Human Tissue Network (CHTN) of the National Institutes of Health, Bethesda, MD.

Immunohistochemistry

IHC was performed to evaluate the expression of six secretory factors: vascularization factors, VEGF (Rabbit IgG, Santa Cruz) and PDGFbb (Rabbit IgG, Abcam); pro-inflammatory cytokines, TNF α (Rabbit IgG, Novus Biologicals) and IL-1 β (Rabbit IgG, Abcam); and pain-related factors, NGF (Rabbit IgG, Abcam) and substance P (Rabbit IgG, EMD Millipore). Optimal conditions for each antibody were first determined. The antibody concentrations were: VEGF 1:100, PDGFbb 1:100, TNF α 1:100, IL-1 β 1:400, NGF 1:500, substance P 1:500. Slides with tissues originally fixed in formalin, as opposed to UMFIX (Sakura Finetek, Torrance, CA), were first treated with an antigen retrieval solution (Vector Labs). All slides were incubated in 0.5% Triton in PBS to enhance permeability, 3%

H₂O₂ in methanol to block endogenous peroxidases, and to block non-specific background in 4% BSA, 0.1% Tween-20 in PBS. Lastly, slides were incubated at 4°C overnight with the primary antibodies. For antibody visualization, samples were incubated with pan-specific secondary antibody, followed by horseradish peroxidase (Santa Cruz) and DAB solution (Vector Labs), and then counterstained with 50% hematoxylin.

Image Analysis

Each stained tissue section was imaged (200X) using an Olympus BX50 microscope (Melville, NY, USA) equipped with a stepper motor-controlled stage. DAB staining was determined by first employing a customized image-threshold operation programmed in MATLAB® (MathWorks Inc, Natick, MA), followed by measuring DAB positive area using NIH ImageJ (National Institutes of Health, Bethesda, MD). In brief, the red, green and blue channels for the 24-bit bright field DAB-labelled images were normalized by the sum of the three channels. Pixel values for 8-bit images were calculated using a published formula that allows for maximal separation of DAB-stained pixels from the background tissue [7].

Statistical Analysis

To statistically compare immunohistochemical levels for tissues from different patient groups, the Wilcoxon test was employed. Correlations for blood vessels, inflammatory cells, wear debris and the six immunohistological markers were determined using Spearman Rho correlation test for non-parametric data. Significance was based on p<0.05.

Results

The mean percent area of expression for VEGF (p=0.04), IL-1 β (p=0.01) and substance P (p=0.01) were significantly higher in TDR tissues when compared to tissues obtained from DDD patients. PDGFbb (p=0.14), TNF α (p=0.06) and NGF (p=0.19) were also increased in the TDR patient tissues. When compared to normal disc tissues, the mean percent area for all six factors was statistically increased in TDR tissues (p<0.05). Interestingly, no statistical differences were observed between DDD and normal disc tissues.

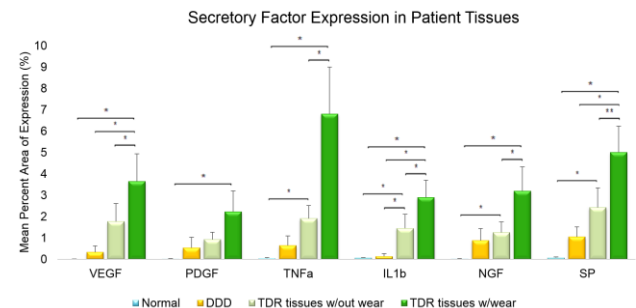


Figure 1: Mean expression of factors in tissues. *p<0.05; ** p<0.01

Based on wear debris comparisons, the expression of all factors, but PDGFbb, was significantly higher (p<0.05) in TDR tissues with UHMWPE wear particles (n=14) when compared to TDR tissues without detectable (>0.461 μ m) particles (n=16) (Fig. 1). Furthermore, the amount of UHMWPE wear debris showed a significant correlation with the percent area of VEGF (p=0.002, ρ =0.56), but not PDGFbb. Nonetheless, both factors were expressed

at low levels when no particles were present. Particles also showed a significant correlation to the percent area of both TNF α and IL-1 β ($p < 0.001$, $\rho = 0.63$; $p = 0.01$, $\rho = 0.50$). These factors were expressed at substantially lower levels when no particles were present, with the exception of highly necrotic tissues (statistical outliers).

Additional significant factor correlations in TDR tissues included NGF and substance P expression with the expression of VEGF, PDGFbb, TNF α and IL-1 β ($p < 0.001$ for all; Fig. 2). Specifically, NGF had a strongly positive relationship with the pro-inflammatory cytokines TNF α and IL-1 β ($\rho = 0.77$; $\rho = 0.79$), while substance P had a strongly positive relationship with the vascularization factor, VEGF ($\rho = 0.77$).

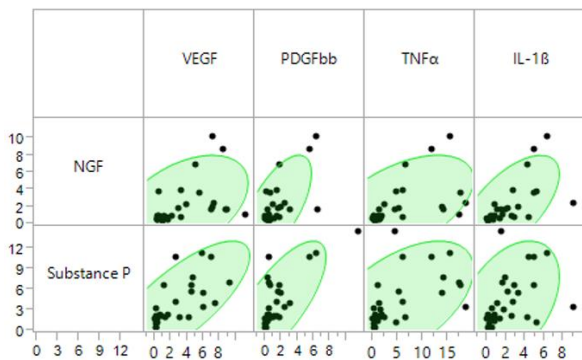


Figure 2: Spearman Rho correlations for NGF & SP

Discussion

The results support our hypothesis that UHMWPE wear-debris induced tissue reactions in the human lumbar spine can be linked to neurovascular and neuroinflammatory invasion, which may ultimately lead to the sensitization of pain. Vascularization, inflammation and innervation secretory factors were all elevated in TDR periprosthetic tissues when compared to tissues from DDD patients and normal disc tissues. Specifically, the vascularization factor VEGF and pro-inflammatory cytokines, TNF α and IL-1 β , correlated to number of UHMWPE wear particles. Furthermore, VEGF, PDGFbb, TNF α and IL-1 β expression correlated with neural innervation and the hypersensitization agents, NGF and substance P, suggesting neural-maladaptive plasticity at periprosthetic sites.

While TDR tissues are initially poorly vascularized, the generation of UHMWPE wear debris increased both vascularization and the infiltration of inflammatory macrophages. Past studies on hip and knee replacement tissues have suggested these changes are initiated by wear debris activation of fibroblasts and the subsequent secretion of the angiogenic factors, VEGF and fibroblast growth factor, and pro-inflammatory cytokines, TNF α and IL-1 β [8]. Moreover, the production of angiogenic factors lead to extensive vascularization of the periprosthetic tissue, and the recruitment of peripheral blood monocytes [9].

The current study is the first to identify vascularization and neurological factors in TDR periprosthetic tissues, however a number of studies of DDD have reported blood vessel ingrowth and inflammatory factors leading to nerve ingrowth into layers of the disc, which are then thought to result in chronic lower back pain [3, 4, 10, 11]. Specifically, NGF expression along blood vessels has been detected and co-localized to sensory nerve fibers in the annulus fibrosis and even deeper into the nucleus pulposus of the spinal disc [4]. These nerve fibers are known to produce neurotransmitters, including substance P, involved in pain transmission [12]. Inflammatory cell recruitment and TNF α and IL-1 β release can further enhance this process, ultimately stimulating the release of more NGF, substance P and other neural factors [13].

Altogether, the current findings, combined with previous research, suggest a possible signaling cascade starting with UHMWPE wear

debris activation of resident fibroblasts, release of factors that regulate vascularization, innervation and inflammatory cell infiltration. Subsequently, fibroblasts, macrophages and nerve cells secrete NGF and/or substance P, which induce nociceptive pain (pain response to tissue damage).

The importance of NGF and substance P production in periprosthetic tissues is 2-fold. First, NGF is a known mediator of sensory and nociceptive nerve function and substance P is a sensory pain-associated neuropeptide released at synapses; thus, both contribute to hyperalgesia (increased sensitivity to pain) [14, 15]. Second, NGF can contribute to nerve ingrowth [13, 16], and without it, all sensory neurons will undergo apoptosis [17]; substance P is also involved in nerve ingrowth and is predominantly secreted at sensory nerve endings during innervation [18]. Both factors work in synergy and may be directly involved in mediating innervation and pain in the lower back [19, 20]. Taken together, their association with wear-debris induced vascularization and inflammation elucidates key mechanisms that may be involved in the development of pain in TDR patients.

Acknowledgements

Funding provided by the National Institutes of Health (NIAMS) R01 AR56264.

References

1. Mooney, V. *Ann Med*, 1989. **21**(5): p. 373-9.
2. Malinsky, J. *Acta Anat (Basel)*, 1959. **38**: p. 96-113.
3. Binch, A.L., et al. *Arthritis Res Ther*, 2014. **16**(5): p. 416.
4. Freemont, A.J., et al. *J Pathol*, 2002. **197**(3): p. 286-92.
5. Veruva, S.Y., et al. *Clin Orthop Relat Res*, 2015. **473**(3): p. 987-98.
6. Kurtz, S.M., et al. *SAS*, 2009. **3**(4): p. 161-177.
7. Brey, E.M., et al. *J Histochem Cytochem*, 2003. **51**(5): p. 575-84.
8. Tunyogi-Csapo, M., et al. *J Orthop Res*, 2007. **25**(10): p. 1378-88.
9. Koreny, T., et al. *Arthritis Rheum*, 2006. **54**(10): p. 3221-32.
10. Melrose, J., et al. *Spine (Phila Pa 1976)*, 2002. **27**(12): p. 1278-85.
11. Peng, B., et al. *J Bone Joint Surg Br*, 2005. **87**(1): p. 62-7.
12. Ashton, I.K., et al. *J Orthop Res*, 1994. **12**(2): p. 186-92.
13. Abe, Y., et al. *Spine (Phila Pa 1976)*, 2007. **32**(6): p. 635-42.
14. Ahmed, M., et al. *Spine (Phila Pa 1976)*, 1993. **18**(14): p. 2121-6.
15. Lewin, G.R., A.M. Ritter, and L.M. Mendell. *J Neurosci*, 1993. **13**(5): p. 2136-48.
16. Korsching, S. and H. Thoenen. *Proc Natl Acad Sci U S A*, 1983. **80**(11): p. 3513-6.
17. Freeman, R.S., et al. *Prog Brain Res*, 2004. **146**: p. 111-26.
18. Wojtys, E.M., et al. *Arthroscopy*, 1990. **6**(4): p. 254-63.
19. Verge, V.M., et al. *J Neurosci*, 1990. **10**(3): p. 926-34.
20. Richardson, S.M., et al. *Arthritis Res Ther*, 2009. **11**(4): p. R126.



SESSION
SIX:

**New Frontiers in
UHMWPE:
Fibers and
Beyond**

Advances in Medical-Grade UHMWPE Fiber Development: Additives for Visualization

H. Smelt¹, K. Boon-Ceelen¹, L. Panella¹, P. de Bueger¹

¹DSM, Geleen, NL

harold.smelt@dsm.com

Introduction: Since long, molded UHMWPE is the material of choice for total joint replacements in orthopedic surgery. UHMWPE fibers are also attractive for medical applications and, because of their strength, flexibility and durability, they have become the gold standard for high-strength orthopedic sutures.

Naturally, UHMWPE fiber has a white color. However, for differentiation between multiple sutures, the availability of several fiber colors is desirable since it allows multiple suture designs¹. For example, for rotator cuff soft tissue repair, a device equipped with multiple colored sutures is used to facilitate the surgeon during the procedure. Intrinsically, UHMWPE fiber also lacks radiopacity and therefore the possibility for adequate postoperative radiological assessment. A radiopaque UHMWPE fiber can potentially replace metal wire in the design of trauma or spine applications².

This abstract summarizes the latest advancements in the visualization of medical-grade UHMWPE fiber technology and its use in medical applications. The examples provided relate to the development of both a blue and a radiopaque UHMWPE fiber.

Methods and Materials: UHMWPE fiber's chemical inertness and high crystallinity makes it a difficult material to dye. The very low percentage of amorphous or semi-crystalline phase and the apolar nature of the aliphatic C₂H₂ backbone of the UHMWPE polymer does not provide sufficient compatibility with most available color dyes. In this respect, the addition of the color as a pigment during the gel-spinning process would be a better alternative, as the pigment would be well dispersed in the solution of solvent and disentangled UHMWPE, facilitating a homogeneous physical incorporation. To facilitate regulatory approval, blue fibers with Chromium-Cobalt-Aluminum Oxide were produced, as this pigment is listed on the FDA's 21 CFR part 73 on *Color Additives Exempt from Certification* for coloring linear polyethylene surgical sutures for use in general surgery.



Figure 1: A braided suture made of Dyneema Purity® VG fiber containing Chromium-Cobalt-Aluminum Oxide (left) and a woven wire made of Dyneema Purity® RP fiber containing Bi₂O₃ (right).

Radiopacity can be achieved by applying a metal-containing coating on the fiber or textile construct, but to obtain sufficient radiopacity the thickness of the coating layer might compromise the fiber or textile flexibility and introduces the danger of metal based coating debris. An alternative is the integration of radiopaque particles within each fiber via the gel-spinning process. During the development of Dyneema Purity® RP fiber, a very high density radiopacifier, Bi₂O₃, was selected. The use of

such a high density radiopacifier allows to limit the total volume fraction added to the fiber to guarantee visibility, whilst preserving the fiber characteristics. From a process point of view, the density difference between the particles of Bi₂O₃ and of UHMWPE required the incorporation of excellent mixing during the gel spinning to avoid segregation during the process and final poor distribution in the fiber product. The main questions to be answered for these fibers with additives are 1) Are fiber properties affected? and 2) How are the pigment/radiopacifier particles distributed and entrapped after removal of the solvent and after the drawing process?

Therefore, the new fibers were benchmarked against natural white fibers on mechanical properties and particle release was tested by means of leaching tests following ISO 10993-12 and USP37 NF32.

Results:

The integration of particles had no negative influence on the tensile properties. Both the blue fiber and the radiopaque fiber had tensile properties in the order of 3,5-4.0 GPa, equivalent to natural white fiber without additives.

SEM images of cross and length sections showed that the integrated Bi₂O₃ particles were homogeneously distributed in the fiber (figure 2).

The leaching test according to ISO10993-12 at 50°C for 72 hours for the radiopaque fiber resulted in a maximum of 1.5 ppm Bi₂O₃ in the used extraction solvents saline, cyclohexane and ethanol based on 0.2 g sample per ml of solvent. The leaching test according to USP37 NF32 showed a transparent color extract and thus no blue pigment was extracted from the fiber based on this test method.

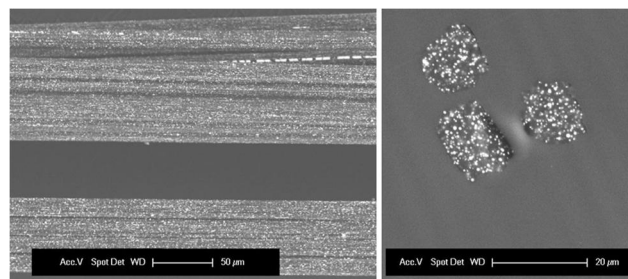


Figure 2: SEM images of filaments of UHMWPE fibers containing Bi₂O₃ (left: lengthwise; right: cross-section).

Discussion: The high crystallinity and the chemical inertness of UHMWPE fibers make it a difficult material to dye or coat to add a visualization function. The physical integration of particles forms a suitable alternative. Sufficient particles can be homogeneously integrated in the fiber for visualization. Both blue fibers, with CrCoAl pigment, and radiopaque fibers, with Bi₂O₃ particles, were produced and had comparable tensile strength levels to natural white UHMWPE fibers (> 3 GPa). The particles are well entrapped between the filaments and diffusion to the fiber surface seems difficult, as demonstrated by the leaching and extraction tests which were performed.

¹ Ceelen K et al.; Blue pigmented Dyneema Purity® fibers for arthroscopy. EORS poster2010

² Bogie R, Roth A et al. Novel Radiopaque UHMWPE Sublaminar Wires in a Growth-Guidance System for the Treatment of Early Onset Scoliosis: Feasibility in a Large Animal Study. Spine (Phila Pa 1976) 2014.

Mechanical, tribological and chemical stability performance of a novel 1-2 layered graphene/UHMWPE composites

Pascual, F.J.¹; Alonso, P.J.²; L. Quiles³; P. Castell³; Puertolas, J.A.¹

¹Department of Materials Science and Technology, I3A, Universidad de Zaragoza, Zaragoza, Spain.

²Aragón Materials Science Institute, ICMA, Universidad de Zaragoza-CSIC, Zaragoza, Spain.

³AITIIP Technological Center, Zaragoza, Spain

jpascual@unizar.es

Introduction: UHMWPE-based composites have been developed as an alternative to the current highly crosslinked UHMWPE obtained by gamma or electron beam irradiation and stabilized by thermal treatments or antioxidants [1]. The first and unique commercially available implantable-grade carbon reinforced UHMWPE was a mechanically blended short carbon fiber composite, known as Poly II [2]. Several attempts to improve the UHMWPE have been attained in the recent years by blending with carbon-based materials [3]. Graphene materials are new and potential candidates for reinforcement polymers owing to their high strength close to 130 GPa, stiffness around 1TPa and excellent thermal conductivity. In the present work, we evaluate the UHMWPE composites based on 1-2 layered graphene from a mechanical, tribological and chemical stability point of view.

Methods and Materials: Uniaxial tensile tests (n=4) were carried out according to ASTM D638M (UNE-EN ISO 527-2) in an Instron machine (model 5565) at a constant displacement rate of 10 mm/min. Izod tests were carried out by Cemitec (Noain, Spain). Differential Scanning Calorimetry (DSC) were performed heating in air from 20 to 200 °C at 10 °C/min in a Q200 Thermal Analysis DSC. Wear ball-on-disk test (n≤3) were performed in a TRB tribometer (CSM instruments, Peseux, Switzerland) for 24 hours. Rotating UHMWPE sample disks, 20 mm in diameter, were immersed in diluted bovine serum at 37°C and opposed to an alumina ball, 6 mm in diameter. The load applied was 5 N resulting in a contact pressure of 37 MPa. The radius of the circular track was 4 mm and the sliding speed was 0.05 m/s. Worn volume is calculated by confocal microscopy using a SENSOFAR PLU 2300 optical imaging profiler. Electron Paramagnetic Resonance (EPR) measurements were taken at room temperature in a Bruker Elexsys E580 spectrometer working at X-band. The microwave power was 0.2 mW and the modulation amplitude 0.1 mT. Prismatic shape samples (2x2x10 mm³) were fixed with vacuum grease to a methacrylate sample holder.

Medical grade GUR1050 UHMWPE powder was gently supplied by Celanese (Irving, USA) with an average particle size of 150 µm. The near-monolayer graphene used in this work is considered to be 1-2-layered graphene and was provided by Avanzare (Spain). It was blended with the UHMWPE to concentrations of 0.1, 0.3, and 0.5

wt% in a ball mill for 8 hours at 400 rpm to obtain a homogeneous dispersion. The consolidation process was carried out using a 15 Ton press with hot plates (Specac, UK) for 30 minutes at 175°C under 15 MPa pressure, followed by cooling in air down to 40°C under the same pressure. Samples were denoted as GUR1050+X%GR1-2L, where X stands for the weight % of reinforcements in the polymer matrix. Some composites underwent a further high temperature thermal treatment in a vacuum oven (LTE, UK) for 8 hours at 240°C and were denoted GUR1050+X%GR1-2L HT. Some specimens were gamma irradiated in Aragogamma (Spain) to a final dose of 90 kGy.

Results: Tensile performance of the untreated composites showed a slight increase in secant modulus for all GR1-2L amounts and yield stress remained unchanged. However, fracture stress, fracture strain and work to fracture decreased as additive amount increased. For example, at the lower concentration, 0.1 wt%, the decrease was about 20%. Conversely, Izod impact toughness pertained the unloaded metrics until the 0.5 wt%, where a diminution of about 40% arisen. When thermal treatment is considered, both secant modulus and yield stress underwent a considerable increase of 30% and 10%, respectively, for all the percentages. For the 0.1 wt% composite, fracture stress, fracture strain and work to fracture kept similar values to the pristine GUR1050 while Izod impact toughness increased about 10%. On the other hand, the 0.5%wt composite showed a reduction of about 20% in fracture stress, fracture strain and work to fracture compared to pristine polyethylene. Compared to the thermally untreated equivalent, the improvement in properties is evident, ranging from 20-50%.

From DSC data, we can infer that T_m (136.9 °C) and the degree of crystallinity (48.1 %) practically remain constant with the addition of GR1-2L up to 0.5 wt %. High temperature thermal treatment increases the T_m about 1.25 °C, the crystallinity in about 2% for the composites.

Ball-on-disk tribological tests reveal that coefficient of friction did not show any significant difference for the untreated composites. However, a strong reduction (about 50%) in friction coefficient of the composites when the high temperature thermal treatment was applied, as shown in Table 1. Worn areas considered to be the “flooded” area, i.e. the area results from subtracting the area placed

over the surface level of the unworn sample from the total worn area.

Table 1. Friction coefficient (μ) and wear factor (k) of GUR1050/GR1-2L composites.

Material	μ (2000-4000 m)	$k \cdot 10^{-6}$ (mm^3/Nm)
GUR1050	0.085 ± 0.013	2.41 ± 0.07
GUR1050+0.1%GR1-2L	0.093 ± 0.023	2.60 ± 0.45
GUR1050+0.3%GR1-2L	0.087 ± 0.007	2.44 ± 0.75
GUR1050+0.5%GR1-2L	0.082 ± 0.016	2.51 ± 0.98
GUR1050 HT	0.059 ± 0.002	N/A
GUR1050+0.1%GR1-2L HT	0.047 ± 0.002	N/A
GUR1050+0.3%GR1-2L HT	0.047 ± 0.002	N/A
GUR1050+0.5%GR1-2L HT	0.049 ± 0.002	N/A

In order to study chemical stability, EPR spectra have been measured before and after irradiating the samples. Prior to irradiation, no signals were detected in any case while a complex spectrum was observed after irradiating the sample with a 90 kGy dose. Figure 1 show the spectra observed in composite samples with different content of 1-2 layered graphene. For comparison purposes the EPR spectra of pristine UHMWPE (PE) and of a MWCNT/UHMWPE composite with a 0.5 % content of Nanocyl™ NC7000 labelled as NCYL) have been also include in the figure. The spectra observed in all the cases are similar and they consists of a dominant central signal ($g \approx 2$, and a peak-to-peak width of about 1 mT), labelled with S, and other one with complex structure that is marked with stars, similar to observed in [4]. So, the star-labelled signal is associated to more stable polyallyl radicals and the S-labelled one to oxygen-centered radicals [5]. However the relative intensities of these contributions are markedly different that that previously found. The S signal results dominant in the present case while the polyallyl contribution is markedly lower. Moreover no intensity variation is observed in this last signal with the addition of either CNT or different amounts of graphene.

On the other hand the intensity of the S-signal is affected by the presence of the carbonaceous materials. Its intensity decreases as the graphene content increases. It has been summarized in Figure 2 where the peak-to-peak height (Y_{pp}) of the S-signal (normalized to its values in neat UHMWPE) is plot as a function of the graphene content. However this decrease is less than that found when CNT are added as it is depicted by open circles.

Conclusion: The present work proposes a high temperature thermally treated 1-2 layered-graphene/UHMWPE composite as an alternative to current HXLPS.

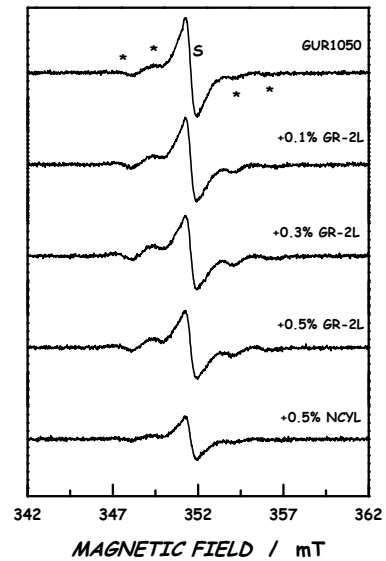


Figure 1. EPR spectra of γ -irradiated samples.

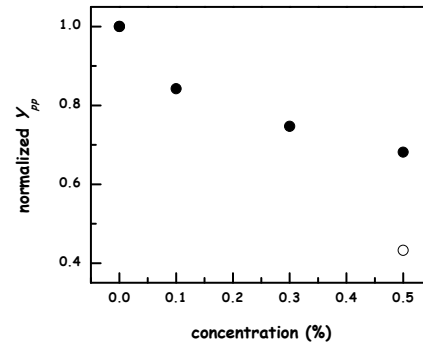


Figure 2. Normalized peak-to-peak height (Y_{pp}) of the S-signal for the GR1-2L/UHMWPE composites.

A very strong reduction in friction coefficient ($\approx 50\%$) and a noticeable improvement in secant modulus ($\approx 30\%$) and yield stress ($\approx 10\%$) have been found. Additionally, in EPR tests, it has been found a reduction in free radicals when the composite is γ -irradiated comparable to the MWCNT/UHMWPE one. Additional studies concerning bioactivity of wear debris should be programmed before to consider the proposed composite material as a potential substitute to highly crosslinked UHMWPEs.

References:

- [1] Kurtz S, UHMWPE Biomaterials Handbook. AP 2009.
- [2] Farling G, inventor; Zimmer Inc., assignee. (1977) U. S. Patent No. 4, 055,862. [3] Puértolas JA and Kurtz SM. J Mech Behav Biomed Mater 39 (2014) 129-145. [4] Potts JR, Polymer 52 (2011) 5-25. [5] Martínez-Morlanes MJ et al. Carbon 50 (2012) 2442-2452. [6] Castel P et al. J. Mater Sci. 48 (2013) 6549-6557.

Effect of Supercritical Fluid Sterilization on Microstructure and Properties of Porous UHMWPE

Senatov F.S.¹, Maksimkin A.V.¹, Zalepugin D.Yu.², Chernyshova I.V.², Tilkunova N.A.², Anisimova N.Yu.³, Kiselevsky M.V.³, Tcherdyntsev V.V.¹, Senatova S.I.¹, Kaloshkin S.D.¹

¹ National University of Science and Technology "MISIS", Moscow, Russian Federation

² State Plant of Medicinal Drugs, Moscow, Russian Federation

³ N.N. Blokhin Russian Cancer Research Center, Moscow, Russian Federation

Senatov@mis.ru

Introduction:

Ultra-high molecular weight polyethylene (UHMWPE) is a widely used material for implantology because of bioinertness and high mechanical properties. UHMWPE porous structure simulating cancellous bone tissue provides osteoconductive properties and acts as the substrate for cells adhesion and new bone formation for reparative osteogenesis.

Implants may introduce pathogens into the body from their surfaces. Therefore, in order to minimize the number of pathogenic microorganisms sterilization of the implant before the surgery is carried out. The most common method of sterilization of UHMWPE products is a radiation method, which consists in irradiating of the implant by γ -rays. The radiation causes the formation of free radicals; thereby it contributes to breaking of UHMWPE molecular chains. Degradation of the polymer causes a decrease in its properties.

An alternative method for sterilization of the material may be treatment in the supercritical fluid [1].

Methods and Materials:

In this study porous UHMWPE implants were obtained. Porosity was formed by mixing the polymer powder with soluble filler (90% wt.) and thermopressing of mixture under load of 70 MPa, followed by washing with subcritical water (water flow rate of 3 ml / min) at a temperature of 120 °C and a pressure of 250 bar to remove salt [2].

The porous UHMWPE samples were sterilized in supercritical carbon dioxide. The effect of sterilization on the microstructure of UHMWPE was studied by SEM, DSC and FT-IR spectroscopy. Mechanical properties in compression and decontamination of samples after sterilization were also studied.

Studies of decontamination UHMWPE specimens after sterilization were carried out according to the guidelines MUK 4.2.2942-11 "Methods of control. Biological and microbiological factors. Methods of sanitary-biological study of environmental objects, air and sterility control in medical organizations". Thioglycolic broth medium (to detect microaerophilic bacterial and fungal microflora) and Sabouraud broth containing the growth inhibitor of foreign microflora - potassium tellurite or chloramphenicol (psychrophilic to detect saprophytic fungal microflora) (Pronadisa, Spain) were used.

Bulk (nonporous) samples of UHMWPE were prepared to analyze the depth of penetration of supercritical fluids. The treated layer was colored with orange dye.

Results:

Porous samples of UHMWPE were obtained with porosity of 79 % vol. Pores are open and interconnected with size of 80-700 microns as shown in Figure 1.

Compressive strength at 40% strain for UHMWPE with high porosity was 1.36 MPa; Young's modulus in compression - 14.3 MPa. Sterilization by supercritical CO₂ had no effect on mechanical properties of UHMWPE samples.

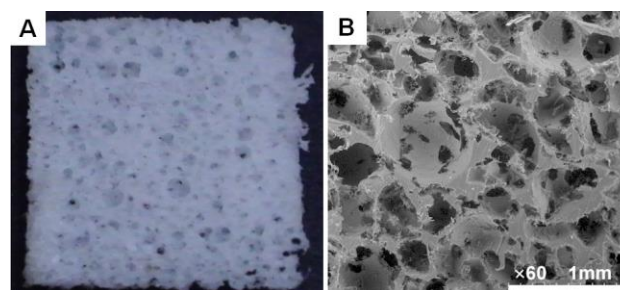


Fig.1 – Porous UHMWPE: photograph (A) and SEM microphotograph (B)

There was no contamination of fungal and bacterial microflora after sterilization with supercritical CO₂. The lack of colony forming in thioglycolic broth and Sabouraud broth after 14 days of cultivation was observed as shown on Figure 2.

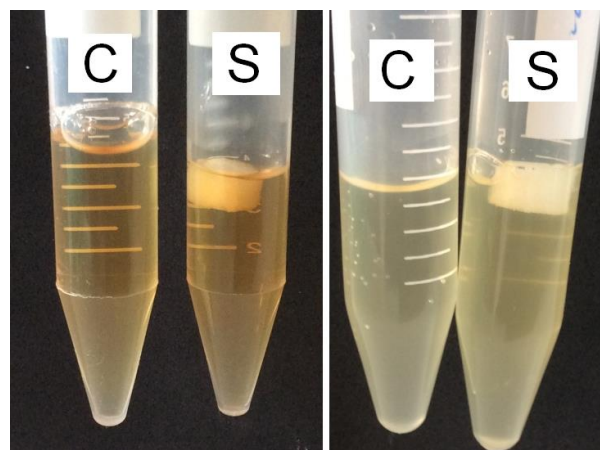


Fig.2 – Control (C) and porous UHMWPE sample (S) in thioglycolic broth (left) and Sabouraud broth (right) after 14 days of cultivation

Treatment with supercritical fluids led to deep penetration of CO₂ as it was shown in Figure 3.

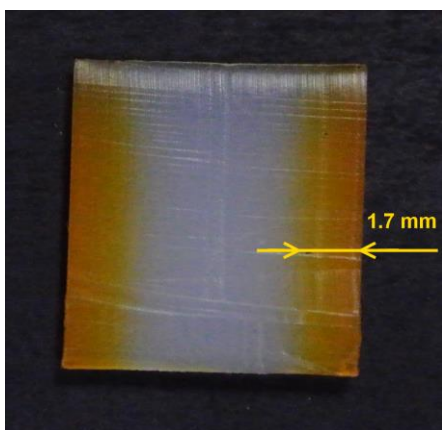


Fig.3 – Nonporous UHMWPE sample after treatment with supercritical fluids. The depth of penetration of the fluid is shown with orange color

Discussion:

Porous UHMWPE samples were obtained by treatment with soluble filler (salt) in planetary ball mill and washing out with subcritical water. Mechanical activation in planetary ball mill may lead to varying of pore size by grinding of salt particles. Mechanical activation with high energy intensity may also lead to the formation of low molecular weight polymer chains which help to increase the rate of interdiffusion between the borders of the polymer particles and lead to better sintering of UHMWPE particles and higher mechanical properties [4-6].

The obtained results of the analysis of UHMWPE samples with high porosity showed no signs of colony formation of bacteria and fungi in specialized growth medium and showed no contamination of the samples with microflora after sterilizing treatment by supercritical carbon dioxide. Deep penetration (1.5-2 mm) of CO₂ into bulk nonporous UHMWPE samples was observed. However, it is important to note that at the end of the sterilization supercritical fluid was completely out of the structure of UHMWPE, without creating additional porosity, which was confirmed by microscopy.

Acknowledgements

This work is supported by the Federal Targeted Program “Research and development in priority directions of development of scientific technological complex of Russia in 2014–2020 years”, with the financial support from the Ministry of Education and Science of Russian Federation: agreement 14.578.21.0055, 19 September 2014. Unique identifier of applied scientific researches: RFMEFI57814X0055.

[1] Silva M.J. et al. Effect of pressure, depressurization rate and pressure cycling on the inactivation of *Escherichia coli* by supercritical carbon dioxide // *Food Control*. –2013. –V.29.No.1. –P.76-81

[2] D.Yu. Zalepugin et al. The use of subcritical water in the technology of porous ultrahigh molecular weight polyethylene obtaining // *Russian Journal of Physical Chemistry B*. (in print)

[3] Senatov F.S., Gorshenkov M.V., Kaloshkin S.D., Tcherdyntsev V.V., Anisimova N.Yu., Kopylov A.N., Kiselevsky M.V. Biocompatible polymer composites based on ultrahigh molecular weight polyethylene perspective for cartilage defects replacement / *Journal of Alloys and Compounds*, 586 (2014) S544–S547

[4] F.S. Senatov, M.V. Gorshenkov, V.V. Tcherdyntsev, S.D. Kaloshkin, V.A. Sudarchikov. Fractographic analysis of composites based on ultra high molecular weight polyethylene // *Composites Part B*, 56 (2014) 869–875

[5] F.S. Senatov, A.A. Baranov, D.S. Muratov, M.V. Gorshenkov, S.D. Kaloshkin, V.V.Tcherdyntsev. Microstructure and properties of composite materials based on UHMWPE after mechanical activation // *Journal of Alloys and Compounds* (2014), 615 S1, pp. 573-577

[6] F.S. Senatov, A.N. Kopylov, N.Yu. Anisimova, M.V. Kiselevsky, A.V. Maksimkin. UHMWPE-based nanocomposite as a material for damaged cartilage replacement / *Materials Science and Engineering C* 48 (2015) 566–571

Prevention of bacterial adherence and biofilm formation on implant surface by a highly hydrophilic and electrically neutral phospholipid polymer layer

Kyomoto M^{1,2,4}, Shobuike T⁵, Moro T², Yamane S^{1,2,4}, Tanaka S³, Miyamoto H⁵, Ishihara K¹

¹Department of Materials Engineering, School of Engineering; ²Division of Science for Joint Reconstruction, ³Sensory and Motor System Medicine, Graduate School of Medicine; The University of Tokyo, Tokyo, Japan

⁴Research Department, KYOCERA Medical Corporation, Osaka, Japan

⁵Department of Pathology and Microbiology, Faculty of Medicine, Saga University, Saga, Japan

kyomoto@mpc.t.u-tokyo.ac.jp

Introduction: Three major complications, i.e., aseptic loosening, dislocation, and infection, greatly limit the duration and clinical outcomes of total hip arthroplasty. Implant-related infection is also a serious issue and often results in septic failure. Hence, in the construction of artificial hip joint replacements, the surface and substrate of a cross-linked polyethylene (CLPE) liner are designed to achieve high wear resistance and prevent infection by bacteria. Our ultimate goal in manipulating the surface and substrate of the CLPE liner was not just to obtain high wear resistance, but also high antibiofouling and anti-infection properties for life-long orthopedic bearings. In this study, we fabricated a highly hydrophilic and antibiofouling poly(2-methacryloyloxyethyl phosphorylcholine [MPC]) (PMPC)-graft layer on the vitamin E-blended CLPE (HD-CLPE(VE)) surface [1].

Methods and Materials: Compression-molded bar stock of 0.1 mass% of vitamin E-blended polyethylene (GUR1020E resin) was irradiated with a high dose of gamma-rays (100–150 kGy) and annealed at 120°C for 12 hours for cross-linking (HD-CLPE(VE)). As the control, a

compression-molded bar stock of PE without any additives (GUR1020 resin) was irradiated with a 50-kGy dose of gamma-rays and annealed to facilitate cross-linking (CLPE). HD-CLPE(VE) coated with benzophenone were immersed in a 0.5 mol/L aqueous MPC solution. The photo-induced graft polymerization on the HD-CLPE(VE) surface was carried out under ultraviolet irradiation of 5 mW/cm² at 60°C for 90 min (PMPC-grafted HD-CLPE(VE)). All samples were then sterilized by gamma-ray irradiation under N₂ gas.

Surface properties of the samples were examined by static water-contact angle and surface zeta-potential measurements. Surface morphologies were analyzed using atomic force microscopy (AFM). The amount of protein (bovine serum albumin or bovine blood γ -globulins) adsorbed on the surfaces was measured by the micro bicinchoninic acid (BCA) method. Two gram-positive bacteria strains, i.e., *Staphylococcus aureus* UOEH6 and NBRC12732 (ATCC 6538P), were used in this experiment. To allow adhesion to the disk samples, 10⁸ bacterial cells were inoculated on the disk samples in 24-well plates and incubated for 1 h at 37°C. To allow biofilm formation, 3 ×

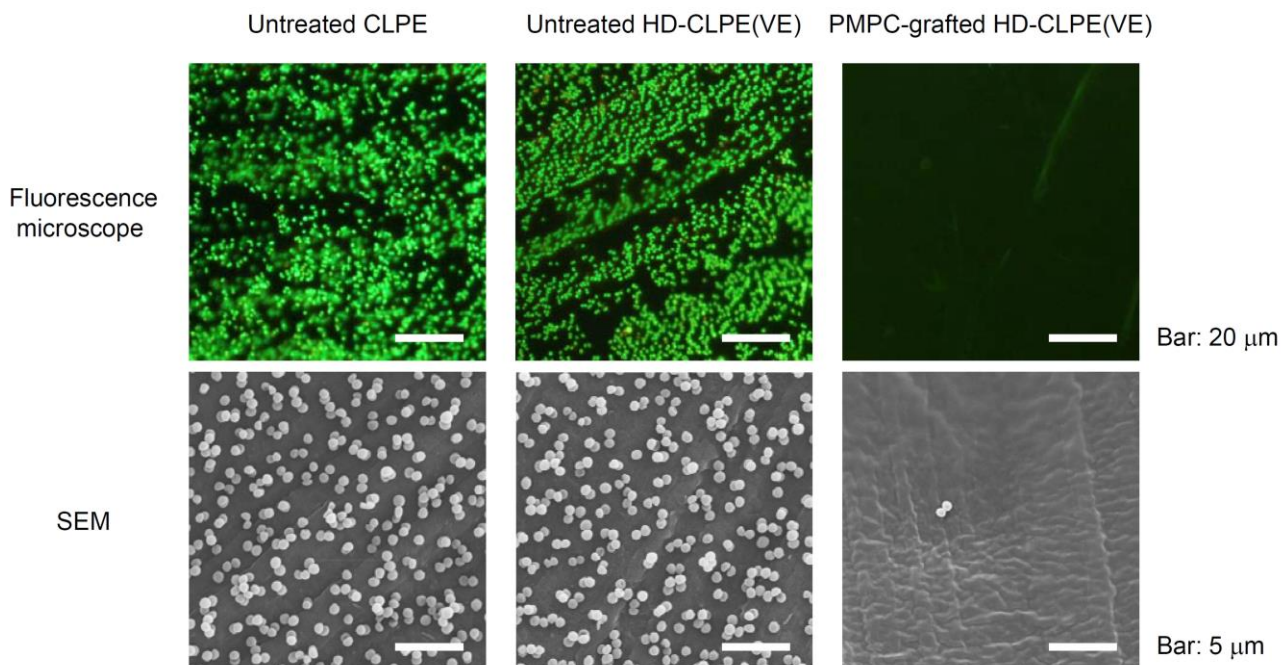


Figure 1. Adherence of biofilm-producing *Staphylococcus aureus* (UOEH6) on the CLPE, HD-CLPE(VE), and PMPC-grafted HD-CLPE(VE) after 1 h of incubation. (A) Fluorescence microscope and SEM images of bacteria-adherent surfaces.

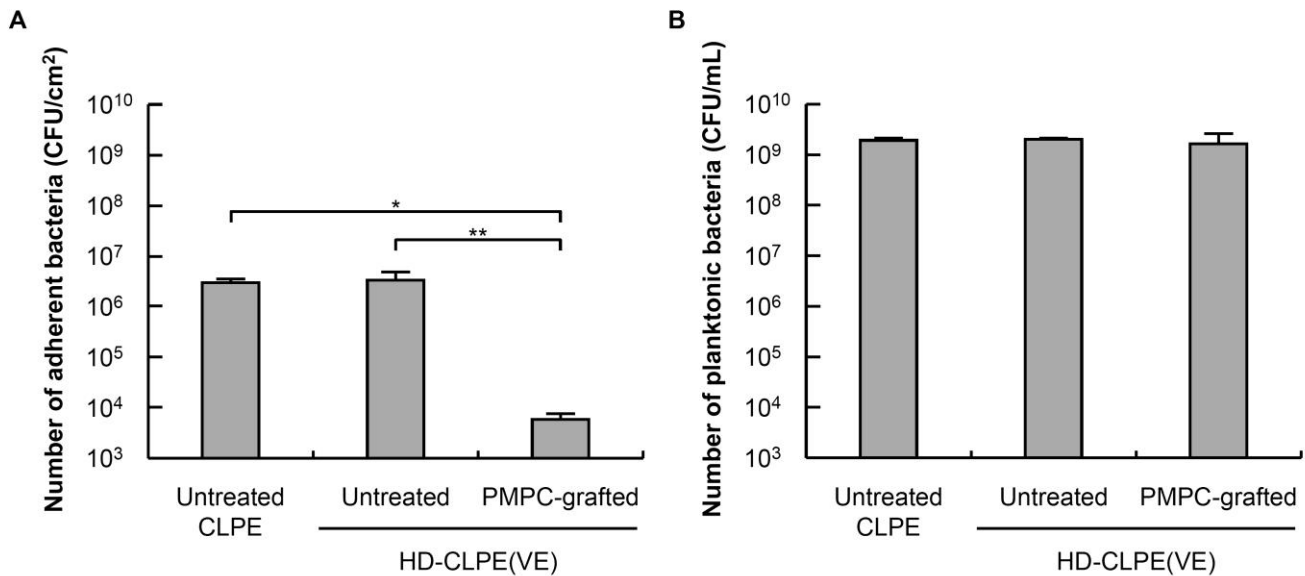


Figure 2. Numbers of (A) adherent and (B) planktonic bacteria on the CLPE, HD-CLPE(VE), and PMPC-grafted HD-CLPE(VE) after 1 h of incubation. Data are expressed as means \pm 95% confidence intervals. * indicates $p < 0.05$, ** indicates $p < 0.01$.

10^6 bacterial cells were inoculated on the disk samples and incubated for 24 h at 37°C. Disk samples were analyzed using fluorescence microscopy and SEM, and the numbers of adherent and planktonic bacteria were counted.

Results: The 100-nm-thick, smooth (surface roughness $<$ approximately 1 nm), highly hydrophilic (water contact angle $<$ approximately 30°), and electrically neutral (surface zeta-potential = almost zero) PMPC layer was successfully fabricated on the HD-CLPE(VE) surface using photoinduced graft polymerization. Only the surface modification by PMPC resulted in high antibiofouling, which can serve as an extremely efficient antibiofouling layer. The amount of each protein (BSA and γ -globulins) adsorbed on the surface did not differ significantly between untreated CLPE and HD-CLPE(VE) groups. In contrast, the amount of each protein adsorbed on the PMPC-grafted HD-CLPE(VE) surface was considerably lower than that on the untreated surfaces. The PMPC-grafted HD-CLPE(VE) was found to prevent bacterial adherence and biofilm formation by biofilm-producing and non-producing *Staphylococcus aureus* on the surface (Figs. 1&2). The number of bacterial adhered on the PMPC-grafted HD-CLPE(VE) surface was reduced by 100-fold or more by PMPC grafting, regardless of the biofilm-production characteristics of the strains. In contrast, vitamin E blending did not affect bacterial adhesion. Moreover, the number of planktonic bacteria did not differ significantly, regardless of PMPC grafting and vitamin E blending. Similar interactions of stable bacterial adhesion of *Staphylococcus aureus* were observed. The extent of biofilm formation was observed on the untreated CLPE and HD-CLPE(VE) surfaces after 24 h of incubation. In contrast, after PMPC grafting, very few observable bacteria were adhered on the PMPC-grafted HD-

CLPE(VE) surface. Significantly different numbers of dislodged bacteria colonies by biofilm formation were achieved on surfaces with and without PMPC grafting, highlighting that the bacterial adhesion capacity of *Staphylococcus aureus* significantly lower on the PMPC-grafted HD-CLPE(VE) surface compared with those on both the untreated surfaces, regardless of the biofilm production capacity of the strains. Indeed, the number of stable bacteria adhering to PMPC-grafted surfaces was decreased by 1000-fold.

Discussion: Since bacterial adhesion is a multifactorial process, it was not surprising that the benefits of PMPC surface layer were associated with the characteristics of the surface, including the smoothness, hydrophilicity, and electrostatic charge, affecting nonspecific bacterial adhesion and biofilm formation [2]. In conclusion, the PMPC-grafted HD-CLPE(VE) provided bacteriostatic effects associated with smooth, highly hydrophilic surfaces with a neutral electrostatic charge owing to the zwitterionic structure of the MPC unit. Thus, this modification may prove useful for the production of artificial hip joint replacement materials.

References:

- [1] Kyomoto M, et al., Poly(2-methacryloyloxyethyl phosphorylcholine) grafting and vitamin E blending for high wear resistance and oxidative stability of orthopedic bearings. *Biomaterials* 2014;35(25):6677-6686.
- [2] Kyomoto M, et al., Prevention of bacterial adherence and biofilm formation on a vitamin E-blended, cross-linked polyethylene surface with a poly(2-methacryloyloxyethyl phosphorylcholine) layer. *Acta Biomater* 2015, in press.

Woven UHMWPE fibers for use in cardiovascular applications

K. Boon-Ceelen¹, H. Smelt¹, P. Gründeman²

¹DSM, Geleen, NL; ²Utrecht University Medical Center, NL
karlien.boon-ceelen@dsm.com

Introduction: Although UHMWPE has been used for decades in various kinds of implants with satisfactory results, its use in cardiovascular applications has been limited. For heart valve replacement surgery, both mechanical heart valves and biological valves with leaflets of bovine or porcine origin are currently in use. Mechanical heart valves have lifelong durability, but require lifelong strong anticoagulant therapy and cannot be folded for transcatheter based implantation. In contrast, biological valves don't require anticoagulants, suffer from moderate durability, but can be implanted via transcatheter approach. In vascular surgery, current delivery systems for stent grafts however still have a relatively large diameter, thus limiting the patient selection.

Because of the flexibility, strength, fatigue and tear resistance of UHMWPE fibers and their good biocompatibility, a woven fabric of these fibers seems promising for use in the design of vascular and valvular constructs. They could actually combine good durability with the possibility of transcatheter implantation without the need for anticoagulants. To investigate this, in vitro bio-/hemocompatibility tests were done, followed by an in vivo study with a handmade stented heart valve prototype made out of thin woven fabric of Dyneema Purity[®] fibers.

Methods and Materials: First, the following in vitro hem-/biocompatibility tests were done: 1) Platelet adhesion on filaments of polyester and UHMWPE fibers and 2) Plasma thrombin generation, platelet and erythrocyte adhesion and bacterial adhesion on woven fabric of UHMWPE fibers and commercially available polyester and ePTFE cardiovascular patches.

Secondly, a woven fabric was made out of Dyneema Purity[®] TG 10dtex fibers. This fabric was implanted as a patch in the carotid artery of sheep with follow-up times of 1 and 6 weeks. No anticoagulation other than aspirin was used. Commercial ePTFE cardiovascular patches were used as reference materials. Histological analysis was performed at 1 and 6 weeks to analyze healing and new tissue formed.

Thirdly, a handmade stented heart valve prototype was constructed with this fabric, using UHMWPE sutures (figure 1). No surface modification was applied. This valve was tested in an in vitro mock circulation test (80 bpm, 88mmHg afterload) to check its opening and closing behavior as well as its durability. Subsequently, 16 sheep were implanted with this valve in pulmonary position with follow-up times of 1 week and 1, 3 and 6 months. Again, no anticoagulation other than aspirin was used during implantation and follow-up. Biological valves were implanted in reference animals. Echocardiography, histology and X-ray were used to assess valve function and tissue deposition.



Figure 1 Stented heart valve made of fabric of UHMWPE fibers.

Results: The results obtained from the in vitro hem-/biocompatibility studies showed that Dyneema Purity[®] fibers performed at least on the same level as the reference materials in all of these tests.

The patch implantation studies showed anatomical healing of the arteries without intimal hyperplasia, endothelial cells were observed and there was no calcification.

The heart valve in the mock circulation showed good opening and closing behavior and survived more than 7 million cycles without any visual damage, after stopping these tests.

All animals implanted with the heart valve survived in good health without clinical signs of thrombo-embolization in the lungs. All explanted heart valves were fully intact (commissures, sutures, free edges and leaflets). Echocardiography, after implantation, confirmed in vivo good opening and closing behavior of the valve (figure 2).



Figure 2 Echo of heart valve in closed position (left) and explanted valve after 3 months (right).

From 3 to 6 months, leaflet flexibility decreased due to tissue deposition, which lead to leaflet retraction and some insufficiency in leaflet closure at 6 months. Histology showed organization of the adhered tissue over time and endothelial cells after 1 month. X-ray confirmed the absence of calcification.

Of the biological control valves, one was severely stenotic, requiring early termination of the animal after 4 months. The other control valves were competent after 3 and 6 months.

Discussion: All the above tests confirm that a woven fabric of Dyneema Purity[®] fibers seems a promising material for use in mentioned cardiovascular applications. In vitro results qualified the material for in vivo animal testing. The patch implantation study showed anatomical healing after 6 weeks. Valve implantation, in a worst-case scenario of testing in a low-pressure condition with only antiplatelet therapy, showed that the currently tested novel UHMWPE valve concept performed satisfactorily without any visual signs of physical damage to the valve after 6 months. Intact endothelialized UHMWPE valves showed acceptable function, with some insufficiency at 6 months related to tissue overgrowth.

The promising results of this study for the use of UHMWPE fibers in the design of cardiovascular applications allow for further investigation of fabric type, design concepts and implantation locations.



Poster
Presentations

Improvements in Efficiency of Oxidation Index and Trans-Vinyl Index Measurements by FTIR in UHMWPE

Abshagen, S; Besemer, D; Grosjean, B; Mimnaugh, B; Rufner, J.

Zimmer Biomet, P.O. Box 708, Warsaw, IN 46581-0708

scott.abshagen@zimmerbiomet.com

Introduction: Two of the key factors that influence the clinical performance of orthopedic ultra-high molecular weight polyethylene (UHMWPE) are oxidation and the degree of crosslinking, which are quantifiable using Fourier transmission infrared spectroscopy (FTIR) [1-2]. Oxidation index (OI) measures the amount of oxidation in a sample and trans-vinylene index (TVI) measures the degree of crosslinking.

Current ASTM standards stipulate a minimum of 32 scans per spectrum [3-4]. This study compares the data acquired using 16 and 32 scans and demonstrated that 16 scans can significantly reduce OI and TVI analysis time, without sacrificing the quality of the results.

Methods and Materials: The samples were UHMWPE knee inserts (Figure 1). OI was measured in an aged conventional UHMWPE sample at various depths below the articulating surface. TVI was measured using three crosslinked UHMWPE samples, each representing a different radiation dose.

200 μ m thick films were microtomed from each knee, roughened on both sides using 400-grit paper, and rinsed with dichloromethane.

The microtomed films were analyzed using a Bruker Vertex 70 infrared spectrometer with a Hyperion microscope. The instrument settings included a resolution of 4 cm^{-1} and a rectangular aperture of approximately 200 μ m by 200 μ m. Data were collected at a 200 μ m step size, creating a profile through the thickness of the sample.

Testing for each sample was repeated 10 times at both 16 and 32 scans per spectrum. The x-y microscope stage coordinates were maintained to ensure that the same linear mapping path was used across the sample.

The spectra were integrated using peak area absorbance. OI was calculated using the integration limits 1850-1650/1392-1330 cm^{-1} . TVI was calculated using the integration limits 980-947/1392-1330 cm^{-1} . These values were normalized against the C-H peak area absorption at 1370 cm^{-1} [3-4]. All 10 data sets for each scan setting were averaged. OI results were calculated at specific depths below the articulating surface. TVI results were calculated as an average from all data points.

Results: The OI results for 16 and 32 scans produced overlapping confidence intervals at each specific depth, demonstrating method equivalency (Figure 2).

The TVI results for 16 and 32 scans produced overlapping confidence intervals for the low and medium radiation doses. The high radiation dose confidence intervals were within 0.4% of the overall mean (Figure 3).

Instrument run time at 16 scans was reduced to approximately 50% of the run time for 32 scans while maintaining equivalent results.

Figure 1: (a) Knee Insert; (b) Microtomed Film

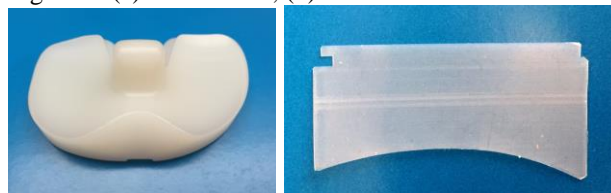


Figure 2: (a) Average OI results; (b) OI Profiles with Confidence Intervals

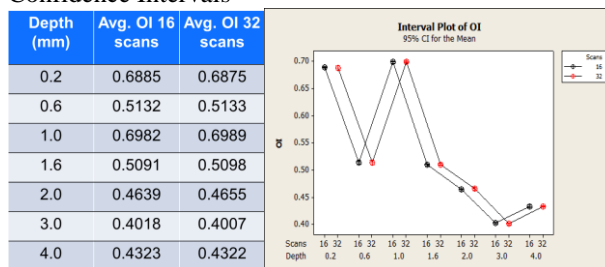


Figure 3: Average TVI results

Radiation Dose	Avg. TVI 16 Scans	Avg. TVI 32 Scans
Low: 25-37 kGy	0.0115	0.0114
Medium: 65 kGy	0.0364	0.0364
High: >110 kGy	0.0809	0.0807

Discussion: The findings demonstrated that decreasing the number of scans per spectrum had a minimal effect on both OI and TVI data. Using 16 scans gave equivalent results to 32 scans and the method was not impacted by instrument noise at lower radiation doses or various oxidation levels.

Lowering the number of scans per spectrum substantially reduced the instrument run time, which will increase the throughput of existing test methods. OI and TVI measurements are key indicators of UHMWPE performance. Improving these test methods will make new product development and retrieval studies more efficient.

References: 1. Kurtz, S.M., et al., ORS, p, 98, 1999. 2. O.K. Muratoglu and W.H. Harris, J Biomed Mater Res 56: 584-592, 2001. 3. ASTM F2102-13. 4. ASTM F2381-10.

Dose Uniformity of Commercial High Power X-Ray, in the Manufacture of Highly Crosslinked UHMWPE

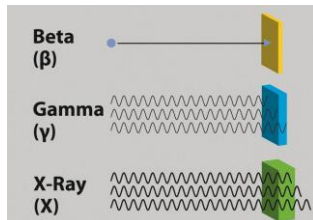
Allen M.D (mallen@orthoplastics.com)

Orthoplastics Ltd, Unit A, Beech Ind. Estate, Bacup, Lancashire, OL13 9EL, UK.

Introduction

The use of Gamma and e-Beam to manufacture highly crosslinked Ultra High Molecular Weight Polyethylene (UHMWPE) for orthopaedic applications has been undertaken historically. Recently commercial X-ray processing techniques have been developed at Synergy Healthcare (Daniken Switzerland) utilising a high energy electron beam accelerator. X-rays are produced by deceleration or deflection of energetic electrons (7 MeV) in a target material. When an electron passes close to an atomic nucleus, the strong coulomb field causes the electron to deviate its original motion.

The processing of UHMWPE is extremely difficult due to the very high density, thus attenuation occurs. However, X-rays enhanced penetrative power when compared to the alternatives yield an improved dose uniformity ratio. Therefore with a high density product the induced cross link density will be more uniform throughout the cross section and the total area processed. The purpose of this study was to evaluate the physical mechanical performance of UHMWPE processed through X-Ray and Gamma (Co₆₀) irradiation processes at different administered doses.



Materials and Methods

Compression moulded (Celanese GUR1020) was evaluated at five nominal irradiation doses (50, 75, 100, 125 and 150kGy).

X-ray processing was also conducted on three polymer lots from Celanese.

Irradiation Method	Orthoplastics Batch Ref	Celanese Polymer Batch
X-Ray	20909M	CM0000415499
X-Ray	20994M	CM0000493126
X-Ray	21036M	CM0000508571
Gamma	21016M	CM0000508571

Processing was completed on a small scale development with product 84mm Ø x 500mm

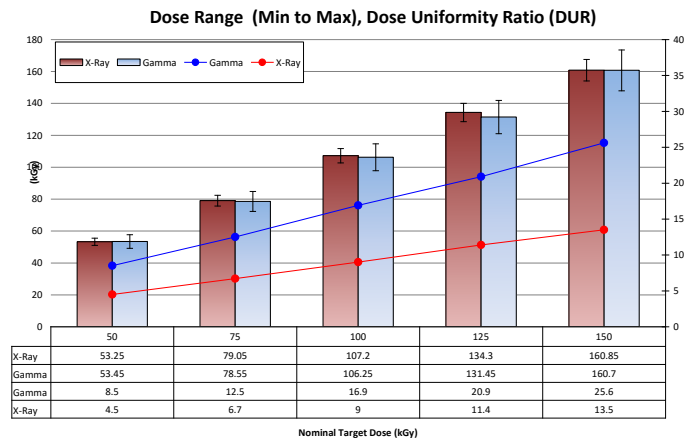
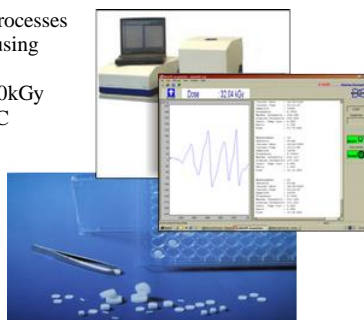
Analysis

Processed materials were analysed in accordance with the principle guidance of ASTM F2565, namely the characterisation of Extensively Irradiation-Crosslinked Ultra-High Molecular Weight Polyethylene Fabricated Forms for Surgical Implant Applications. Testing of the materials included;

Trans-Vinylene Index Analysis ASTM F2381

Results and Discussion

Both Gamma and X-Ray processes were monitored and controlled using Alanine dosimeters pellets. Pellets: dose range 10kGy to 150kGy
Temperature range -10 to +80 °C
Total uncertainty < 4 %±



The actual administered dose was calculated based upon multiple dosimeter reading from the processed bar.

The dose range (min to max) was calculated from single dosimeters reading for both X-ray and Gamma processes.

Trans-Vinylene index analysis was completed on the cross section of the material specimens from surface to core, thus evaluating attenuation and penetration.

	Gamma	X-Ray	X-Ray	X-Ray
STVI	0.04591	0.04362	0.04416	0.04348
STD	0.00589	0.00495	0.00375	0.00495
MTVI	0.05069	0.04757	0.04758	0.04758
BTVI	0.03641	0.03706	0.03581	0.03647
STD	0.00075	0.00733	0.00081	0.00066
Range	0.01428	0.01050	0.011779	0.01110

STVI - Surface Trans-Vinylene Index

STD - Standard Deviation

MTVI- Maximum Trans-Vinylene Index

BTVI - Bulk Trans-Vinylene Index

Conclusions

- X-Ray reduces significantly the dose uniformity ratio when compared to Gamma, in both cross section and surface area treated.
- Evaluation of Trans-Vinylene via FTIR within the study concludes that the dose distribution observed in the Alanine dosimeters was reflected in penetrative capability of X-Ray
- Attenuation in X-Ray processed UHMWPE is lower than conventional Gamma and therefore e-beam.

Notch Fatigue of UHMWPE: A Linear Elastic Fracture Mechanics Approach

Ansari, F¹; Bonnheim, N¹; Gajudo, Gio¹; Purviance, Connor¹; Ries, M²; Pruitt, L¹

¹University of California, Berkeley, Berkeley, CA; ²Tahoe Fracture & Orthopedic Medical Clinic, Inc., Carson City, NV
fansari@berkeley.edu

Introduction: *In vivo* fatigue fracture of total joint replacement (TJR) components made of ultra-high molecular weight polyethylene (UHMWPE) has been documented for hip, knee and shoulder devices (**Fig. 1**) [1-3]. Fracture events often initiate at a design feature or “notch” that serves as a stress riser, such as at the locking mechanism of acetabular liners in total hip replacements (THA) or at the tibial post of posterior-stabilized tibial inserts in total knee replacements (TKA) [1-2]. The influences of irradiation dosage (crosslinking), post-irradiation heat treatments, and crystallinity on fatigue crack growth in UHMWPE have been well established [4,5]. However, little is known about the influence of notch geometry on fatigue crack propagation (FCP) behavior. This work presents a linear elastic fracture mechanics (LEFM) evaluation of fatigue crack growth emanating from various notch geometries in three UHMWPE formulations: virgin, remelted highly crosslinked, and Vitamin E blended highly crosslinked.

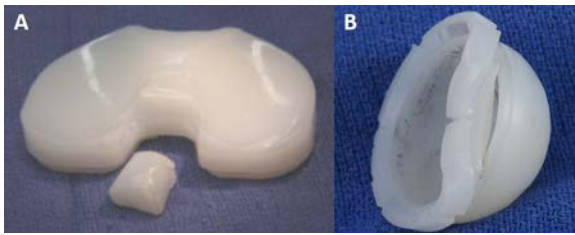


Figure 1. Retrieved devices revealing catastrophic failure for (A) knee and (B) hip UHMWPE components in which fracture occurs at a notch. Both components received a moderate irradiation crosslinking dosage (25-50 kGy) [3].

Methods and Materials: Sharp and blunt notch compact tension (CT) specimens (**Fig. 2**) were machined from virgin GUR 1020 UHMWPE (UHMWPE), irradiated (75kGy) and remelted GUR 1020 UHMWPE (RXLPE), and irradiated (75 kGy) and Vitamin E blended (0.1 wt%) GUR 1020 UHMWPE (VXLPE) (Orthoplastics, Lancashire, United Kingdom). A pre-crack 0.3 - 0.5 mm in length was created at the tip of each notch using a razor blade [4]. Samples were cycled in an Instron 8871 servohydraulic system (Norwood, MA) using a load-controlled sinusoidal wave function at a frequency of 5 Hz. Testing was performed at room temperature and an air cooling system was used to minimize hysteretic heating [4,5]. The load ratio (minimum load / maximum load) was held constant at 0.1. Crack length was measured using a variable magnification optical system (Infinivar CFM-2/S, Boulder, Colorado, 5 μm/pixel) and a digital CCD video camera (Sony XCD-SX910, Tokyo, Japan). For each material and notch combination, 3-5 specimens were tested.

The Paris equation was used to map FCP as a function of cyclic stress intensity, ΔK [6]. For blunt notch specimens, a modified Dowling approximation [7] for stress intensity was used when cracks were within the notch-affected zone (“short cracks”, K_s) (**Fig 3**). For cracks that extended beyond the zone of notch-affect (“long cracks”, K_l) the stress intensity was equivalent to that of sharp crack specimens [7], as tabulated in [8]. The transition length (l^*) (i.e. the size of the notch-affected zone) is defined as the intersection of short and long crack approximations, as shown in **Table 1** and **Fig. 3**. Finite element analysis (FEA) (ABAQUS v. 6.12) was used to validate the use of Dowling’s approximation in predicting the stress intensity values for various crack lengths using 2D plane strain models of 2500-4000 quadratic elements for each notch root radius. FEA was also used on 3D specimens composed of 14000 to 30000 20-node quadratic elements to measure the local notch plastic zone as a function of applied load for the four blunt notch root radii.

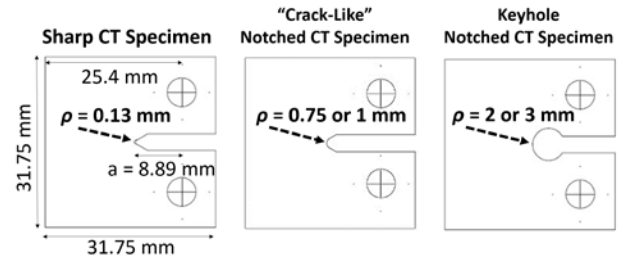


Figure 2. CT Specimens used for fatigue analysis, including sharp (LEFT) and blunt (MIDDLE, RIGHT) geometries. Blunt geometries were machined as a crack-like notch (MIDDLE) for small radii (0.75, 1 mm) or a keyhole notch (RIGHT) for large radii (2, 3 mm). Specimens were 8.13 mm thick.

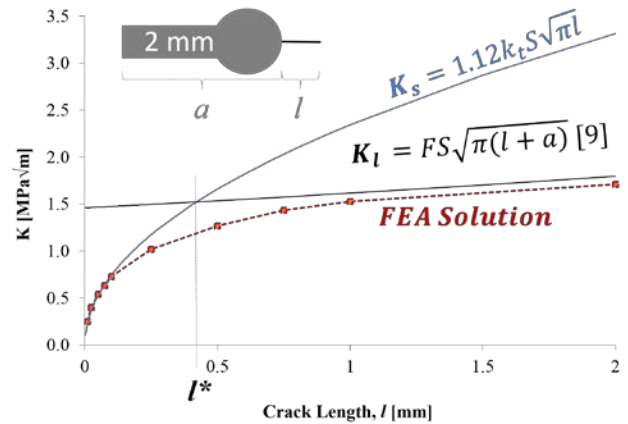


Figure 3. The stress intensity driving crack growth was modeled using “short crack” (K_s) and “long crack” (K_l) equations, as per [7]. Shown here is the approximation for a 2 mm notch root radius. (k_t = stress concentration factor; S = far-field stress; l^* = transition length; F = specimen geometry factor [8]).

Results: FCP data for all notched data is seen in **Fig. 4**. Both crosslinked formulations display reduced resistance to FCP compared to UHMWPE. VXLPE displays a slight improvement in fatigue performance compared to RXLPE. In general, crack growth ahead of notches overlaps with sharp crack data for all material formulations. When engulfed by the notch plastic zone, short cracks are denoted with open symbols (**Fig 4**). While this “plastic” data resulted in increased scatter, it followed the general trend of FCP resistance for all three materials. Transition lengths (notch-affected zone size) for each blunt notch are also shown in **Table 1**.

Table 1. Size of the notch-affected zone (transition length) for each notch geometry, as calculated using [7].

Notch Radius [mm]	0.75	1.0	2.0	3.0
Transition Length [mm]	0.15	0.20	0.40	0.60

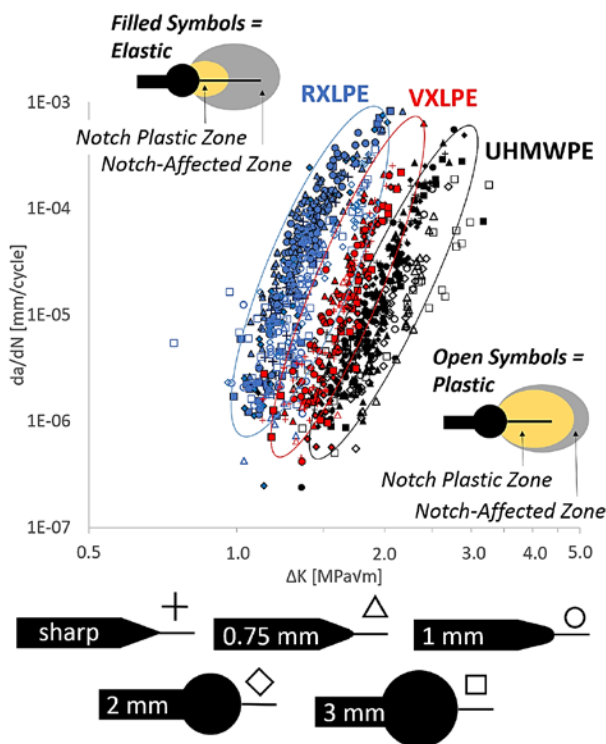


Figure 4. FCP data for UHMWPE (black), RXLPE (blue) and VXLPE (red). Filled symbols represent long crack elastic data, while open symbols demarcate short cracks growing within the notch plastic zone (plastic data). Notch radii are differentiated by symbol geometry (see illustrative legend at bottom of graph).

Discussion: Notches or sharp corners in UHMWPE components for TJRs are often present in implants for a variety of reasons including acetabular cup/liner locking mechanisms and posterior stabilization posts. Explants reveal that UHMWPE implants are susceptible to crack formation in as little as one month of use, often in the vicinity of a notch, and can lead to *in vivo* fracture [1-3,9].

Previous work has been performed to evaluate notch influence on monotonic fracture as well as its effect on the stress-life fatigue performance of UHMWPE formulations [10]. Our work represents the first effort at using existing LEFM methods with clinically-relevant notch geometries to evaluate the impact of these design features on crack growth in UHMWPE.

FCP data in **Fig. 4** shows overlap between crack growth rates for blunt and sharp specimens for RXLPE, VXLPE and UHMWPE formulations. Regardless of notch geometry or crack length, RXLPE and VXLPE consistently show reduced resistance to FCP compared to UHMWPE. This is consistent with trends seen for sharp crack data [4,5], and is attributed to the reduction of local plasticity that results from increased crosslinking in the amorphous region. The higher resistance to fatigue exhibited by VXLPE compared to RXLPE is thought to be the result of reduced crosslinking efficiency concomitant with blended Vitamin E formulations [11].

The size of the notch-affected zone for all four clinically-relevant notch radii approach the sizes of cracks seen in retrieved devices in as little as one month after implantation [9]. Thus, cracks growing in UHMWPE TJR components likely fall into “long crack” elastic growth regimes, and may not succumb to the same plasticity seen in the laboratory. Even with this consideration, both long and short crack growth do not appear to display differences between the notch geometries. Our data thus suggests that FCP in UHMWPE is more dictated by microstructure than design, which has direct implications for existing TJRs and the design of new systems.

Acknowledgements: We would like to thank David Brooks and Mark Allen at Orthoplastics for their generous donation of material used in this study.

References:

- [1] Furmanski et al. (2009), *Biomaterials* 30.29: 5572-5582.
- [2] Ansari et al. (2013), *The Knee* 20.6: 609-613.
- [3] Ansari et al. (2014). World Congress Biomechanics. July 9, 2014: Session 18-16.
- [4] Atwood et al. (2010), *Journal of the Mechanical Behavior of Biomedical Materials* (4): 1033-45.
- [5] Baker et al. (2000), *Polymer* 41.2: 795-808.
- [6] Paris et al. (1961), *Trends in Engineering*. 13: 9-14.
- [7] Dowling et al. (1979), *Fatigue of Engineering Materials & Structures* 2.2: 129-138.
- [8] Tada et al. (1973), *Stress Analysis of Cracks*. Dell Research Corp, PA.
- [9] Furmanski et al. (2011) *J Arthroplasty* 26.5: 796-801.
- [10] Sobieraj et al. (2013), *Journal of the Mechanical Behavior of Biomedical Materials* 28: 244-53.
- [11] Oral et al. (2006), *Biomaterials* 27.32: 5580-87.

Murine model of particle-induced osteolysis using a titanium tibial implant to test the influence of aging on bone turnover

Bichara DA¹, Langlois J^{1,2}, Bertrand D³, Micheli B¹, Wannomae KK¹, Hamadouche M², Muratoglu OK¹.

¹Massachusetts General Hospital, Harvard Medical School, Boston, MA

²Laboratoire de Bioingenierie et Biomecanique Osteo-articulaires, UMR CNRS 7052, Faculté Paris 7-Denis Diderot

³Ecole Centrale Paris, UMR CNRS 8579

omuratoglu@mgh.harvard.edu

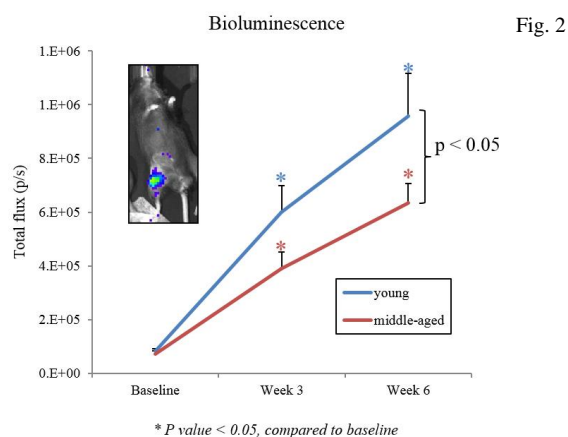
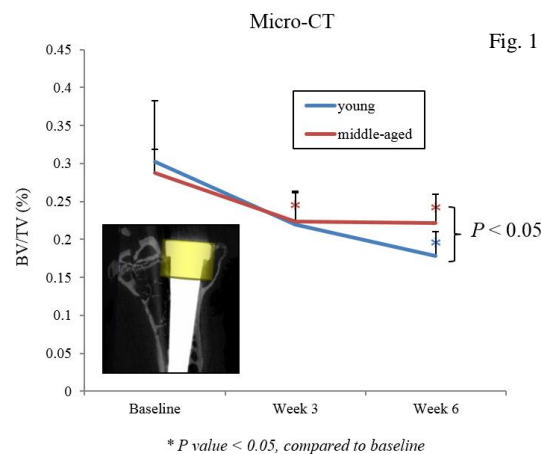
Introduction: The clinical context of aseptic loosening is not fully represented in preclinical studies determining the underlying mechanisms responsible for particle-induced osteolysis; a vast majority of the experimental models involve murine species using unloaded (calvarial) bone and limited short-term endpoints. Modification of the murine model to obtain more accurate, clinically-relevant endpoints can shed new light on the *in vivo* reaction to wear particles. The objective of this study was to determine the effects of UHMWPE particle-induced osteolysis in a murine model after the implantation of an intramedullary tibial titanium (Ti) pin. In addition, we compared the effects of particle-induced osteolysis between 2-month (mo.) old mice and 12-mo. old mice to determine the influence of age on bone turnover.

Methods and Materials: All actions were approved by the IACUC of the Massachusetts General Hospital. A total of $n=80$ male C57/BL6 mice were used in this study. **Study groups:** Control group (mice with Ti implant, no particle exposure) versus UHMWPE group (mice with Ti implant and particle exposure via intra-articular injection). For each group, half of the mice were young (2 mo. old), and half were middle-aged (12-month old). **Surgical procedure:** After an anteromedial incision over the R knee, the patella was dislocated laterally, the tibial plateau was exposed, pierced with the beveled tip of a 25G needle, and drilled using a 0.5 mm bit. The Ti implant (TiAl6V4, 1 mm diameter with a conical shape and 5 mm length, 14.9 μm surface roughness) was press-fitted into the canal; the top of the implant was flush with the articular surface. Buprenorphine (0.05-0.1 mg/kg intraperitoneal) was administered for the first 3 post-operative days. After a 4-week period of osseointegration, endpoints were performed at the following intervals: (i) baseline (after the 4-week osseointegration period), (ii) week 3 (after $n=2$ intra-articular UHMWPE particle injections; 4E08 in 0.1 ml were administered per injection), and (iii) week 6 (after $n=4$ particle injections, using the same concentrations as previously described). **Endpoints:** Bioluminescence for inflammation (using IVIS imaging system from Xenogen and L-012 luminescent probe injection, 50mg/kg SC), micro-CT scanning ($\mu\text{CT}40$ from Scanco Medical AG, with a 10- μm nominal resolution), and histological analysis using hard MMA embedding and Sanderson's Rapid Bone Stain. All values are expressed as means \pm SD. Non parametric paired or unpaired comparison tests were performed, as dedicated. A p value < 0.05 was considered statistically significant.

Results: No intra or postoperative deaths or infections were encountered. All implants were successfully implanted into the tibial canal. Histologically, implants were osseointegrated after 4 weeks. Less bone was visualized around the implant after the particle injections, but there were no subjective histological differences between $n=2$ (week 3) or $n=4$ particle injections (week 6) between groups. In addition, UHMWPE particles were only visualized via polarized light in the proximal one third of the implant. Micro-CT analyses are shown in **Fig. 1** (region of interest: 1.5 mm diameter and 1 mm length of proximal tibia). Bone volumes, compared to baseline, decreased significantly after 2 injections in the middle-aged group ($0.22 \pm 0.04\%$ vs. baseline $0.29 \pm 0.03\%$, $p=0.02$), while 4 injections were

required in the young group ($0.18 \pm 0.03\%$ vs. baseline $0.30 \pm 0.08\%$, $p=0.03$) to observe a difference in bone volumes between groups. In summary, young mice showed significantly more osteolysis than old mice ($p=0.04$) at the 6-week timepoint. Baseline luminescence signals were similar between both groups. Distinct luminescent signals between young and old mice were measured after 2 and 4 injections (respectively $p=0.04$ and $p<0.01$) (**Fig. 2**). A higher inflammatory reaction was observed in the young mice group.

Discussion: Although this new murine tibial implant model more closely mimics the clinical time course of aseptic loosening – osteolysis progressively developing around the proximal part of the Ti implant before surrounding its entire length – possible model modifications are granted for future experiments. These include the following: (i) increasing the number of particle injections, or the implantation of an osmotic pump for continuous particle delivery; (ii) reducing the osseointegration period so particles are allowed to travel distally; (iii) implanting a particle-coated Ti implant. A bone-implant interface that was tight enough to prevent particles from travelling distally after 4 weeks was an unexpected finding. Interestingly, these results are contradictory to similar experiments based on the calvaria osteolysis model, where we observed that older mice (24-month) demonstrate greater patterns of both inflammation and osteolysis. This study suggests that the effects of particle induced-osteolysis might be both model-dependent and age



Storage of UHMWPE Powder Blended with Peroxides

*Chan, DS; *Konsin, ZB; *Wannomae, KK; +*Muratoglu, OK
 +* Harris Orthopaedic Laboratory, Massachusetts General Hospital, Boston, MA 617-726-3869
 omuratoglu@partners.org

Introduction:

Highly crosslinked ultra high molecular weight polyethylene (UHMWPE) is the bearing material of choice for total hip replacements. The cost of the current methods of crosslinking using ionizing radiation can be considerably high. A cheaper and viable alternative is the use of chemical crosslinkers, such as peroxides, to induce crosslinking of UHMWPE without compromising the integrity of the polyethylene. Since the crosslinking chemical will be blended in the UHMWPE powder prior to consolidation, it is imperative that the blended powder not change in composition while it is stored. This study will determine any changes in a peroxide blended polyethylene powder during storage.

Methods and Materials:

2,5-dimethyl-2,5-di(t-butylperoxy)-hexyne-3 (P130, Sigma Aldrich) was blended with UHMWPE GUR1020 powder using a shaker (Turbula Shaker T 2 F). A low concentration (0.2 wt.%) P130 and a high concentration (0.9 wt.%) P130 blend was created, and both of these materials were stored under three different conditions:

- In an open container (no lid) at room temperature
- In a closed container at room temperature
- In a closed container at 4°C

The open containers were covered with a stainless steel wire mesh that allowed air to circulate into and out of the container but prevented large particulates from contaminating the blend.

The stored blends were tested at 10 different time points between 0 and 120 days. Pellets were consolidated and immediately analyzed via FTIR (Varian 670-IR Spectrometer) to quantify peroxide content. Peroxide content was calculated by normalizing the absorbance of a double peak at 864 cm⁻¹ and 881 cm⁻¹ by 1895 cm⁻¹.

On Days 0 and 120, closed container of high concentration blend was compression molded into pucks that were then machined into Izod samples for double notched impact strength testing per ASTM F648 and 3.2 mm thick Type V dog-bone specimens for tensile testing per ASTM D638. Low concentration blends and open container high concentration blends were not molded for mechanical testing.

Results:

The day to day measured peroxide concentrations via FTIR are given in Figure 1 and the mechanical properties and Izod impact strength for consolidated 0.9 weight percent blended pucks are given in Table 1

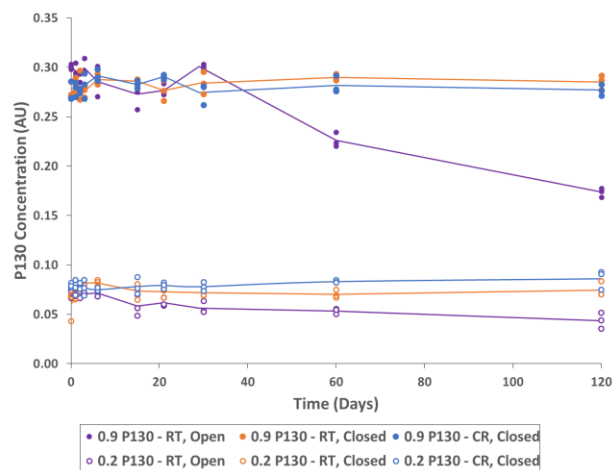


Figure 1: Measured P130 content after 120 days for various storage methods. All purple groups have been stored in open containers at room temperature. All blue samples were stored at 4°C in closed containers. All orange groups were stored at room temperature in closed containers. All filled markers are from 0.9 weight percent P130 while unfilled markers are from 0.2 weight percent P130 blended powders.

Table 1: Mechanical Properties for 0.9 wt.% Peroxide Consolidated Pucks

	Modulus (GPa)	UTS (MPa)	EAB (%)	Izod (kJ/m ²)
Day 0, (Fresh)	0.64±0.06	41.0±2.2	206±20	52.1±2.3
Day 120, RT, Closed	0.56±0.05	47.1±2.1	242±15	54.3±0.9
Day 120, 0°C, Closed	0.68±0.09	43.8±3.6	229±14	54.3±0.5

Discussion: For all blends stored within a closed container, the peroxide concentration measured after 120 days of storage were comparable to those measured at day 0. The blends that were stored in an open container showed a significant drop in P130 concentration at day 120 as compared to day 0. There was no difference in the mechanical properties and the impact strength of the high concentration blend after being stored in a closed container for 120 days.

This study suggests that, as long as the material is kept in an air-tight closed container, P130 blended UHMWPE can be stored for multiple months without any detrimental effects.

Effectiveness of AO Polyethylene: What early retrievals can tell us

Currier, BH,¹ Currier, JH,¹ Levine RAC,¹ Van Citters, DW¹

¹Dartmouth College, Hanover, NH USA

barbara.h.currier@dartmouth.edu

Introduction: Assessing the effectiveness of anti-oxidant (AO) polyethylene in minimizing oxidation compared to conventional gamma-sterilized or remelted highly cross-linked (HXL) polyethylene is necessary to set realistic expectations of the service lifetime of AO polyethylene in the knee. The hypotheses explored in this study are: retrieved AO tibial inserts will exhibit (1) lower oxidation than conventional or remelted highly cross-linked tibial inserts and (2) better mechanical properties than remelted highly cross-linked tibial inserts.

Methods and Materials: An IRB-approved retrieval laboratory received 20 AO polyethylene tibial insert retrievals from three manufacturers with in vivo time of 0-3 years. These were compared with 16 conventional gamma-inert sterilized and 29 HXL (65-kGray, remelted) tibial inserts of the same in vivo duration range. The retrievals were sectioned with a microtome through the medial condyle in the A-P plane. These vertical cross-sections were analyzed for oxidation and trans-vinylene index (TVI) using a Thermo Scientific iN-10 FTIR microscope. Oxidation was reported as the maximum ketone peak height oxidation measured in the scan from the articular surface to the backside of the bearing.

Inserts of sufficient size and thickness were evaluated for mechanical properties by uniaxial tensile testing and small punch testing (SPT). A series of 250-micron thin sections (n=12-15, dependent on the initial thickness of the retrieved insert), were cut parallel to the nonarticular surface of the insert with a microtome. These parallel sections were cut with a die into ASTM Type V samples for uniaxial tensile testing, carried out on an Instron 5544 load frame equipped with a 2-kN load cell, pneumatic sample grips, and video extensometer. Samples were loaded at a rate of 25.4 mm/minute, corresponding to a strain rate of 100%/minute. Small punch tests, modified to capture changes of material properties with depth, were run as described previously [1-2].

Results: None of these short term retrievals showed oxidation-related cracking or delamination. AO polyethylene retrievals exhibited oxidation that was significantly less than that measured in conventional gamma-inert sterilized retrievals (p=0.024); however, the oxidation measured in AO retrievals was not significantly different from that measured in that in HXL retrievals (p=0.110, Figure 1). Trans-vinylene index correlated positively with irradiation dose (p<0.001). Mechanical properties varied by material, with toughness correlating negatively (p<0.001) with increasing irradiation dose (TVI).

Discussion: AO polyethylene was developed to address

the problem of free radicals in polyethylene resulting from irradiation used in cross-linking or sterilization. Each manufacturer uses a different antioxidant or method of incorporating the antioxidant. However, all of the antioxidant materials appear to be effective at minimizing oxidation over the in vivo period of this study, reducing oxidation significantly compared to conventional gamma-sterilized. The toughness, or ability of the material to resist fatigue damage, varies with irradiation dose. These AO polyethylenes have lower toughness than conventional poly, but they avoid the loss of toughness due to remelting.

References:[1] Reinitz S, Franklin K, Carlson E, Collier J, Van Citters D. Application of small punch test to depth dependent mechanical property testing for retrieved UHMWPE bearings. ORS 2013 Annual Meeting, San Antonio, TX. 2013. p. 1054. [2] Reinitz S, Franklin K, Carlson E, Paniogue T, Van Citters D. Thickness dependence of small punch test for thin specimens. ORS 2013 Annual Meeting, San Antonio, TX. 2013. p. 1829.

Figure 1: Maximum oxidation by material

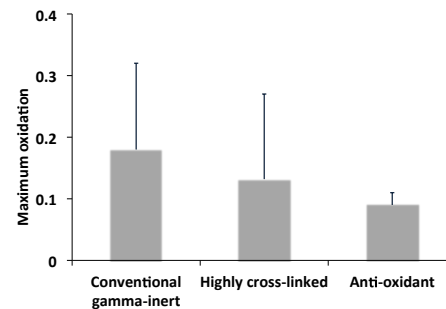


Table 1: Trans-vinylene index and mechanical properties vary by manufacturer. AO materials manufactured using higher irradiation doses have lower toughness.

Material	TVI 1370	UTS (MPa)	UE (%)	Toughness (MPa)
AO Poly 1	0.029	73	365	139
AO Poly 2	0.05	68	271	109
AO Poly 3	0.088	64	290	95
HXL remelted	0.036	50	357	95
Conventional	0.011	70	367	169

Table 2: SPT properties vary by material.

Material	TVI 1370	Maximum Load (N)	Ultimate Extension (mm)	Work to Failure (J)
AO Poly 1	0.029	-40.9	3.4	0.10
AO Poly 2	0.05	-51.4	3.5	0.12
AO Poly 3	0.088	-46.2	3.8	0.11
Conventional	0.011	-52.4	4.2	0.15

An Alternative Vitamin E-Diffused UHMWPE with Improved Toughness

Doshi BN¹, Oral E^{1,2}, Muratoglu OK^{1,2}

¹Harris Orthopaedic Laboratory, Massachusetts General Hospital; ²Department of Orthopaedics, Harvard Medical School
eoral@mgh.harvard.edu

Introduction: Antioxidant stabilization of radiation cross-linked UHMWPEs were introduced with post-irradiation diffusion of the antioxidant vitamin E into radiation cross-linked UHMWPE [1]. Currently available implants using this method are prepared by a two-step doping and homogenization, where the former introduces the antioxidant to the surface of the material and the latter helps make the concentration of the antioxidant uniform. Previously, we have shown that high temperature melting (HTM) of UHMWPE at around 300°C improved impact toughness [2]. We hypothesized that increasing the homogenization temperature used in incorporating the antioxidant into UHMWPE would improve its toughness.

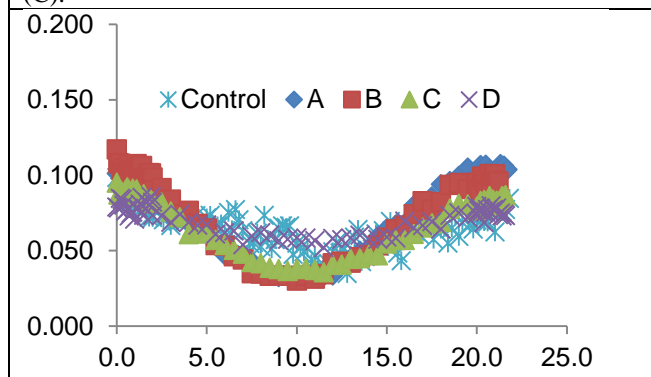
Methods and Materials: Medical grade GUR1020 UHMWPE blocks (diameter 6.7 cm, thickness 2.3 cm) were compression molded and radiation cross-linked at 100 kGy. After radiation, these blocks were doped with vitamin E at a temperature below the melting point for 4 hours in inert atmosphere. A control block was homogenized at 130°C with the current homogenization procedure. Other blocks were high temperature homogenized with the following parameters:

	Temperature (°C)	Duration (hrs)
Control	130	NA
A	250	9
B	300	4
C	310	3
D	300	8

Vitamin E concentration profiles were determined using Fourier Transform Infrared Spectroscopy (FTIR). Microtomed sections (150 micra) were analyzed at every 100 micra and a vitamin E index was calculated as the ratio of the area under the peak at 1265 cm⁻¹ to that of the peak at 1895 cm⁻¹. Tensile mechanical properties were determined using ASTM D638. IZOD impact toughness was determined using ASTM D256 and F648. Wear rate was determined using a bidirectional pin-on-disc (POD) tester with cylindrical pins of UHMWPE (diameter 9 mm, length 13 mm) against polished CoCr discs in undiluted, preserved bovine serum. The wear rate was determined as the linear regression of weight loss from 0.5 to 1 MC.

Results: After homogenization, the vitamin E concentration profiles among the blocks were substantially similar (Figure 1), showing that a similar vitamin E concentration profile could be achieved using high temperature homogenization. The sample homogenized at 300°C for 8 hours was more homogenous than the others (3-mm surface average index to 3-mm bulk index ratio= 0.8 compared to 0.66 for control).

Figure 1. The vitamin E profiles for blocks homogenized at 130°C (Control), 250°C (A), 300°C (B, D) and 310°C (C).



The general mechanical properties represented by the ultimate tensile strength (UTS) and the wear rate were similar for all homogenized UHMWPEs (Table 2). In contrast, the impact toughness represented by the IZOD impact strength was improved for all high temperature homogenized UHMWPEs compared to control.

Table 2. Comparative properties of vitamin E-doped UHMWPE homogenized at different temperatures. Control was terminally gamma sterilized.

	UTS (MPa)	IZOD (kJ/m ²)	Wear (mg/MC)
Control*	46.7±0.7	64.7	0.64±0.08
A	49.9±0.6	68.3	0.54±0.04
B	47.9±1.2	71.9	0.67±0.09
C	46.1±2.7	65.5	NT
D	50.0±1.2	74.1	0.89±0.11

Discussion: Radiation cross-linked and vitamin E-diffused UHMWPE is used successfully since 2007 in total hip and since 2008 in total knee replacements. Early clinical results indicate excellent wear resistance similar to the predicate radiation cross-linked UHMWPEs with good clinical performance [3].

The toughness of cross-linked UHMWPEs is limited by crystallinity and cross-link density. Here, we used high temperature melting as part of vitamin E incorporation to improve the toughness of this cross-linked UHMWPE. An additional benefit is the shortening of the manufacturing time; homogenization at 300°C is much faster than at 130°C.

References: [1] Oral et al. Biomaterials (2004) 25:5515-22; [2] Fu et al. Polymer (2010) 51:2721-31; [3] Greene et al. AAOS (2013):560.

Nanoparticle reinforced UHMWPE for orthopaedic applications “parameters affecting the manufacturing process and mechanical properties”

Emami N

¹ Biotribology research group, Dept. of Engineering Sciences and Mathematics, Luleå University of Technology, Sweden

*nazanin.emami@ltu.se

Introduction

Total joint arthroplasty (TJA) is considered as the 20th century's greatest surgical success, starting in 1958 when Sir John Charnley introduced PTFE in total hip replacements (THR). PTFE was soon abandoned on behalf of ultrahigh molecular weight polyethylene (UHMWPE). UHMWPE has, since its introduction in total joint arthroplasty in 1962, where metal/ceramic is used as counterface, been considered as gold standard bearing couple. It has excellent mechanical and tribological properties compared to other polymers. Despite the success of UHMWPE in TJA, these joint replacements have a limited lifetime. The main drawbacks with these systems is osteolysis initiated by UHMWPE wear particle which causes failure of the total implant. Increasing the wear resistance and fracture toughness of UHMWPE is a necessity especially for younger and more active patients with higher demands on longevity and sustainability. In this work we compare nanocomposites based on UHMWPE reinforced with Multiwalled Carbon nanotubes (MWCNT), Graphene Oxide (GO) and nanodiamonds (ND). The dispersion of nanofillers, their interaction with matrix, crystallinity of the final nanocomposites and mechanical properties of the designed nanocomposites were studied.

Materials and Methods

UHMWPE, GUR 1020 was supplied by Ticona, with an average molecular weight of 3.5×10^6 g/mol and an average particle size 140 μm . It has a specific density of 0.93 g/cm³. The multiwalled carbon nanotubes (MWCNT) was Nanocyl-3150 with a purity of >95% and a tube diameter of 5-10 nm and a length of 1-5 μm . Surface modification was performed as described by Singh *et al* [1]. Graphene oxide (GO) was prepared according to the procedure described by Gonçalves *et al* [2]. The Nanodiamonds were supplied by International Technology Center in Raleigh, USA. These nanodiamonds have a high purity level (>98%), in a cubic phase and have a primary particle size of 4 up to 5 nm. The functional groups of our NDs are in forms of a carboxyl group which includes both carbonyl and hydroxyl.

The composite was ball-milled in ethanol in a planetary ball mill, using a container volume of 500 mL and a ratio of ball to composite of 22. Ball-milling times between 1 and 8 hours were carefully investigated to obtain an optimum mixture of the composites, without damaging the UHMWPE. UHMWPE reinforced with 0.5, 1 and 2wt% MWCNTs, GO or ND was investigated and compared to virgin UHMWPE. The morphology of the composites was investigated by scanning electron spectroscopy (SEM). Thermal characterisation was carried out using Differential scanning calorimetry (DSC) and Thermogravimetry (TGA) in order to measure the degree of

crystallinity and oxidation degradation for manufactured composites in comparison to virgin UHMWPE. Universal instron. Differential scanning calorimetry (DSC) was used to investigate the crystallinity.

Mechanical properties of the nanocomposites and virgin UHMWPE were measured using tensile, fracture toughness and microhardness testing. Tensile testing was performed using a tensile machine (Instron 3366, USA) and Young's modulus, yield stress, fracture stress and fracture strain properties were determined from the strain-stress curves registered. Contact angle measurements were performed to investigate the wettability of the nanocomposites and compare it with that of virgin UHMWPE. The water contact angles were determined using the sessile drop method, where a 4 μl of distilled water was deposited on the surface of the samples and measurements were taken after one second.

Effect of irradiation and aging was investigated on selected nanocomposite compositions.

Results and Discussion

The high melt viscosity of UHMWPE makes it difficult to process the polymer with conventional processing techniques. When subjecting UHMWPE to ball milling, one needs to take into consideration the harsh conditions that are used. The ball milling time was optimized to SEM indicates a fairly good distribution of nano fillers on the UHMWPE surface. Thermal characterisation showed that the oxidation degradation is extended to higher temperature for nanocomposites in comparison to virgin UHMWPE, though the DSC indicated rather similar degree of crystallinity for nanocomposites and virgin UHMWPE. Contact angle were increased indicating higher hydrophobicity for nanocomposites. The addition of MWCNTs, GO and ND showed a positive effect on the mechanical properties of UHMWPE.

Acknowledgment: UHMWPE (GUR 1020) was generously supplied by Ticona/Celanese.

- Past and present members of the group: S. Suner, A. Gomez, E. Enqvist, D. Ramanenka, R. Joffe and J. Tipper are highly acknowledged for their contributions to the studies which are partly presented here.

References

- 1 M. Singh, T. Shokuhfar and J. Gracio, *Advanced Functional Materials*, 2008, **18**, 694-700
- 2 Gil Gonçalves, Paula A.A.P. Marques, Carlos Granadeiro, Helena Nogueira, Manoj Singh, José Grácio, *Chemistry of Materials*, 21 (2009) 4796-4802
- 3 S Suñer, R. Joffe, J. Tipper, N. EmamiUltra High Molecular Weight Polyethylene/Graphene Oxide Nanocomposites: Thermal, Mechanical and Wettability Characterisation. *Composites part B*, 2015;78(7).

Surface functionalisation of MWCNTs to Improve Behaviour of UHMWPE-Based Nanocomposites

Emami N, McLaren H*

Biotribology research group, Department of Engineering Sciences and Mathematics, Luleå University of Technology, Sweden

*nazanin.emami@ltu.se

Hip and knee joints are the most common joints in the body that require complete replacement. Replacement materials require low friction and a low wear rate to minimise damage. Wear particles can cause problems such as osteolysis (bone resorption) and aseptic loosening. A common material in total joint replacement (TJR) is ultra-high molecular weight polyethylene (UHMWPE), which has a low coefficient of friction and good wear characteristics. However, wear particles are still a serious problem with UHMWPE and multi-walled carbon nanotubes (MWCNT) have been added to UHMWPE in an attempt to form a composite with improved properties. Surface modification of MWCNTs could improve the interface between matrix and reinforcement. A better interface results in more efficient load transfer and thus improved properties. MWCNTs were functionalised with octadecyltrichlorosilane (OTS) and combined with UHMWPE by ball milling. The following characterisations were carried out:

- Differential Scanning Calorimetry (crystallinity), Thermal Gravimetric Analysis (degradation)
- Bending (flexural modulus)
- Contact Angle (hydrophobicity)
- Pin-on-Disc Friction & Wear Test
- XHR-SEM

Results and Discussion: Table 1: Tribological test results for the three materials. The modified composite has a lower friction coefficient and both composites have a much lower wear rate than UHMWPE.

Material	Wear Factor ($\times 10^{-6}$ mm ³ /Nm)	Coefficient of Friction
UHMWPE	17.0 (± 1.1)*	0.21 (± 0.015)*
UHMWPE/CNT	2.8 (± 1.2)*	0.18 (± 0.012)*
UHMWPE/CNT-OTS	3.2 (± 1.0)	0.16 (± 0.013)

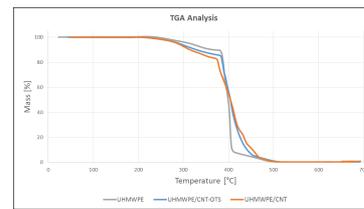


Figure 1: TGA, composites begin to degrade earlier.

It can be said that the composites, modified or otherwise, are less thermally stable than the pure polymer. Complete degradation arrives later for the composites due to more energy needed to burn the reinforcement.

UHMWPE/CNT-OTS observations:

- Low friction and Low wear rate
- Hydrophobic, Good dispersion of MWCNT
- Slightly higher crystallinity and less thermally stable than UHMWPE
- Small clusters of MWCNT and good adhesion to UHMWPE
- Fracture surface is more brittle than UHMWPE

Surface modification of multi-walled carbon nanotubes improves dispersion within UHMWPE. The interface is improved compared to unmodified MWCNT composites. These factors result in better friction and wear properties. Although these tests are only the first step, this material has potential for use in artificial joints.

Acknowledgment: UHMWPE (GUR 1020) was generously supplied by Ticona/Celanese.

- Dr. Y. Shi and Dr. A. Golchin are highly acknowledged for their great contribution to this study.

Fatigue crack propagation testing in UHMWPE

Kozak, A.¹, Leisinger, S.², Spiegelberg, S.¹, Narayan, V.²

¹Cambridge Polymer Group, Inc., ²Depuy J&J
stephen.spiegelberg@campoly.com

Introduction:

Static test methods, such as tensile and compression testing, provided needed information about the basic mechanical properties of ultra high molecular weight polyethylene (UHMWPE). The application of this material as a bearing surface in articulating implants subjects it to fatigue behavior, which is not captured by static tests. In particular, crack growth resistance is an important parameter, as rim cracking in acetabular liners has been observed in the past,¹ and concerns about crack resistance effects on the locking mechanism and post strength of tibial inserts.²

Highly crosslinked UHMWPE introduced in the late 1990's addressed clinical issues with wear debris generation, but required the compromise of reduced mechanical properties, including resistance to fatigue crack propagation.³ Fatigue crack propagation resistance has conventionally been tested according to ASTM E647.⁴ This general testing standard is more focused on metals testing, rather than tough plastics like UHMWPE. Additionally, the only reportable material value in the standard is the ΔK_{th} , or the threshold asymptomatic value of stress intensity factor ΔK where da/dN approaches 10^{-10} m/cycle (approximating zero). Researchers working with UHMWPE typically also report the Paris regime parameters (C and m), which are obtained from the fitted da/dN vs ΔK curve for zone II of the fatigue crack growth curve.⁵ Differences in test methodology, equipment, sample geometry, and data analysis techniques can make comparisons of fatigue crack test data challenging. To this end, a new ASTM test method for fatigue crack propagation (FCP) specific to UHMWPE is being developed. As part of this method, a new optical system has been developed to aid in collecting crack propagation data, in an effort to improve the quality and density of the data, and to provide more uniformity in data comparison between labs. This paper discusses a comparison of the new optical system tested at two laboratories on a highly crosslinked UHMWPE.

Methods and Materials:

The material tested was GUR 1050, gamma irradiated to 50 kGy and remelted (Marathon). A single set of test specimens were machined and razor pre-notched at one lab, using compact tensile specimens ($W = 40$ mm, $B = 10$ mm). Samples were tested at a ΔP of 347 N, an R of 0.1, a frequency of 3 Hz, and a sinusoidal wave form. Lab 1 used an electrodynamic load frame with chilled air blowing on the test specimen, and Lab 2 used a servohydraulic load frame with ambient air cooling the test specimen.

The same custom developed optical system using dual cameras on either side of the test specimen was used at each lab (see Figure 1). Validated software collected images at a frame rate of 21 FPS, while the samples were being flexed in the load frame and the crack length a was computed in real time as a function of load cycles N , reported as an average of the crack length from each camera. Fatigue crack growth rate da/dN was calculated using the secant method.⁴ Eight specimens were tested at Lab 1, and five specimens were tested at Lab 2. Exemplary data is shown in Figure 2. The higher stress intensity factors and tail off for Lab 2 data is likely caused by feedback loop problems on the servohydraulic load frame at high displacements occurring near sample failure. ΔK_{th} was calculated by performing a linear regression on data obtained in growth rates between 10^{-10} m/cycle and 10^{-8} m/cycle and determining the required ΔK to produce a da/dN of 10^{-10} m/cycle. Linear regression was also performed in the Paris regime (defined here as da/dN values between 10^{-7} and 10^{-5} m/cycle) for determination of m and C parameters.

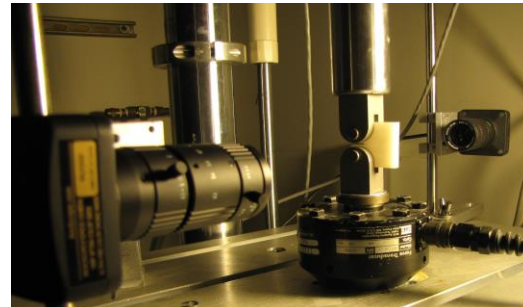


Figure 1: Dual camera optical system.

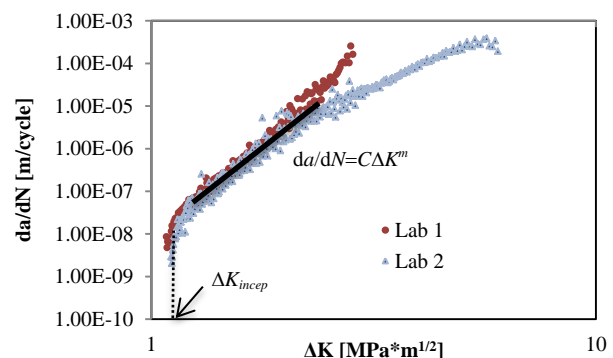


Figure 2: Exemplary processed data from FCP testing at two laboratories. The reportable parameters are indicated on the plot.

Results:

The computed parameters from the two labs are shown below. Statistical analysis of the results (T-test, two tail, heteroscedastic), shows no statistically significant difference in results in C ($p=0.039$), but a statistically

significant difference in the ΔK_{th} and m ($p=0.006, 0.001$). The difference in ΔK_{th} was 2.5%, and was 18% for m . Given the commonality of the test specimen and crack analysis system, the only potential differences were due to the sample temperature and load frame characteristics. Rinnac and co-workers observed temperature dependency on the Paris regime parameters, with higher temperature (37°C) showing a decreased C , along with a reduced ΔK_{th} compared to samples tested at room temperature.⁵ The parameter m was not statistically significantly different in the highly crosslinked samples in the Rinnac study, however. The 37°C data was collected in PBS, which introduced a second variable. The challenge in interpreting ΔK_{th} is that this parameter is dependent on the initial crack length, the load regime used, the temperature, and the material. Since all the parameters except for temperature were held constant between the two labs, it is speculated that Lab 1's used of chilled air, versus room temperature air, may have resulted in a reduction in ΔK_{th} . The servohydraulic load frame used by Lab 2 is also expected to generate additional heat during operation as compared to the electrodynamic load frame used by Lab 1. In addition, feedback loop problems on the servohydraulic load frame at high crack growth rates likely contribute to the difference in Paris regime parameters—inability of the load frame to maintain adequate force control during large sample deformations results in an undershoot of the nominal force value, which would manifest as a downward bowing of the da/dN vs ΔK curve.

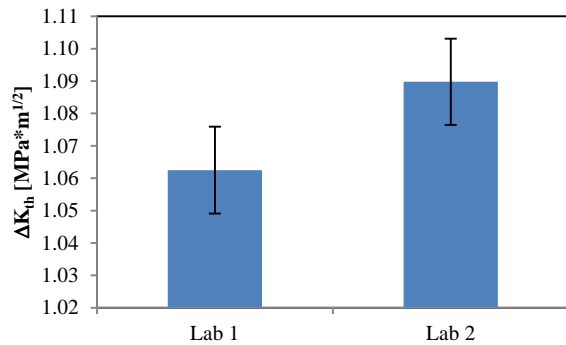


Figure 3: Computed stress intensity factor at crack inception at each lab.

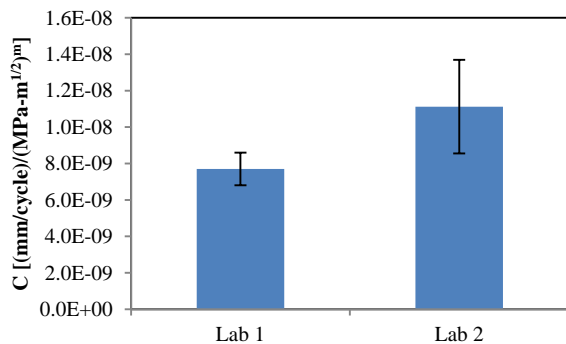


Figure 4: Computed Paris regime parameter C at crack inception at each lab.

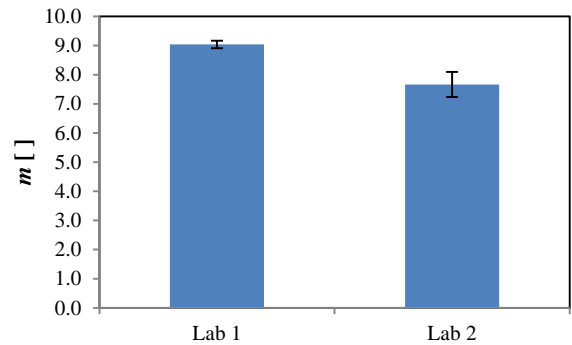


Figure 5: Computed Paris regime parameter m at crack inception at each lab.

Discussion:

The results indicate the utility of the automated optical system for measuring crack growth resistance in fatigue in UHMWPE. Samples did not have to be removed from the load frame for crack length analysis, avoid potential distortions of the samples, and tests could be run continuously until sample failure. The results also point out the need for more attention to temperature control and the feedback loops employed by the test load frame. Automated optical systems are being installed in two additional labs, which will permit a more extensive round robin study in anticipation of the ASTM standard for FCP in UHMWPE. Temperature effects and load frame feedback loop parameters will be considered in this study, with the possibility of active temperature control during the test.

References:

1. Birman, M.V., Noble, P.C., Conditt, M.A., Li, S., Mathis, K.B., J. Arthroplasty, Vol 20, 87-92 (2005).
2. Chakrabarty, G., Vashinshtha, M., Leeder, D., J. Clin. Orthop and Trauma, vol 6, 108-112 (2015).
3. Bradford, L., Baker, D., Ries, M., Pruit, L., Clin. Orthop. Rel. Res., vol 440, 149-156 (2005).
4. ASTM E647: Standard test method for measurement of fatigue crack growth rates.
5. Varadarajan, R., Rimanc, C.M., 9th International Fatigue Congress (2006).

Disclosures:

Materials were provided by Depuy J&J. No funding was received for this work.

Effect of Knee, Ankle and Hip Joint Replacements on Vitamin E Infused Highly Crosslinked UHMWPE Wear Particles Size, Shape and Morphologies Using a New Modified Base Digestion Method

Saurabh Lal and Jun Jie Wu

Biophysical Sciences Institute, School of Engineering and Computing Sciences, Durham University, UK
junjie.wu@durham.ac.uk

Introduction: UHMWPE wear debris isolation methods including acid digestion, base digestion, enzymatic digestion, were assessed and compared [1-8]. The potential limitations include incomplete digestion, presence of impurities, bacterial contamination and low reproducibility. Therefore, a novel UHMWPE wear debris isolation method was developed to overcome these limitations. This proposed method successfully isolated UHMWPE wear debris by using modified base digestion and by purifying the wear particles using a two-stage density gradient ultracentrifugation. High-resolution scanning electron microscopy was used to capture digital images of the wear particles deposited on 15 nm pore size membrane filters. Particle analyses software was developed to provide understanding of particle size, shape and morphologies. Two current commercial size analysers (i.e. Nanosight and Mastersizer) were compared to SEM image analysis for characterising UHMWPE wear debris. Large size range and complex shapes of the UHMWPE wear particles have posed real challenges for complete characterisation using Nanosight and Mastersizer. Moreover, no shape analysis was available in both commercial particle analysers. Therefore, SEM imaging image analysis was chosen for particle characterisation. Custom software was developed at Durham University to automatically analyse SEM images and characterise particles using a range of size and shape descriptors.

Methods and Materials: Base digestion was used to digest the serum proteins due to its proven efficacy of digesting serum proteins as well as by previous studies (Discussed in Section 6.1, page 224). A two-stage density gradient centrifugation was used to purify the particles. The detailed description of the method is given in the Figure 1. In order to verify the complete removal of proteins, lipids and other impurities, control serum lubricants were also isolated. No banding was found between isopropanol layers at the end of step 2 (Figure 2). Moreover, SEM images of control serum showed no particles or impurities.

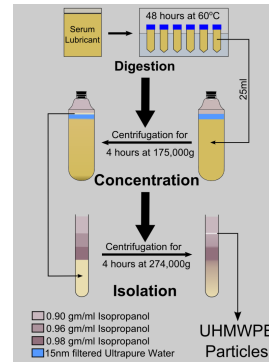


Figure 1 Schematic diagram for the modified base digestion method developed in the current study showing three key stages: Digestion, Concentration and Isolation.

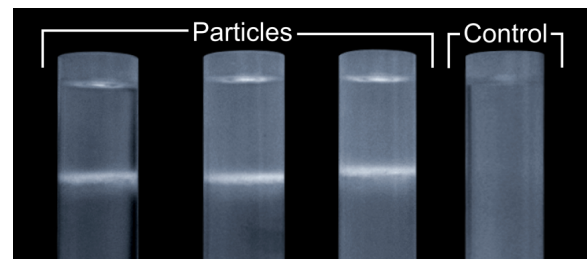


Figure 2: E1 UHMWPE particles seen as opaque white banding between 0.90gm/ml and 0.96gm/ml isopropanol layers and the control serum going through the same method (schematic diagram indicating the method – see Figure 1) showed no particles or impurities.

Results: In this study, FEI Heios Nanolab 600 SEM was used for imaging particles. The dimensions of all captured images were 1024 pixels by 943 pixels. Moreover, a minimum of 100 images were captured for each sample, which captured 500 or more particles for characterisation.

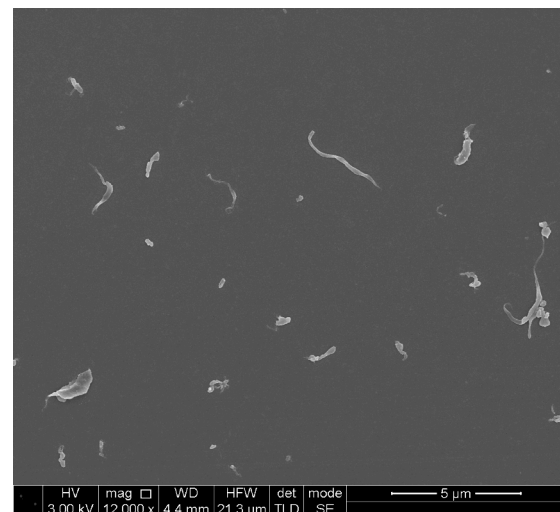


Figure 3. Example of E1 UHMWPE particles isolated by modified base digestion method and deposited on a 15nm pore size membrane filter.

EDX analysis was used to distinguish UHMWPE wear particles from the background or any impurities present in the samples. Figure 2.20 shows the EDX analysis of UHMWPE wear debris. SEM image shows the selection of a UHMWPE wear particle in red colour and selected of the background in blue colour. The EDX graph showed carbon (C), oxygen (O) and gold (Au) peaks for background, while only carbon (C) and gold (Au) peaks for UHMWPE wear particle. Samples were coated with gold. Therefore, a peak for gold was observed for both particle and background. No oxygen peak was observed for UHMWPE because UHMWPE is only composed of carbon and hydrogen elements. Both carbon and oxygen peaks were observed for background because the background material was polycarbonate, which is composed of carbon, hydrogen and oxygen. Absence of any other elements indicated the complete isolation of UHMWPE and cleanliness of particle isolation and SEM sample preparation methodologies. EDX does not detect lighter elements such as hydrogen. Therefore, no peak was generated by hydrogen in EDX graph for both UHMWPE wear debris and background.

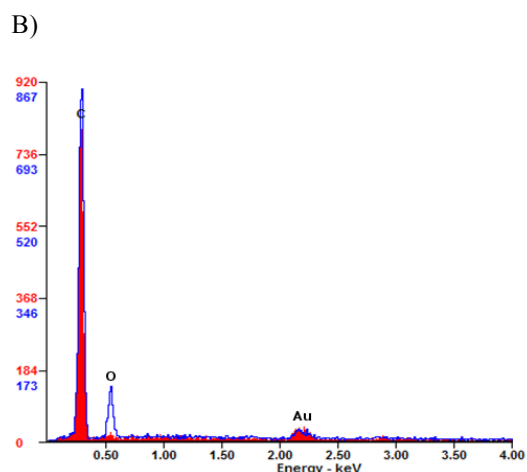
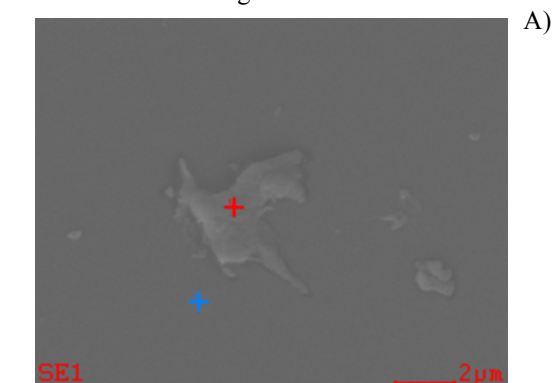


Figure 4: EDX analysis of UHMWPE wear debris isolated by using modified base digestion method developed in this study. A) SEM image showing a point selection inside UHMWPE particle (red cross) and point selection for background (blue cross). B) EDX graph showing carbon(C), oxygen(O) and gold(Au) peaks for background (blue line) and for E1 UHMWPE particle (red filled area).

No oxygen (O) peak was observed for UHMWPE particle due to absence of oxygen in its elemental composition.

Discussion: Vitamin E Infused Highly Crosslinked UHMWPE (E1) knee and ankle joints were wear tested to 5 million cycles using Prosim Knee Wear Simulator at Durham University. E1 hip joints were tested using Prosim Hip Wear Simulator at Durham. Their E1 wear particles were analysed thoroughly and we have found that they are predominantly submicron in size. Noncrosslinked direct compression moulded (DCM) ArCom UHMWPE generated more elongated and fibrillar wear particles; whilst highly crosslinked E1 generated less elongated and more compact shaped wear particles.

References:

1. P. Campbell, S. Ma, B. Yeom, H. McKellop, T. P. Schmalzried, and H. C. Amstutz, "Isolation of predominantly submicron-sized UHMWPE wear particles from periprosthetic tissues.," *J. Biomed. Mater. Res.*, vol. 29, no. 1, pp. 127–31, Jan. 1995.
2. S. Niedzwiecki, C. Klapperich, J. Short, S. Jani, M. Ries, and L. Pruitt, "Comparison of three joint simulator wear debris isolation techniques: Acid digestion, base digestion, and enzyme cleavage," *Techniques*, 2001.
3. A. P. D. Elfick, "The quantitative assessment of UHMWPE wear debris produced in hip simulator testing: the influence of head material and roughness, motion and loading," *Wear*, vol. 249, no. 5–6, pp. 517–527, Jun. 2001.
4. J. L. Tipper, A. L. Galvin, S. Williams, H. M. J. McEwen, M. H. Stone, E. Ingham, and J. Fisher, "Isolation and characterization of UHMWPE wear particles down to ten nanometers in size from in vitro hip and knee joint simulators.," *J. Biomed. Mater. Res. A*, vol. 78, no. 3, pp. 473–80, Sep. 2006.
5. ISO, "ISO 17853 Wear of implant materials — Polymer and metal wear particles — Isolation and characterization," 2011.
6. M. Scott, M. Morrison, S. R. Mishra, and S. Jani, "Particle analysis for the determination of UHMWPE wear.," *J. Biomed. Mater. Res. B. Appl. Biomater.*, vol. 73, no. 2, pp. 325–37, May 2005.
7. J. Tipper, P. . Firkins, a. . Besong, P. S. . Barbour, J. Nevelos, M. . Stone, E. Ingham, and J. Fisher, "Characterisation of wear debris from UHMWPE on zirconia ceramic, metal-on-metal and alumina ceramic-on-ceramic hip prostheses generated in a physiological anatomical hip joint simulator," *Wear*, vol. 250, no. 1–12, pp. 120–128, Oct. 2001.
8. F. Billi, P. Benya, A. Kavanaugh, J. Adams, E. Ebramzadeh, and H. McKellop, "The John Charnley Award: an accurate and sensitive method to separate, display, and characterize wear debris: part 1: polyethylene particles.," *Clin. Orthop. Relat. Res.*, vol. 470, no. 2, pp. 329–38, Feb. 2012.

Tribological Behaviour of the “Reverse” Inverse Shoulder Prosthesis: Shoulder Simulator Study with four Different Material Pairings

Lerf R¹, Reimelt I², Dallmann F², Delfosse D¹

¹Mathys Ltd Bettlach, Bettlach, Switzerland, ; ²Mathys Orthopaedie GmbH, Moersdorf, Germany
reto.lerf@mathysmedical.com

Introduction: When reversing the hard-soft articulation in inverse shoulder replacement, i.e. hard inlay and soft glenosphere (cf. Figure 1), the tribological behaviour of such a pairing has to be tested thoroughly. Therefore, two hard materials for the inlay, CoCr alloy and alumina toughened zirconia ceramic (ceramys[®]) articulating on two soft materials, conventional UHMWPE and vitamin E stabilised, highly cross-linked PE (vitamys[®]) were tested in a joint simulator.

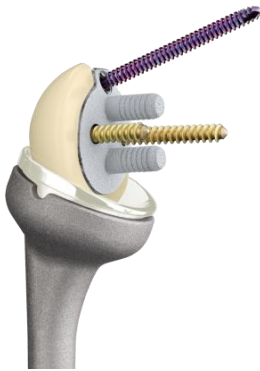


Figure 1: Affinis Inverse shoulder prosthesis by Mathys with vitamin E stabilised, highly cross-linked PE (vitamys[®]) glenosphere and alumina toughened zirconia (ceramys[®]) inlay.

Methods and Materials: The simulator tests were performed at EndoLab GmbH, Rosenheim, Germany, analogue to standardised gravimetric wear tests for hip prosthesis (ISO 14242-1) with load and motion curves adapted to the shoulder. The test parameters differing from the standard were the maximum force (1.0 kN) and the range of motion (flexion / extension +25° / -18°, abduction / adduction +7° / -4°, internal / external rotation +2° / -11°). A servo-hydraulic six station joint simulator (EndoLab) was used to run the tests up to 5*10⁶ cycles with diluted calf serum at 37° C as lubricant. Visual inspection and mass measurements were done at 0.1, 0.5, 1, 2, 3, 4 and 5 million cycles using a high precision scale (Sartorius CP225D) and a stereo microscope, respectively.

The inlays tested were commercial Mathys implants, i.e. inlays made from CoCr alloy bar stock and inlays made from the Mathys proprietary dispersion ceramic ceramys[®]. The Glenospheres were sterile sample implants made from conventional UHMWPE and vitamin E stabilised, highly cross-linked PE vitamys[®]. Three sets of each pairing were tested.

Results: The wear rates measured in the simulator are summarised in the table below and illustrated in Figure 2.

Material pairing	Shoulder simulator study “reverse – inverse”	
	Wear rate [mg/10 ⁶ cycles]	Std Dev [mg/10 ⁶ cycles]
CoCr – UHMWPE	32.50	3.48
CoCr – vitamys [®]	10.65	2.36
ceramys [®] – UHMWPE	20.34	1.14
ceramys [®] – vitamys [®]	5.99	0.79

Table 1: Wear rates of inverse shoulder prosthesis pairings measured by simulator study.

Replacing standard UHMWPE by the cross-linked vitamys[®], the wear rate is reduced to about 1/3 for both hard counterparts, i.e. CoCr inlay and ceramys[®] inlay, respectively. Replacing the CoCr inlay by a part made from ceramys[®] lowers wear by about 37 % in articulation against UHMWPE. This difference is significant (p = 0.002, significance level 5 %). And comparing CoCr and ceramys[®] against vitamys[®], yields a reduction of about 44 %. Which is significant again (p = 0.015, significance level 5 %). The lowest wear rate, with a reduction of about 80 % compared to the standard CoCr inlay–UHMWPE glenosphere, exhibits the pairing of both advanced materials, ceramys[®] – vitamys[®].

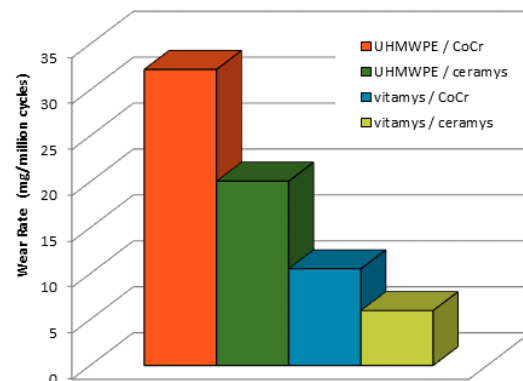


Figure 2: Graphical illustration of the wear rates of inverse shoulder prosthesis pairings measured in the present simulator study.

Discussion: The simulator wear rate of the standard articulation CoCr – UHMWPE is similar to that found in the corresponding pairing for hip endoprosthesis. This results probably from opposing trends: the lower maximum force (1.0 kN vs. 3.0 kN), which reduces wear, and the larger articulation diameter of the glenospheres tested (42 mm compared to 28 – 32 mm in hip joints), which increases wear. All in all, the magnitude of wear rates found seems to be plausible and in-line with results

published by a group from Hamburg, Germany (Helmers 2015).

The reduction of wear rate of about 65 %, observed when standard UHMWPE is replaced by vitamys[®], is the same as found in other shoulder simulator studies with the usual pairing shoulder head against glenoid made from UHMWPE and vitamys[®], respectively (data on file, to be published).

Reference:

Helmers N, Betthäuser A, Obere Extremität 2015;10:47-54

Hybrid Porous UHMWPE Scaffolds for Bone Defects Replacement

Maksimkin A.V.¹, Senatov F.S.¹, Anisimova N.Yu.², Kiselevsky M.V.², Zalepugin D.Yu.³, Chernyshova I.V.³, Tilkunova N.A.³, Kaloshkin S.D.¹

¹National University of Science and Technology "MISIS", Moscow, Russian Federation

²N.N. Blokhin Russian Cancer Research Center, Moscow, Russian Federation

³State Plant of Medicinal Drugs, Moscow, Russian Federation

Senatov@mis.ru

Introduction:

Currently, reconstruction of the structural integrity of the damaged bone tissue is an urgent problem. Bone tissue has a natural ability to regenerate, but in case of large defects this ability is extremely limited.

Development of scaffolds with architecture of bone tissue and capable to function under the mechanical load is a promising direction for solving this problem.

UHMWPE is a promising polymer material which was already widely used in implantology. UHMWPE may be recommended for the manufacture of implants simulating as closely as possible the porous cancellous bone structure because of a combination of high chemical resistance and bioinertness. But the extremely high molecular weight of the polymer does not allow to use traditional methods of foaming. The creation of hybrid scaffolds with nonporous bulk layer and porous layer with three-dimensional structure of UHMWPE with the ability to control the pore size was studied in this work.

Methods and Materials:

The formation of the porous structure is based on obtaining of UHMWPE powder composite polymer / soluble by solid phase method of mixing using a planetary ball mill [1]. The size filler determines the size pores. Mixing was performed in low energy conditions to keep the size of the particles. The forming of the composite powder of polymer / soluble filler was carried out by thermopressing. Optimal regimes of thermopressing were selected to achieve the best sintering of UHMWPE particles.

The soluble filler was removed after thermopressing with subcritical water (water flow rate of 3 ml / min) at a temperature of 120 °C and a pressure of 250 bar to remove salt [2].

A method allowing to form hybrid materials based on UHMWPE combining solid and porous structure was also developed.

The obtained porous and hybrid UHMWPE samples were studied with scanning electron microscopy (SEM) and tested for compressive and flexural strength. Volume porosity and pore size distribution were studied.

Study of porous samples *in vivo* was performed by orthotopic implantation of cylindrical samples with average size 5 × 1.5 mm into tibial bones of "Wistar" rats (n=5) for 60 days. Skin and muscles on rat's leg were dissected during the surgery in order to get access to the surface of tibial bone. After that a small defect (1.8 mm) was created with a drill and implant was placed into the defect. Tibial bones were taken out after implantation and

then they were histologically studied with haemotoxilyn-eosin stain.

Results:

The studies of porous UHMWPE showed that the pores are open and interconnected. Volume porosity of the obtained samples was over then 80%. The pore size range was from 80 to 700 microns. These porous samples had high plasticity and could be bent several times. The sample recovers its dimensions and shape after unloading. All UHMWPE particles were sintered.

Possibility of producing hybrid materials combining nonporous reinforcing UHMWPE layer and porous layer was demonstrated (Fig.1).

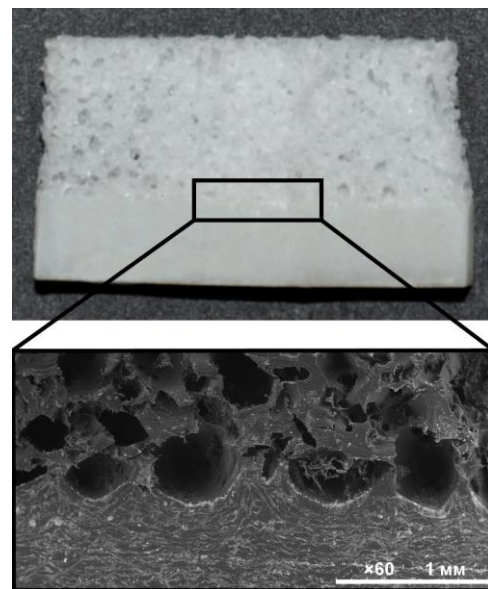


Fig.1 – Hybrid UHMWPE scaffolds with nonporous bulk layer and porous layer

Histology of implanted porous UHMWPE samples and the surrounding tissues was studied. Important indicators are the state of the bone tissue that contacts with the implant and a motor activity of the animals. Histology of the implant and the surrounding tissue is shown in Figure 2.

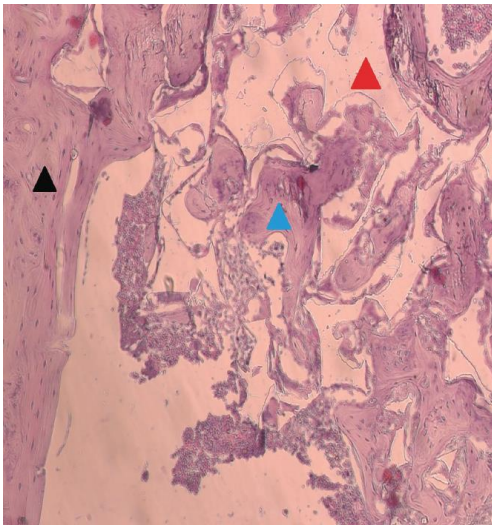


Fig.2 – Porous UHMWPE implant inside the bone. Black arrow – bone tissue, red arrow - material of the implant, blue arrow - sites of neosteogenesis. H & E stain. Magnification $\times 100$

Discussion:

The size of the formed pores and their distribution in the porous UHMWPE depends on the size of the soluble filler particles. The use of low energy modes of ball milling of polymer / soluble filler composite powders allows to save the distribution of particles size, which greatly simplifies the programming of required pore size.

The main influence on the quality of the sintering of UHMWPE particles in the process of thermoforming had temperature and pressure.

There were no signs of acute rejection and no macrophages in the contact zone after implantation of porous UHMWPE sample into bone defect. It should be noted that during functioning of implant in the joint for 2 months there were no motor activity disorders. After surgery the animals has used limbs with implant for moving without any lameness. No signs of inflammation and rejection were observed. The same situation was also discussed in case of nonporous UHMWPE for cartilage defects replacement [3].

Acknowledgements

This work is supported by the Federal Targeted Program “Research and development in priority directions of development of scientific technological complex of Russia in 2014–2020 years”, with the financial support from the Ministry of Education and Science of Russian Federation: agreement 14.578.21.0055, 19 September 2014. Unique identifier of applied scientific researches: RFMEFI57814X0055.

[1] A.V. Maksimkin et al. Technologies for manufacturing ultrahigh molecular weight polyethylene based porous structures for bone implants // *Biomedical Engineering*. – 2013. -V. 47(2). – P.73-77.

[2] D.Yu. Zalepugin et al. The use of subcritical water in the technology of porous ultrahigh molecular weight polyethylene obtaining // *Russian Journal of Physical Chemistry B*. (in print)

[3] F.S. Senatov, A.N. Kopylov, N.Yu. Anisimova, M.V. Kiselevsky, A.V. Maksimkin. UHMWPE-based nanocomposite as a material for damaged cartilage replacement / *Materials Science and Engineering C* 48 (2015) 566–571

Oriented bulk nanocomposites based on UHMWPE/MWCNT

Maksimkin A.V., [Chukov D.I.](#), Senatov F.S., Mostovaya K.S., Kaloshkin S.D, Gorshenkov M.V.
National University of Science and Technology "MISIS", Moscow, Russian Federation
aleksey_maksimkin@mail.ru

Introduction:

Ultrahigh molecular weight polyethylene (UHMWPE) is a unique polymeric material with huge potential. But obtaining of nanocomposites based on UHMWPE is associated with technical difficulties of its processing. UHMWPE does not have a plastic state that makes it almost impossible to introduce fillers into the melt. Moreover, it is a polar polymer that prevents the formation of strong interfacial interactions with reinforcing fillers.

In this work oriented bulk nanocomposites based on UHMWPE and multi-walled carbon nanotubes (MWCNTs) with high mechanical and tribological properties were developed. MWCNTs were functionalized by direct fluorination to improve the interfacial interaction between the fillers and the polymer matrix.

Methods and Materials:

GUR 4120 UHMWPE resin with a molecular weight of $5 \cdot 10^6$ g/mol was used for the preparation of oriented nanocomposites. Multi-walled carbon nanotubes ("Taunit", Russia) were used as fillers. The average diameter of the nanotubes is 30 nm, length more than 2 microns. Fluorination of MWCNTs was conducted in a steel reactor at a pressure of fluorine gas $0.9 \div 1$ atm at 150 °C. Duration of the treatment was 2 hours.

Introduction of fluorinated MWCNTs in the UHMWPE matrix was carried out by solid phase mixing using a planetary ball mill.

Formation of the oriented nanocomposites was carried out in several stages [1]. In the first stage monolithic nanocomposites with isotropic structure were prepared by compression molding. In the second stage the formed nanocomposites were subjected to uniaxial low-orientation drawing. Drawing was carried out at room temperature till the sample residual elongation of 200%. During these operations oriented precursors of nanocomposites were obtained. In the third stage oriented precursors were formed into oriented nanocomposites by compression molding.

Results:

The obtained oriented bulk nanocomposites based on UHMWPE reinforced with fluorinated MWCNTs have shown great efficiency of using low-orientation drawing and fillers functionalization in terms of mechanical properties of the composites, as shown in table 1.

Table 1. Mechanical properties of the nanocomposites

Materials	Ultimate strength, MPa	Tensile Modulus, MPa	Elongation, %
neat UHMWPE	22±2	700	>200
Oriented UHMWPE	94±9	767±11	71±4
Oriented UHMWPE/0,1%MWCNT	99±11	896±71	60±3
Oriented UHMWPE/0,5%MWCNT	94±2	950±50	63±7
Oriented UHMWPE/1%MWCNT	101±8	974±62	66±12
Oriented UHMWPE/0,1%FMWCNT	103±10	897±35	78±20
Oriented UHMWPE/0,5%FMWCNT	122±2	867±61	48±3
Oriented UHMWPE/1%FMWCNT	132±0,3	919±10	53±5

The tribological tests showed a decrease in the coefficient of dry friction from 0.24 for the initial (neat) polymer to 0.14 for the oriented UHMWPE composites reinforced with 1wt.% MWCNT.

Discussion:

The proposed regimes of obtaining of oriented bulk nanocomposites lead to the formation of nanofibrils in the structure of UHMWPE. A particularly large number of nanofibrils was observed in the materials which were reinforced with fluorinated MWCNTs as shown in Figure 1. Nanofibrils consist of a more or less continuous crystalline phase with dispersed and rare defects [2]. The theoretical strength of the nanofibrils may reach up to 19 GPa. Formation of the nanofibrils is possible due to the formation of folded crystalline structures on the surface of MWCNTs during molding of nanocomposites and its further unwrapping to nanofibrils during loading of the material.

Nanofibrils have a positive influence on the tensile strength of obtained nanocomposites, especially in case of using fluorinated carbon nanotubes, when the number of nanofibrils dramatically increases.

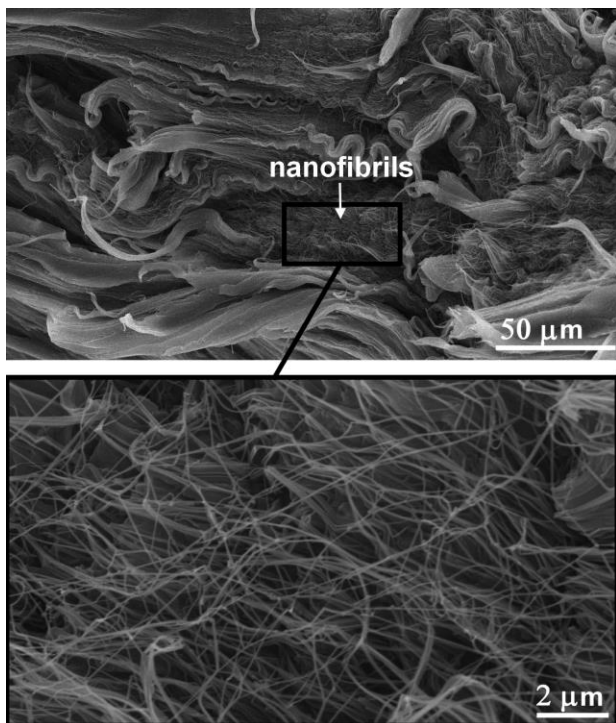


Figure 2 – Scanning electron microscopy images of fracture surface of oriented UHMWPE/FMWCNT

Acknowledgements

This work is supported by the Federal Targeted Program “Research and development in priority directions of development of scientific technological complex of Russia in 2014–2020 years”, with the financial support from the Ministry of Education and Science of Russian Federation: agreement № 14.578.21.0083, 27 November 2014. Unique identifier of applied scientific researches: RFMEFI57814X0083.

[1] A.V. Maksimkin, S.D. Kaloshkin, M.S. Kaloshkina, M.V. Gorshenkov, V.V. Tcherdyntsev, K.S. Ergin, I.V. Shchetinin. Ultra-high molecular weight polyethylene reinforced with multi-walled carbon nanotubes: Fabrication method and properties // *Journal of alloys and compounds*. – 2012. – V.536S. – P.s538-s540

[2] L. Berger, H.H. Kausch, C.J.G. Plummer. Structure and deformation mechanisms in UHMWPE-fibres // *Polymer*. – 2003. – V. 44 – P. 5877-5884.

Finite Element Evaluation of the Newest ISO Testing Standard for Polyethylene TKR Liners

Mell SP¹, Wimmer MA¹, Lundberg HJ¹

¹Rush University Medical Center, Chicago, IL, USA

steven_p_mell@rush.edu

Introduction: With highly crosslinked polyethylenes becoming more prevalent in total knee replacements (TKRs), proper testing protocols become important to evaluate any perceived benefits. Generic walking profiles applied to mechanical knee simulators are the current gold standard in wear testing of TKRs. Recently, there was a change in the ISO standard for knee testing (ISO 14243-3): the direction of motion in the anterior/posterior (AP) direction was reversed. The effects of this change have not been investigated. Using a finite element analysis (FEA) model of a TKR, we investigated differences in wear scar areas for both ISO 14243-3(2004) and ISO 14243-3(2014). Kinematic inputs from the older and newer ISO were compared against each other, and wear scar areas predicted by the FEA model were validated against simulator generated wear scar outlines. The null hypothesis of this study was that the wear scars from new and old ISO inputs would be similar but mirrored in the medial-lateral directions.

Methods and Materials: A FEA model was created from CAD models of a left sided NexGen Cruciate Retaining TKR (Zimmer, Warsaw, IN). 8 node hexahedral elements were used to model the UHMWPE component. The CoCrMo femoral component and titanium tray were modeled as rigid surfaces, utilizing a mix of 2nd order quadrilaterals and tetrahedrons (Figure 1). The UHMWPE component was modeled using the J-2 Plasticity model [1] with a density of 9.4E-7kg/mm³. Contact between the tibial tray, UHMWPE insert, and femoral component was modeled as penalty contact, with the friction coefficient set to 0.04 on the articular surface and 0.2 at the backside. The tibial tray was fixed during the simulation and the UHMWPE insert was left free in all 6 degrees of freedom. Initial contact between the tibial tray and the UHMWPE insert was modeled as an interference fit. Internal/external rotation, flexion/extension, and anterior/posterior translation were applied to the femoral component as velocity boundary conditions at a reference point located at the center of rotation as defined during simulator testing. Medial/lateral translation and abduction and adduction were left free. Axial force was applied through the femoral reference point. FEA models were run using ABAQUS v6.13-2/Standard (Dassault Systèmes, Waltham, MA). The loads and motions specified by simulator standard ISO 14243-3(2014) were compared to ISO 14243-3(2004). Wear scars were generated using a custom Python script using an energy-based wear model [2], adapted to FEA, though without the effects of cross shear. The wear model utilizes a parameter, unit work, defined as the frictional energy required to remove a unit volume of material. A unit work value of 8.473E-8 J/mm³ was used and predicted wear was scaled to 1 million cycles. Preliminary validation of the FEA model was carried out by comparing wear scar

areas to contact areas produced using a mechanical knee simulator (Endolab GmbH, Germany). The articulating surface of NexGen CR PE inserts were colored with marker and simulator tests run in displacement control for 10 cycles using the same kinematic and force profiles as the FEA model. A coordinate measuring machine (Smartscope, OGP, Rochester, NY) was used to outline the contact areas. ImageJ (NIH, Bethesda, MD) was used to calculate the area and dimensions of both the FEA and simulator generated contact areas. Wear areas and the length of contact area in the AP direction were compared between the old and new ISO profiles. The same outputs were used to compare the simulator contact areas to the FEA generated wear scars.

Results: FEA predicted wear scars for new ISO inputs (Figure 2A) covered a larger area of the articular surface and were longer than the old standard (Figure 2B). Locations of higher wear predicted by the wear model varied considerably between profiles, with high wear in the old standard being more anterior on the tibial component, but more posterior in the new standard. FEA predictions compared well with the simulator as shown by the large overlap between FEA predicted wear scars and simulator generated contact areas (Figure 2). The average differences in area and length between the FEA model and the simulator tested components was 16.6mm² and 0.1mm respectively. The average overlap between simulator contact areas and predicted FEA contact areas was 67.2%.

Discussion: Contrary to the hypothesis, there was no obvious relationships between the wear scars from the old and new ISO profiles. The new ISO profile coverage predicted by the FEA model was 35.6%, while the old ISO was 26.3%. Contact area coverage of the total articular surface for retrievals of the same component has been shown to be 50.3±12.23% [3]. Wear scars from the old and new profiles were over one standard deviation smaller than that measured on retrievals. The FEA model performed well when compared against simulator tested components. Although FEA and simulator wear scar shapes and sizes were similar, differences in wear scar location can be attributed to variations in the setup or start position of simulator tests. In the future, the wear model should be adapted to account for cross-shear, and the mesh updated periodically in order to predict wear rate. More sophisticated material models are planned to be implemented, and models representing different UHMWPE materials such as highly crosslinked polyethylene could be investigated. Future validation of the model should include volumetric analysis with comparisons between the FEA model and components that have undergone a full simulator study. This could lead to a

better understanding of the relationship between polyethylene material properties and wear.

The results of the study suggest that major differences between the old and the new ISO standard exist and therefore historical wear results are not comparable to newly obtained results. In addition, this study demonstrates the utility of FEA in wear analysis as a supplement to simulator testing.

References: [1] Bergström et al., *Biomaterials*, 2002, 23(11):2329–43. [2] Schwenke et al., *Wear*, 2013, 301(1–2):168–74. [3] Elmira Moslemi Rad., MS Thesis, UIC, 2015.

Acknowledgements: Funding for this study was provided by NIH R01AR059843 (MAW) and RTSC Pilot Project 13061104-GR01 (HJL). Thanks to Zimmer for providing CAD models of the NexGen Cruciate Retaining TKR.

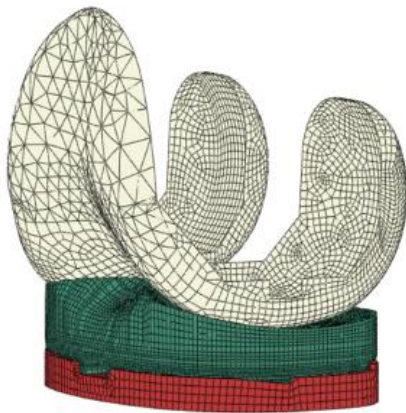


Figure 1: The completed FEA assembly representing the 3 components of the TKR design.

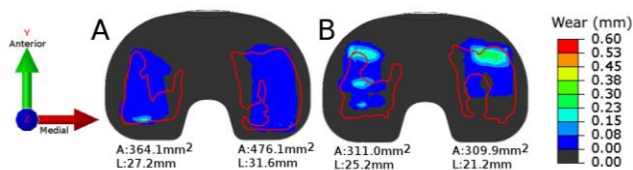


Figure 2: Predicted wear scar areas from FEA simulations (contours) and wear scar outlines from simulator tests (red outlines). A) ISO 14243-3(2014), B) ISO 14243-3(2004). The newest ISO had a larger percentage of the articular surface with contact than the older standard. Areas (A) and lengths (L) are for FEA results.

Quantification of the Cytokine Release from Macrophages Stimulated with Spherical Ultra-High Molecular Weight Polyethylene Particles of Varying Size Using Inverted Cell Culturing Process

Miho Niikura¹, Shuya Nogi¹, Ye Han¹, Alex Turner¹, Naohide Tomita¹

¹Kyoto University, Kyoto, Japan

niikura.miho.73u@st.kyoto-u.ac.jp

Introduction: Although the biological response to Ultra-High Molecular Weight Polyethylene (UHMWPE) particles differs based upon the size ⁽¹⁾ and shape ⁽²⁾ ⁽³⁾ of the wear particles, dosage dependency to the particle size on the macrophage response has not yet been clarified yet. In this study the macrophage response spherical UHMWPE particles of different size is quantified by using an inverted macrophage cell model.

Methods and Materials: Spherical UHMWPE particles, 10 and 30 μ m in diameter (Mitsui Chemicals, Japan) were used. The particles were tested to be endotoxin free by using a Pierce LAL Chromogenic Endotoxin Quantitation Kit (Thermo, USA). To analyze the macrophage biological response, an inverted cell culturing process was used ⁽⁴⁾. The mouse macrophage-like cells from the cell line RAW264 were seeded at densities of 1×10^5 cells and 2×10^5 cells per well in a 96-well culture plate and incubated at 37°C, in a 5%CO₂ environment for 1h to allow the cells adhere to the plate surface. UHMWPE particles suspended in the culture medium were then added to each well in the corresponding amount. After that, fresh medium was added to fill the wells, and a sealing film for cell and tissue culture (BM, Japan) was used to cover the culture plate. The culture plate was then inverted to cause the UHMWPE particles float up and interact with the adhered macrophages. The inverted culture plate was incubated for 24h. The amount of tumor necrosis factor α (TNF- α) was measured by enzyme-linked immunosorbent assay (ELISA) using a TNF-Alpha Quantikine ELISA Kit (RSD, USA). Also, Giemsa staining was performed after the 24h incubation and an inverted microscope was used to obtain the image of the bottom surface.

Results and Discussion: The state of the macrophages reacting to the 10 μ m and 30 μ m UHMWPE particles is shown in Figure 1. The concentrations of TNF- α released by the 1×10^5 macrophages stimulated by each of the two different UHMWPE particles and that from the 2×10^5 macrophages are summarized in Figure 2 and 3 respectively. It was shown that regardless of the particle size, the amount of cytokine released is most directly proportional to the total UHMWPE particle surface area. The concentrations of TNF- α released by 1×10^5 and 2×10^5 macrophages stimulated by 10 μ m and 30 μ m the UHMWPE particles are plotted in Figure 4 with respect to particle surface area. It was shown that the amount of cytokine released was not

proportional to the number of the macrophages.

Figure 1 shows that the 10 μ m UHMWPE particles were phagocytosed by the macrophages one by one, whereas the 30 μ m UHMWPE particles were surrounded by several macrophages to complete phagocytosis. Although there was a difference in the way macrophages responded to the 10 μ m and 30 μ m UHMWPE particles, the result showed that TNF- α release was proportional to the total surface area regardless of the particle size. Fisher et al. proposed a functional biological activity (FBA) parameter to evaluate the influence of wear debris in osteolysis ⁽⁵⁾. In this FBA parameter, debris length (0.1-1.0, 1.0-10, 10-100 micrometer) and wear volume were used to estimate the potential for osteolysis. From the results of this study, however, it is suggested that the macrophage response may be more directly dependent on debris surface area compared to debris volume.

References

- (1) Green TR, Fisher J, Stone M, Wroblewski BM, Ingham E. Polyethylene particles of a 'critical size' are necessary for the induction of cytokines by macrophages in vitro. *Biomaterials*. 1998 Dec; 19(24):2297-302.
- (2) Yang SY, Ren W, Park Y, Sieving A, Hsu S, Nasser S, Wooley PH. Diverse cellular and apoptotic responses to variant shapes of UHMWPE particles in a murine model of inflammation. *Biomaterials*. 2002 Sep; 23(17):3535-43.
- (3) Ren W, Yang Y, Fang W, Hsu S, Wooley H. Distinct gene expression of receptor activator of nuclear factor-kappaB and rank ligand in inflammatory response to variant morphologies of UHMWPE particles. *Biomaterials*. 2003 Nov; 24(26):4819-26.
- (4) Fang H, Ho Y, Yang C, Liu H, Ho F, Lu Y, Ma H, Huang C. Preparation of UHMWPE particles and establishment of inverted macrophage cell model to investigate wear particles induced bioactivities. *Journal of Biochemical and Biophysical Methods*. 2006 Oct; 68(3):175-87.
- (5) Fisher J, Bell J, Barbour PSM, Tipper JL, Matthews JB,

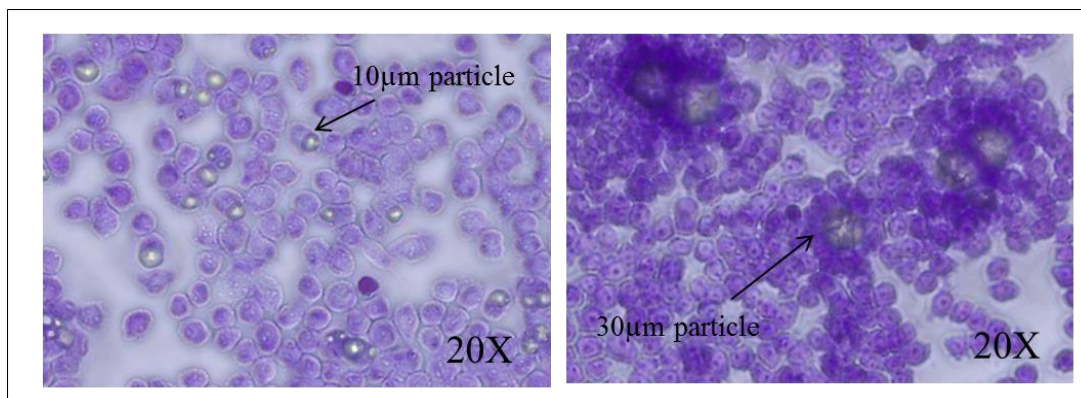


Figure 1. The state of the macrophages reacting to 10 μ m and 30 μ m UHMWPE particles.

Besong AA, Stone MG, Ingham E. A novel method for the prediction of functional biological activity of polyethylene wear debris. Proceedings of the Institution of Mechanical Engineers, PartH: Journal of Engineering in Medicine. 2001 Feb; 215(2): 127-32.

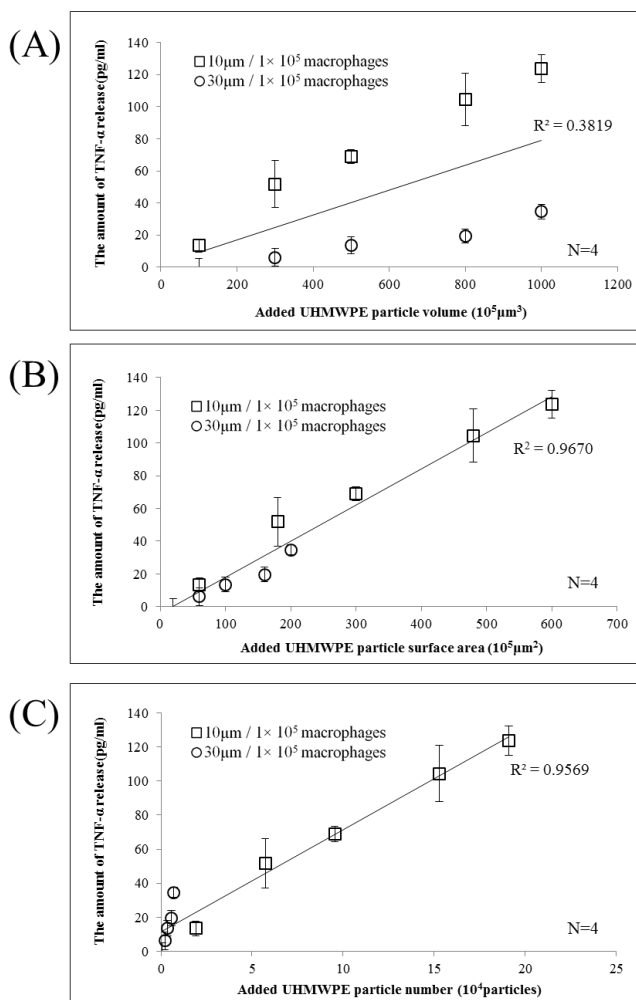


Figure 2. TNF- α released by 1×10^5 macrophages stimulated by $10 \mu\text{m}$ and $30 \mu\text{m}$ UHMWPE particles. (A) Plotted with respect to particle volume μm^3 . (B) Plotted with respect to particle surface area μm^2 . (C) Plotted with respect to particle number. The coefficient of determination (R^2) was evaluated regardless of the difference between the particle sizes.

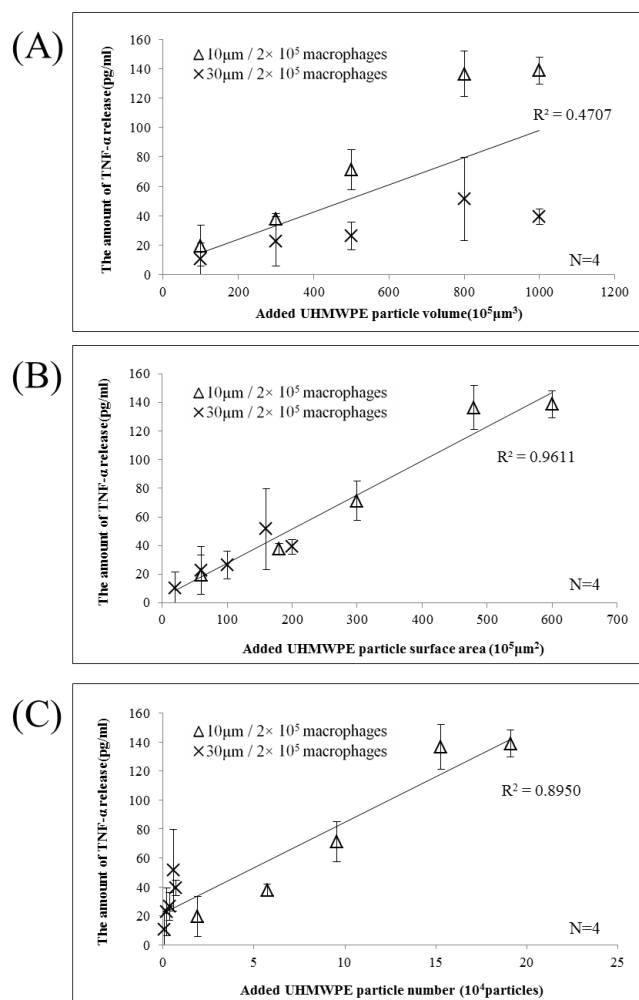


Figure 3. TNF- α released by 2×10^5 macrophages stimulated by $10 \mu\text{m}$ and $30 \mu\text{m}$ UHMWPE particles. (A) Plotted with respect to particle volume μm^3 . (B) Plotted with respect to particle surface area μm^2 . (C) Plotted with respect to particle number. The coefficient of determination (R^2) was evaluated regardless of the difference between the particle sizes.

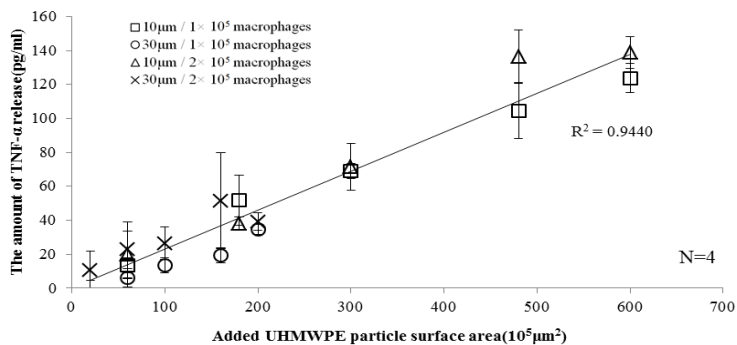


Figure 4. TNF- α released by 1×10^5 and 2×10^5 macrophages stimulated by $10 \mu\text{m}$ and $30 \mu\text{m}$ UHMWPE particles plotted with respect to particle surface area μm^2 . The coefficient of determination (R^2) was evaluated regardless of the difference between the particle sizes and macrophage number.

Spatially cross-linked UHMWPEs using chemical cross-linking: Increased toughness for thinner implants

Oral E^{1,2}; Doshi BN¹; Kayandan S¹; Muratoglu OK^{1,2}

¹Harris Orthopaedic Laboratory, Massachusetts General Hospital; ² Department of Orthopaedics, Harvard Medical School, Boston, MA

eoral@partners.org

Introduction: Radiation cross-linking of UHMWPE is used to increase the wear resistance of UHMWPE; highly cross-linked UHMWPEs have reduced the incidence of wear-debris induced periprosthetic osteolysis significantly over the last decade. On the other hand, increased cross-link density results in decreased fracture toughness. Decreased toughness and its implications are a concern.

Dislocation is a major complication in total hips and its incidence can be decreased with the use of larger femoral heads [1]. Metal-on-metal implants, which were preferred for the larger sizes possible, were recently eliminated from the clinic due to the disastrous consequences of metal wear debris. This has created a great need for the alternative metal-on-UHMWPE implants to accommodate larger head sizes, which can be done by the use of thinner UHMWPE liners.

Here we describe a chemical cross-linking method of making tougher UHMWPEs for use as thinner liners by surface cross-linking.

Methods and Materials: An aqueous emulsion of 30 mg/ml of dicumyl peroxide (DCP) with 15 mg/ml vitamin E and 40 wt% Tween 20 was prepared. Medical grade 1020 UHMWPE blended with 0.1, 0.3 and 0.8 wt% vitamin E was consolidated and doped with the above emulsion for durations up to 16 hours at 100°C. The doped samples were heated further at 150°C to decompose the peroxide and cross-link the surface.

Cross-link density was measured by swelling 3 mm cubes in xylene pre-heated to 130°C for 2 hours. The gravimetric swell ratio was converted to a volumetric swell ratio using the density of polyethylene as 0.94 g/cc and the density of xylene at 130°C as 0.75 g/cc. The crosslink density was calculated as previously described [2]. Pin-on-disc (POD) wear testing was performed on cylindrical pins (dia. 9 mm, height 13 mm) as previously described [3] at 2 Hz for 1.2 million-cycles (MC). Wear was determined gravimetrically every ~0.16 MC and the wear rate was determined by the weight change from 0.5 to 1.2 MC. The IZOD impact strength was determined by double notching and testing of the samples (6.35 × 12.7 × 63.5 mm, n=5) according to ASTM F-648. It is reported as (kJ/m²). The oxidation induction time (OIT) was determined using a differential scanning calorimeter. The samples (~5mg) were heated from 20 to 200°C at a rate of 20°C/min under nitrogen. After 5 minutes at 200°C the gas was switched to oxygen and the onset of oxidation was recorded (OIT) as the intercept of the extended baseline and the steepest tangent drawn to the exotherm. Statistical significance was calculated using student's t-test and the significance was attributed to p<0.05.

Results: The maximum cross-link density attained by doping the blended materials with a DCP emulsion at 100°C was 302±23 mol/m³ (4 hr doping) for 0.1 wt%

vitamin E-blended UHMWPE, 287±18 mol/m³ (8 hr doping) for 0.3 wt% vitamin E-blended UHMWPE and 227±16 mol/m³ (16 hr doping) for 0.8 wt% vitamin E-blended UHMWPE. The cross-link density of the 100-kGy irradiated and melted control was 245±4 mol/m³. This showed that the desired cross-link density and presumably the desired wear rate could not be reached for 0.8 wt% vitamin E-blended UHMWPE. Further testing was done on 0.1 and 0.3 wt% vitamin E-blended UHMWPEs.

The oxidation induction time of the surface cross-linked UHMWPEs was 13.6 min for 0.1 wt% and 19.5 min for 0.3 wt% vitamin E-blended UHMWPE. A large-scale UHMWPE was prepared using the 0.3 wt% vitamin E-blended UHMWPE.

It was shown that by limiting cross-linking to the surface, the impact strength of the implant material was significantly increased (Table 1).

Table 1. The properties of high vitamin E content, surface cross-linked UHMWPEs.

	IZOD Impact Strength (kJ/m ²)	Wear Rate (mg/MC)	Surface cross-link density (mol/m ³)
0.3 wt%	114±2.0	0.9±0.1	288±16
Control	79±1.0	0.9±0.2	245±4

Discussion: Our goal was to develop a surface cross-linked, highly wear and oxidation resistant vitamin E blended UHMWPE with improved toughness. Our approach was to diffuse the organic peroxide DCP in an emulsified form and cross-link the material during a subsequent decomposition step above the decomposition temperature of this peroxide (137°C)..

We determined that the optimal diffusion durations for 0.1 and 0.3 wt% blends feasible in a manufacturing setting. The wear rate of this surface cross-linked UHMWPE was comparable to a clinically relevant, highly cross-linked UHMWPE (Table 1). There was a substantial improvement (44%) in the impact strength due to the restriction of cross-linking to the surface.

In summary, this method can be used to manufacture thinner cross-linked UHMWPEs with high toughness to be used with larger femoral heads and reduce the risk of dislocation.

References: [1] Cuckler et al. JOA (2004) 19:41-4; [2] Oral et al. Biomaterials (2010) 31:7051-60; [3] Bragdon et al. (2001) 16: 658-61.

Peak Stress Dictates Fatigue Crack Growth in a Hindered Phenol Antioxidant UHMWPE

Parran, K¹, Narayan V², Rimnac, C¹

¹Case Western Reserve University, Cleveland, OH; ²DePuy Synthes, Warsaw, IN
clare.rimnac@case.edu

Introduction: Fatigue and fracture resistance are important properties of cross-linked ultra-high molecular weight polyethylene (UHMWPE) materials for use in total joint replacements. The Paris relationship has been useful for describing fatigue crack propagation behavior in many metallic and polymeric materials and relates the change in crack growth per cycle (da/dn) to the cyclic range of the stress intensity factor at the crack tip (ΔK) (eqn. 1). However, recent work suggests that crack propagation in non-crosslinked and highly crosslinked formulations of UHMWPE occurs in an essentially non-cyclic manner, even under applied cyclic loading [1,2]. It has been found that a relationship between the change in crack growth per time (da/dt) versus the peak stress (K_{max}) more comprehensively describes fatigue crack growth behavior in UHMWPE (eqn. 2).

$$\frac{da}{dN} = C\Delta K^m \quad (\text{eqn. 1}) \quad \frac{da}{dt} = YK_{max}^n \quad (\text{eqn. 2})$$

In this study, we asked if the dependency on peak stress during fatigue crack growth also applies to a 2nd generation highly cross-linked polyethylene that has been modified with a hindered phenol antioxidant for oxidation resistance.

Methods and Materials: Crosslinked polyethylene (XLKTM) (as a control material) and hindered phenol antioxidant polyethylene (AOXTM) were received as ram extruded rods (DePuy Synthes, Warsaw, IN). Round compact tension specimens were machined according to ASTM E647-11 [3] in the transverse direction with: notch depth, $a = 18\text{mm}$; specimen length, $w = 40\text{mm}$; thickness, $b = 20\text{mm}$; and side groove depth of 2 mm on each side. Following machining, one half of the AOX specimens were aged for 40 days using a standard protocol based on ASTM F2003 of 5 atm. oxygen at 70°C [4]. Before testing, specimen notches were razor sharpened an additional 1.6 mm at a rate of 0.16 mm/min making the total initial pre-crack length 19.6 mm.

Three test conditions for each of the three test groups (XLK, AOX, Aged AOX) were evaluated with two specimens tested per condition: (1) Sine wave/frequency = 0.1Hz/R=0.1 (where $R = P_{min}/P_{max}$); (2) Sine wave/frequency = 3Hz/R=0.5; (3) Triangle wave/frequency = 1Hz/R=0.1.

Testing was conducted under ambient laboratory conditions on an Instron 8511 servohydraulic load frame (Instron, Norwood, MA). Cyclic load ranges were held constant and the stress intensity crack tip driving force was allowed to increase via crack extension. A precision traveling microscope (Daedal, Philadelphia, PA) with 5 μm resolution was used to measure crack growth.

Crack growth rates (da/dn and da/dt), applied stress intensity factor range (ΔK), and maximum (peak) stress intensity (K_{max}) were calculated based on ASTM E647-

11 [3]. The data was plotted for both the Paris and the peak stress relationships (eqns 1,2). The parameters C and m were calculated between 10⁻⁴ and 10⁻² mm/cycle for the Paris relationship, while the parameters Y and n were calculated between 10⁻⁴ and 10⁻² mm/s for the peak stress relationship. A velocity normalizing factor (Q) was also employed, which describes the theoretical ratio of average crack velocity under a nonsinusoidal load waveform to that driven by a sine wave with the same peak stress [2]. Statistical analysis of the Paris regression lines for the sine wave/R=0.1 condition was conducted [5].

Results: The fatigue crack growth behavior in the Paris regime was obtained for all test conditions and test groups (Fig. 1). All test groups showed K_{max} dominated crack growth (Figure 2) in that the data effectively collapsed to a single response for the peak stress relationship for each group. The antioxidant material (AOX) behaved similarly in the unaged and aged conditions. Comparison of the Paris regression lines for the unaged and aged AOX groups demonstrated no significant difference in m ($p=0.370$) but a difference in C ($p=0.007$) suggesting a possible marginal loss of fatigue crack propagation resistance due to aging. Both the unaged and aged AOX groups demonstrated no difference in m ($p=0.96$ and $p=0.17$, respectively) but a significant difference in C ($p<0.001$) compared to the XLK group indicating better fatigue crack propagation resistance of both conditions of the AOX material relative to the XLK material (Table 1).

Discussion: The results of this study support that the AOX hindered phenol antioxidant UHMWPE material experiences stable crack growth under cyclic load that is quasistatic, and dependent on K_{max} , not ΔK . The AOX material also behaves similarly in the unaged and aged conditions even under a relatively severe accelerated aging protocol that likely represents more time in vivo than clinically monitored time periods to-date for historical UHMWPE. The significance of the small change noted with aging may need to be assessed further since aging under these conditions have not yielded any substantial changes in other mechanical and physical properties in other studies [6].

These results are consistent with earlier work reported for conventional and highly crosslinked UHMWPE materials that demonstrated that fatigue crack growth is dictated by peak stress (K_{max}) [1, 2]. That is, UHMWPE fractures in an intrinsically brittle manner in the presence of stress concentrations or cracks [1]. The findings of this study further support that the crack growth behavior in crosslinked UHMWPE materials, even when modified with an antioxidant, is dictated by peak stress intensity factor (K_{max}) and not the cyclic stress intensity factor range (ΔK). This brittle behavior means that even a static

load will drive crack growth in UHMWPE; the application of a cyclic load is not needed. Such static crack growth from a stress concentration has in fact been observed and reported for UHMWPE [7]. In regard to the current study, the mechanism of crack growth appears to be unchanged due to the incorporation of an antioxidant molecule into the material.

These findings may be useful in developing more physically-motivated fatigue (and static) crack growth assessments of crosslinked UHMWPE materials than the currently utilized Paris relationship. Such a physically-motivated approach may be more relevant and useful in the design of UHMWPE joint replacement components than the Paris relationship.

Acknowledgements: This work was supported by a research agreement with DePuy Synthes. The Wilbert J. Austin Chair (CMR) is also gratefully acknowledged.

References: [1] Furmanski and Pruitt, Polymer 2007; [2] Sirimamilla, Furmanski, and Rinnac, J Biomed Mater Res Appl Biomat 2012; [3] ASTM 647-11 Standard test method for measurement of fatigue crack growth rates. 2000; [4] ASTM F2003 Standard Practice for Accelerated Aging of UHMWPE after Gamma Irradiation in Air. 2008; [5] Larsen, Master of Applied Statistics, Module 9. 2006; [6] Narayan, King and Senyurt, 56th Trans ORS, Poster 2316, 2010; [7] Sirimamilla, Furmanski, and Rinnac, J Mech Behav Biomed Mater 2013.

Material and Testing Conditions	Paris Relationship	
	m (exponent)	C (coefficient)
XLK, specimen 1, sine wave, f=0.1Hz, R=0.1	8.16	9.35E-06
XLK, specimen 2, sine wave, f=0.1Hz, R=0.1	8.20	9.10E-06
AOX, specimen 1, sine wave, f=0.1Hz, R=0.1	10.25	3.12E-07
AOX, specimen 2, sine wave, f=0.1Hz, R=0.1	8.22	2.28E-06
aged AOX, specimen 1, sine wave, f=0.1Hz, R=0.1	7.99	4.01E-06
aged AOX, specimen 2, sine wave, f=0.1Hz, R=0.1	7.91	4.14E-06

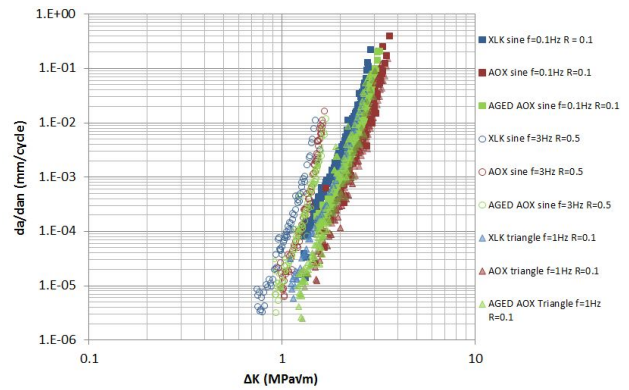


Figure 1. Paris relationship (da/dn vs ΔK) for XLKTM, AOXTM, and aged AOXTM for three different test conditions. Note in particular the distinct difference in fatigue crack propagation resistance between the test conditions of $R = 0.1$ and $R = 0.5$ for each group.

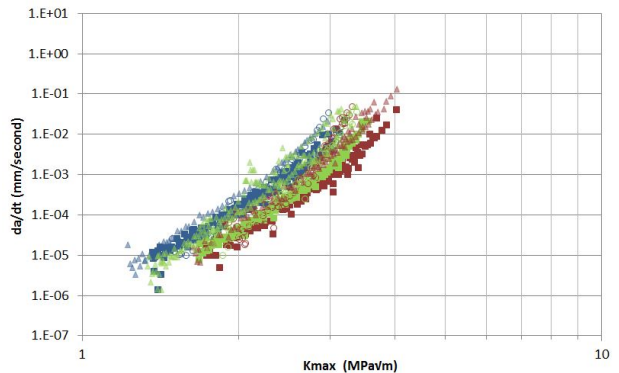


Figure 2. Peak stress relationship (da/dt vs K_{max}) for the three groups. Symbols are the same as in Figure 1. Note that the response generally collapses to a single response for each group, regardless of test condition.

TOUGHNESS IN HIGH TEMPERATURE MELTED UHMWPEs

Pascual, F.J.; Rios, R.; Puertolas, J.A.

Department of Materials Science and Technology, I3A, Universidad de Zaragoza, Zaragoza, Spain.

jpascual@unizar.es

Introduction: Contemporary highly crosslinked UHMWPE obtained by gamma or electron beam irradiation and stabilized by thermal treatment or antioxidant addition have given substantial breakthroughs in wear resistance and oxidative stability [1, 2]. Unfortunately, these improvements usually provoke a diminution in mechanical properties, especially in toughness and fracture resistance. Recently, several studies have introduced high temperature thermal treatments in order to improve mechanical performance of untreated UHMWPE [3]. Different approaches have been used to determine the toughness of UHMWPE, such as the work of fracture obtained from the area below the curve on uniaxial tensile test, Izod or Charpy impact toughness and J-integral experiments. In this work, we use the essential work of fracture (EWF) to assess the fracture resistance of ductile highly crosslinked polyethylenes [4, 5]. This technique allows discrimination between the essential work required to fracture the polymer in its process zone, w_e , and the nonessential or plastic work consumed by various deformation mechanisms in the plastic zone, w_p . Besides, a comparison of the different toughness techniques has been carried out.

Methods and Materials: Medical grade GUR1050 UHMWPE used in this work was manufactured by Celanese (Irwing, USA) and consolidated by Orthoplastics (Bacup, Lancashire, UK) in the form of a consolidated plaque. Some materials were gamma irradiated in air to a final dose of 90 kGy (Aragogamma, Spain). Some blocks underwent high temperature thermal treatments in a vacuum oven (LTE, UK) for X hours at Y °C and were denoted PE+HT(X-Y), while standard temperature remelting treatment is denoted TT(8-150). Work to fracture values were calculated from the area below the engineering stress-strain curves of uniaxial tensile tests per ASTM D638M (n=5). J-integral versus crack growth resistance, J-R, curves were obtained following ASTM D6068-02 guidelines for all material groups (n≥7 per group). Impact Izod tests were carried out at room temperature on double-notched specimens (n=4) following ASTM F648 guidelines.

For the EWF study, double deeply edge-notched tensile (DDEN-T) specimens (85x25x3 mm³) with different free ligament length, l_0 , were tested to fracture. Free ligament lengths were produced in the range $l_0 = 5$ to 10 mm with a fresh razor blade. Specific essential work of fracture (w_e) was determined from linear regression of specific total fracture energy versus ligament length plots.

Results: Figure 1 depicts the load-displacement (F-x) curves of DDENT-T specimens at various ligaments for heat treated (8 hours at 150 °C, vacuum) GUR 1050 specimens. Similar curves were obtained for the remaining materials.

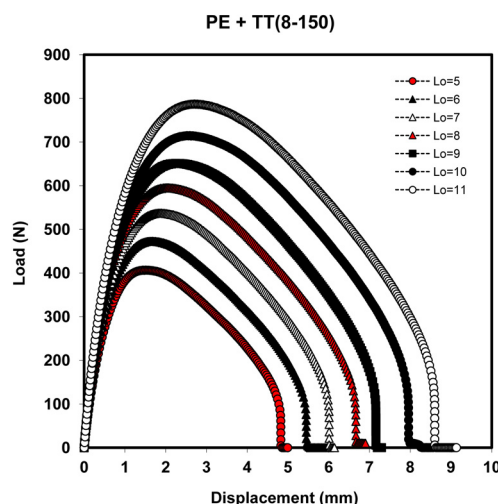


Figure 1 Load-displacement curves for γ -irradiated GUR 1050 EWF specimens.

Table 1 Toughness metrics for all the materials studied.

Material	w_e (KJ/m ²)	Impact Resistance (KJ/m ²)	Work to Fracture (MJ/m ³)	J-integral a=1 mm (kJ/m ²)
PE	45.70 $R^2=0.986$	90.0 ± 4.0	235 ± 17	67.80
PE+TT(8-150)	47.8 $R^2=0.996$	113.6 ± 2.2	281 ± 65	69.69
PE+HT(8-240)	N/A	105.4 ± 3.7	205 ± 31	90.19
PE+HT(8-280)	N/A	158.9 ± 20	291 ± 59	92.76
PE+HT(12-280)	N/A	147.8 ± 6.9	307 ± 57	96.41
PE- γ 90	24.6 $R^2=0.990$	67.9 ± 1.4	167 ± 21	34.56

Table 1 shows a comparison between the toughness values obtained for virgin, irradiated and high temperature thermal treated polyethylenes by the different techniques used in this work.

Discussion and conclusions: The current work presents a remarkable increase in all toughness metrics when high temperature treatment is applied to the UHMWPE. This increase is greater when longer times and higher temperatures are applied. The longer treatment at higher

temperature has proven to increase impact toughness about 65% while tensile work to fracture and $J_c(a=1\text{mm})$ increased about 30%. Conversely, this work also confirms the loss of toughness experienced by GUR 1050 upon irradiation, which is attributed to the high crosslink density induced by γ -radiation, reducing the amorphous deformation modes of the polymer and, therefore, its ductility. This diminution of toughness is represented by a fall of about 50% in the essential work of fracture and $J_c(a=1\text{mm})$. To sum up, this piece of work reveals the convenience of incorporating a post-consolidation high temperature treatment in vacuum to improve the mechanical performance of UHMWPE.

REFERENCES:

- [1] Kurtz S.M. The UHMWPE handbook: ultra-high molecular weight polyethylene in total joint replacement, Academic Press, New York (2009) 2nd edition.
- [2] Gómez-Barrena E. et al. *Acta Orthopaedica* (2008) 79: 832.
- [3] Fu J. et al. *Polymer* 51 (2010) 2721-2731.
- [4] Martínez A.B. et al. *Engineering Failure Analysis* 16 (2009) 2604–2617.
- [5] Naz S. et al. *Journal of Material Science* (2010) 45:448-459.

3D Frictional Torque Results of HXLPE & Vitamin-E Infused UHMWPE against 28 mm Metal & 36 mm Metal & 36 mm Ceramic Heads

W Rodgers III, PhD¹, C Büchele², C Kaddick, Dr.-Ing.², D Schroeder¹

¹Biomet Inc., Warsaw IN, USA, ²Endolab, Rohrdorf, Germany

Dave.Schroeder@Biomet.com

Introduction: Clinically relevant attributes of a bearing material include its strength, oxidative stability, and wear resistance. Recent reductions in wear and oxidation have been realized by crosslinking (HXLPE), and through the incorporation of antioxidants (e.g. α -tocopherol, or VE). VE infusion has been shown to improve the oxidative stability of HXLPE *in vitro* [1] and after *in vivo* use as evidenced by retrievals [2]. However, concern has been raised that adding VE may increase the frictional torque of bearings, potentially increasing the risk of trunnionosis [3]. This study compares the 3D frictional torque results of a HXLPE and a Vitamin-E infused HXLPE, against 28 mm and 36 mm heads, both metal and ceramic.

Methods and Materials: Test samples were machined according to prints for the commercially available Ringloc acetabular system (Biomet, IN). The HXLPE group was made from ArCom XL; isostatically compression molded GUR1050 that is 50 kGy gamma irradiated, mechanically deformed, stress relieved, machined to final dimensions and gas plasma sterilized. The Vitamin-E infused group (VE-HXLPE) was made from E1 HXLPE; isostatically compression molded GUR1020 that is 100 kGy gamma irradiated, infused with VE, machined to final dimensions, and gamma sterilized. The 28 mm femoral heads were of cobalt chrome (ASTM F1537), and the 36 mm heads were of cobalt chrome or ceramic (Biolox Delta™).

All testing was performed at EndoLab®, Germany. An ISO 14242-1 compliant hydraulic six station hip simulator (Endolab®, Germany) was used in conjunction with an ultra-high precision spherical air bearing and two groups of load sensors. Lubrication medium was 350 mL of calf serum, EDTA, and antibiotics diluted in DI water (to 30 g/l of protein). Measurements were made during a 3D gait cycle according to ISO 14242-1. During the cycle, the abduction/adduction range was $-4^{\circ}/+7^{\circ}$, the flexion/extension was $+25^{\circ}/-18^{\circ}$, and the external/internal rotation was $-10^{\circ}/+2^{\circ}$. Testing was performed at $37\pm 2^{\circ}$ C, at 1 Hz, and with a maximum dynamic load of 3.0 kN. Measurements were averaged across 5 full cycles after 120 completed cycles, and again after 200 cycles. Analysis was performed using Minitab with multiple 2-way ANOVAs, with a $p=0.05$ significance threshold.

Results: The 3D frictional torque results are shown in Figure 1. Each column is the average of 4 test samples (\pm SD). Group average frictional torque results after 120 and 200 cycles are in the left and right halves of the chart, respectively. Both the frictional torque means and maximums are shown. The first two columns are 28 mm metal-on-HXLPE, and 28 mm metal-on-VE-infused-HXLPE, respectively. The next two columns are the same materials against 36 mm metal heads, and the last two columns are against 36 mm ceramic heads.

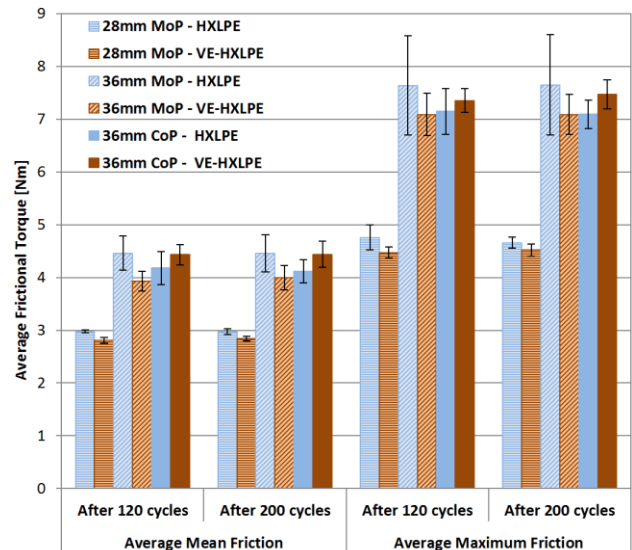


Figure 1: 3D frictional torques of HXLPE and VE-infused-HXLPE against 28 mm metal and 36mm metal and ceramic heads.

There was a statistically significant effect from the head size across all groups ($p<0.0005$). The 36 mm heads exhibited a higher torque (mean of 4.25 ± 0.31 Nm after 200 cycles) compared to the 28 mm heads (2.90 ± 0.08 Nm). Within the 36 mm head groups, there was no statistically significant effect ($p\geq 0.409$, all outputs) from head type (metal vs ceramic). In the 36 mm groups, there was also no statistically significant effect ($p\geq 0.300$, all outputs) from the liner material (HXLPE vs VE-HXLPE). Within the metal head groups, the inclusion of VE statistically significantly decreased ($p\leq 0.018$, all outputs) the average mean torques by $8.07\pm 4.6\%$.

Discussion: A larger head size increased the frictional torque. In the metal head groups the infusion of VE decreased the frictional torque, and VE did not statistically significantly change the torque in the ceramic groups. A previous report found that VE increased torque [3], but evidence herein does not support that conclusion. Limitations of the previous study include; use of a simplified rotation torque method, non-physiologic lubrication, lack of statistical analysis, unknown implant design, and unknown VE concentration and processing methods. Based on these results, no adverse clinical effects are anticipated due to VE-associated changes in frictional torque. Short-to-mid-term clinical results have not shown any adverse effects [4].

References:

- [1] E. Oral & OK Muratoglu, Intl Orthop (SICOT), vol. 35, no. 2, pp. 215–223, Feb. 2011
- [2] S. Rowell *et al*, Bone & Joint Journal Orthop Proc Supp, vol. 96, Supp 11, pp. 201–201, 2014
- [3] RM Meneghini, AAHKS, Poster No: 167, 2014
- [4] AK. Nebergall *et al*, ORS 2014 Annual Meeting: Poster No: 1831, 2014

Biocompatibility Assessment of HALS Stabilized Highly Crosslinked UHMWPE

H. Smelt¹, M. Persson¹, D. Schumann¹, L. Panella¹, F. Linker¹

¹DSM, Geleen, NL

harold.smelt@dsm.com

Introduction: HALS, Hindered Amine Light Stabilizer, is a promising alternative anti-oxidant for highly cross-linked UHMWPE (XLPE) providing long term in vivo oxidation resistance. Compared with Vitamin E stabilized XLPE, it has been shown that crosslink density and wear resistance for HALS stabilized XLPE are significantly higher at the same irradiation dosage¹. Since HALS does not interfere with the crosslinking process and can regenerate itself, the sensitivity for variations in product properties due to local anti-oxidant concentrations is lower in comparison to phenolic anti-oxidants like vitamin E². Next to the mechanical and chemical performance, it is important to assess the biocompatibility and biosafety aspects of HALS as well. Although UHMWPE has been used for decades in various kinds of implants with satisfactory biological safety results, the presence of a stabilizer may play an unexpected role in the biocompatibility of the material. Intended additives and, if applicable, leachable substances may diffuse to the surface of the material and migrate into the surrounding tissue, potentially leading to modified or undesirable tissue reactions. Therefore, the aim of this study was to show that HALS stabilized XLPE wouldn't present a potential harm when used as a biomaterial in the design of permanent class III medical devices.

Methods and Materials: GUR1020 UHMWPE resins (Celanese) doped with 0.10 wt.% HALS Solution (Poly[[6-[(1,1,3,3-tetramethylbutyl)amino]-1,3,5-triazine-2,4-diy]][(2,2,6,6-tetramethyl-4-piperidinyl)imino]-1,6-hexanediy]][(2,2,6,6-tetramethyl-4-piperidinyl)imino]]) (DSM Biomedical) were compression molded into 8 cm thick sheets (Meditech/Quadrant, USA). The material was machined into 2 meter bars and subjected to a dose of gamma irradiation of 75 or 100 kGy (BGS, Germany). Test specimens for all subsequent analyses were machined from the bar stock and ethylene oxide sterilized prior to use.

First leaching characteristics of HALS in 75 kGy XLPE was investigated in "worst-case" scenario experiments, using an extraction solvent in which the solubility of HALS is extremely. The selected leaching liquid was acetone and samples were kept in this solvent for 7 days at 37°C followed by LC-UV/MS analysis.

Next a comparative extractables study between 100 kGy XLPE with and without 0.10 wt.% HALS was performed to identify potential additional polymer additives, impurities and degradation products. Four different methods were applied to release those compounds: headspace enrichment on neat test item (1), reflux extraction with water for injection (2), reflux extraction with dichloromethane (3), and reflux extraction with hexane (4). Calibrated gas-chromatography (GC), and/or liquid-chromatography (LC) in combination with a mass detector (GC/MS) as well as ion chromatography (IC) were used to analyze the extracts.

Finally, *in vitro* biocompatibility studies were accomplished according to ISO 10993 guidelines for the Biological Evaluation of Medical Devices: Part 5 "Test for *in vitro* Cytotoxicity", Part 6 "Tests for Local Effects After

Implantation", Part 10 "Test for Irritation and Skin Sensitization" and Part 11: "Test for Systemic Toxicity".

Results:

The results obtained from the leaching experiments with acetone for the HALS stabilized XLPE blend revealed that negligible traces of HALS had migrated from the 6x6x1cm plaque samples. However, the HALS signals were on the level of the detection limit of the LC-UV-MS and therefore the amount of leachable HALS substance was reported as < 0.002% of the total available HALS in the sample under the applied leaching protocol.

Evaluation of the comparative extractables study did not generate differential compounds in HALS stabilized XLPE versus non stabilized XLPE. In addition, significantly lower amounts of aliphatic hydrocarbons were detected in the HALS stabilized XLPE during the IC analysis. These results reflect the efficacy of the HALS stabilizer in the material to reduce polymer degradation.

Moreover, HALS stabilized XLPE passed all the biocompatibility tests conducted in accordance with the requirements of the ISO 10993:

Test	Result
Cytotoxicity	<u>Passed</u> (non cytotoxic)
Irritation-Sensitization	<u>Passed</u> (test article did not induce any erythema and edema reactions after intracutaneous injection route).
Systemic Toxicity	<u>Passed</u> (no evidence of significant systemic toxicity or mortality)
Intramuscular implantation, 12 weeks	<u>Passed</u> (Does not demonstrate any remarkable difference as compared to the control implant sites (Bioreactivity rating of 1.8) when implanted for 12 weeks)

Discussion: Knowledge of the detailed composition of a biomaterial is exceedingly important in predicting the *in vivo* host response, as this is highly correlated to the biocompatibility of the biomaterial. In general, biomaterials identified as being non-toxic in *in vitro* assays, such as those performed in this study, will most likely be non-toxic in *in vivo* assays³.

In this study, the biocompatibility aspects of HALS intended to be used as antioxidant/stabilizer for UHMWPE was investigated in terms of extractable chemicals, leachable substances as well as *in vitro* and *in vivo* biocompatibility tests.

The results of the performed leaching and extraction tests in conjunction with the positive outcome of the biocompatibility tests, conducted in accordance with the requirements of the ISO 10993-1 standard, substantiate that HALS stabilizer used in XLPE is non-toxic and suitable to be used as a biomaterial in the design of class III medical devices. However, more application-specific testing to assess the biocompatibility of the material under end-use conditions in the final device is still necessary.

¹ Smelt H. et al., UHMWPE Conference 2013, Torino

² Gijssman P. et al., Biomaterials 31 (2010) 6685 - 6691

³ Ratner B.D. Biomaterials Science: An Introduction to Materials in Medicine 3rd edition, Oxford Elsevier, Inc. Academic Press 2013.

Effects of surface modification and bulk geometry on the biotribological behavior of cross-linked polyethylene

Watanabe K^{1,2}, Kyomoto M^{1,2,3}, Saiga K^{1,2}, Yamane S^{1,2,3}, Taketomi S⁴, Kadono Y⁴, Takatori Y², Tanaka S⁴, Ishihara K³, Moro T²

¹Research Department, KYOCERA Medical Corporation, Osaka, Japan

²Division of Science for Joint Reconstruction, Graduate School of Medicine, The University of Tokyo, Tokyo, Japan

³Department of Materials Engineering, School of Engineering, The University of Tokyo, Tokyo, Japan

⁴Orthopaedic Surgery, Sensory and Motor System Medicine, Surgical Sciences, Graduate School of Medicine, The University of Tokyo, Tokyo, Japan

moro-ort@h.u-tokyo.ac.jp

Introduction: The degree of polyethylene (PE) wear is one of the important indicators of the clinical performance of the bearing materials used for artificial joints, regardless of whether highly cross-linked PE (CLPE) is used. To reduce the degree of PE wear and suppress bone resorption, we had previously developed a surface-modification technology that involves synthetic phospholipid-polymer poly(2-methacryloyloxyethyl phosphorylcholine [MPC]) (PMPC) grafting. The grafting of PMPC onto acetabular liners resulted in a drastic reduction in CLPE wear during a long-term hip simulator test; it also yielded good short-term results during clinical trials [1, 2].

Creep deformation resistance is also an important indicator of the clinical performance of acetabular liners. The geometry of the PE part is one of the factors that determine its creep deformation resistance. Similarly, backside wear as well as the damage caused by volumetric penetration and circular scratching is also a serious problem with respect to the PE acetabular liners used in cementless total hip arthroplasty and the PE inserts used in total knee arthroplasty.

The ASTM F732-00 standard defines a method in which a disk-shaped polymer specimen is loaded with a hemispherical cobalt–chromium–molybdenum (Co–Cr–Mo) alloy pin. If one were to employ this method while using a plate with a screw hole as the backplate of the disk specimen, one could evaluate the damage undergone by the backside of the disk without having to perform an expensive joint simulator test. In addition, this method is suitable for evaluating hydrated polymers because a lubricant is applied on the bearing surface during every loading cycle.

The purpose of this study was to evaluate the wear and creep deformation resistances, including the extent of backside damage, of various PE materials using test specimens with 3 and 6 mm in thickness.

Methods and Materials: Compression-molded bars of PE were irradiated with a 50-kGy dose of gamma rays to facilitate cross-linking. PMPC was grafted onto the surfaces of the CLPE samples through photoinduced graft polymerization [1].

The wear and creep deformation resistances of the bearing materials were examined using a pin-on-disk tester, in keeping with the ASTM F732-00 standard (Fig. 1). The various PE materials were used to fabricate disks with a thickness of 3 or 6 mm, while a Co–Cr–Mo alloy

was used for the counter hemispherical pin. The backplate of the disk had a sham screw hole in the center. A mixture of fetal bovine serum was used as the lubricant. Multidirectional pin-on-disk tests were performed; the motion was in the shape of a rectangle with dimensions of 5 × 10 mm. The test conditions were the following: static load of 213 N, motion speed of 30 mm/s, and maximum test duration of 1.0 × 10⁶ cycles. Soak controls were used to compensate for fluid absorption by the specimens of the same group.

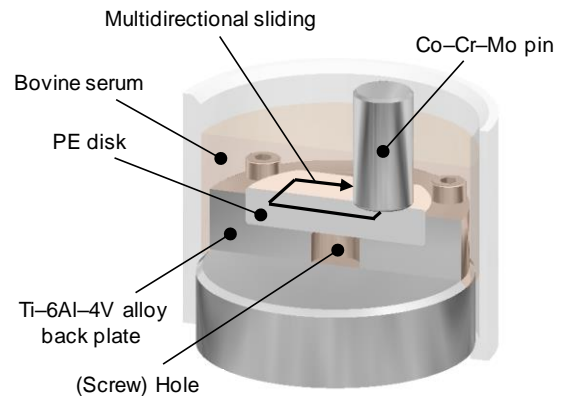


Figure 1. Schematic illustration of the pin-on-disk test

After the completion of the test, the wear of the bearing surface and the depth of penetration in the backside surface of all the disks were measured using a noncontact optical three-dimensional (3D) profiler. To estimate the internal stress in the PE disks, finite element analysis (FEA) was performed using an FEA software program.

The mean values for the three material groups (untreated PE, untreated CLPE, and PMPC-grafted CLPE) were compared using one-factor analysis of variance (ANOVA). The significant differences between the comparable properties were determined through post-hoc testing using Tukey–Kramer’s method. The mean values of the two thickness groups (3 and 6 mm) for each material were compared by using the Student’s *t*-test.

Results: For the 3-mm-thick disk group, the gravimetric wear rate of untreated CLPE and PMPC-grafted CLPE disks were significantly lower than that of the untreated PE disks (Fig. 2). For the 6-mm-thick disk group, the wear rates of untreated CLPE and PMPC-grafted CLPE disks were significantly lower than that of the untreated PE disks. Furthermore, the wear rate of PMPC-grafted

CLPE was significantly lower than that of untreated CLPE. The wear rate of the 3-mm-thick untreated PE disks was significantly larger than that of the 6-mm-thick disks. On the other hand, the wear rate of the 3-mm-thick untreated CLPE disks was significantly lower than that of the 6-mm-thick disks. In the case of PMPC-grafted CLPE, there were no significant differences in the wear rates of the 3 and 6 mm disks.

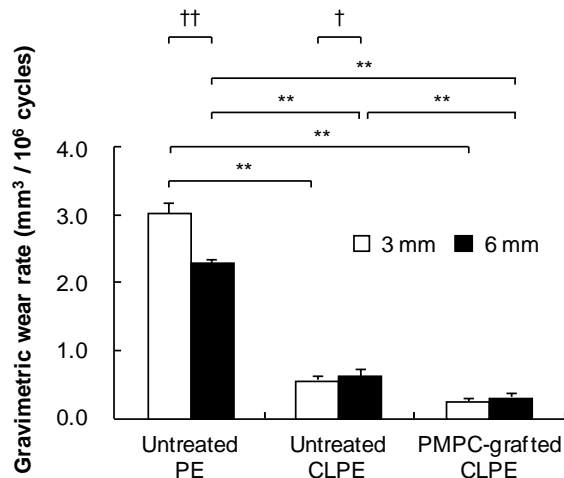


Figure 2. Gravimetric wear rate using disks with 3 and 6 mm in thickness. ** indicates $p < 0.01$ as per Tukey-Kramer's test and † indicates $p < 0.05$ and †† indicates $p < 0.01$ as per Student's t -test.

The 3D profile of the disks showed that all the disks exhibited substantial volumetric wear of the bearing surface, with the backside surface penetrating into the sham screw hole. The differences in the degrees of volumetric wear for the 3-mm-thick disks of the different materials were not significant. For each material group, the volumetric wear of the 3-mm-thick disks was significantly larger than that of the 6-mm-thick disks. The differences in the volumetric penetration for both the 3-mm-thick and 6-mm-thick disks of the various materials were not significant. For each material group, the volumetric penetration of the 3-mm-thick disks was significantly greater than that of the 6-mm-thick disks.

The internal von Mises stress at the bearing side estimated using FEA was almost the same for all the materials. Although the stress at the backside was almost the same for all the material groups for both the 3-mm-thick and the 6-mm-thick disks, the stress in the 3-mm thick disks was computationally much higher than that in the 6-mm-thick disks. Further, it exceeded their respective actual yield strengths by a wide margin.

Discussion: Cross-linking decreased the gravimetric wear of PE significantly, while PMPC grafting decreased it even further. PMPC-grafted CLPE has also been shown to exhibit lower wear than that seen for CLPE; it is thought that the decrease in wear is caused by a surface hydration lubrication mechanism. In the case of natural synovial joints, lubrication is provided by a hydrated layer that consists of chondrocytes; the surrounding matrix

macromolecules are also essential for lubrication, while a surface layer of active phospholipids that covers the surface of the joint cartilage provides hydrophilicity and works as an effective boundary lubricant. Hence, a phospholipid-like layer grafted on the bearing surface of artificial joints may afford ideal hydrophilicity and lubricity, that is, similar to those of physiological joint surfaces.

Even though gravimetric evaluations were performed, measuring the volumetric wear of the bearing surface using an optical 3D profiler did not allow for the detection of significant differences between the three PE material groups in the case of the 3-mm-thick disks and between untreated CLPE and PMPC-grafted CLPE in the case of the 6-mm-thick disks. The internal von Mises stress at the bearing side for both the 3-mm-thick and the 6-mm-thick disks reached the actual yield strength of PE materials. We therefore assumed that the volumetric wear measured in this study consisted of not only the true wear but also the creep deformation of the PE substrate. Since the volume of creep deformation was significantly greater than that of true wear, the differences in the volumetric wear among the three materials for the 3-mm-thick disks as well as that between untreated CLPE and PMPC-grafted CLPE for the 6-mm-thick disks might not be significant.

The volumetric penetration in the backside surfaces increased with a decrease in disk thickness. The internal von Mises stress in all the 3-mm-thick disks was more than 28 MPa in the backside against the edge of the sham screw hole; this was greater than the actual yield strength of the PE materials. It is likely that the fact the internal stress was greater than the actual yield strength is what resulted in the large degree of volumetric penetration. The degree of volumetric wear, which consisted of true wear and creep deformation, was greater in the thinner (3 mm) disks for every material. We assumed that the increase in the degree of volumetric wear in thinner (3 mm) disks was partially owing to the volumetric penetration in the backside surface.

In conclusion, a hydrated bearing surface and a bearing substrate of the appropriate thickness are essential for improving the wear and creep deformation resistances. We believe that PMPC-grafted CLPE is a promising bearing material for increasing the longevity of artificial joints. Further, the pin-on-disk test is a useful one for evaluating bearing biomaterials in a practical and economical manner.

References:

- [1] Moro et al., Long-term hip simulator testing of the artificial hip joint bearing surface grafted with biocompatible phospholipid polymer. *J Orthop Res* 2014;32:369–376.
- [2] Takatori et al., Clinical and radiographic outcomes of total hip replacement with poly(2-methacryloyloxyethyl phosphorylcholine)-grafted highly cross-linked polyethylene liners: Three-year results of a prospective consecutive series. *Mod Rheumatol* 2015;25:286–291.

Effects of extra irradiation on surface and bulk properties of PMPC-grafted cross-linked polyethylene

Yamane S^{1,2,3}, Kyomoto M^{1,2,3}, Moro T², Watanabe K^{1,2}, Hashimoto M⁵, Taketomi S⁴, Kadono Y⁴, Takatori Y², Tanaka S⁴, Ishihara K³,

¹Research Department, KYOCERA Medical Corporation, Osaka, Japan

²Division of Science for Joint Reconstruction, Graduate School of Medicine, The University of Tokyo, Tokyo, Japan

³Department of Materials Engineering, School of Engineering, The University of Tokyo, Tokyo, Japan

⁴Orthopaedic Surgery, Sensory and Motor System Medicine, Surgical Sciences, Graduate School of Medicine, The University of Tokyo, Tokyo, Japan

⁵Materials Research and Development Laboratory, Japan Fine Ceramics Center, Nagoya, Japan

kyomoto@mpc.t.u-tokyo.ac.jp

Introduction: Osteolysis induces implant loosening and is one of the most important complications limiting the longevity of implants. Wear particles of polyethylene (PE) is said to trigger osteolysis, hence, many recent studies have focused on improving wear resistance to reduce the generation of wear particles. We have developed a cross-linked PE (CLPE) bearing surface modified with poly(2-methacryloyloxyethyl phosphorylcholine [MPC]) (PMPC). Graft polymerization of MPC initiated from the CLPE substrate by photoirradiation is an effective method to obtain high-wear resistance for the CLPE surface [1].

To sterilize the CLPE bearing surface, gamma rays and gas plasma are widely used. The energy of gamma-ray irradiation (25–50 kGy) during sterilization is so high that it is well known that gamma-ray irradiation induces chain scission of PE and produces free radicals that lead to cross-linking of PE or other chemical reactions, such as oxidation degradation of PE in the presence of air. On the other hand, various free radicals (e.g., •OH, •OOH, •O, and •H) and ultraviolet (UV) light are generated during the process of gas plasma sterilization [2]. The generated free radicals and secondary UV light may induce changes in the chemical structure at the surface of PE and/or grafted PMPC. Indeed, the effects on the performance of the bearing surface remain unclear.

In this study, we have considered two research questions: Does extra irradiation during the sterilization process induce changes in the properties of (1) the PMPC surface, and (2) the CLPE substrate? From these two perspectives, we evaluated the surface and substrate properties of PMPC-grafted CLPE bearings with extra high-energy (i.e., gamma-ray or plasma with UV light) irradiation.

Methods and Materials: A compression-molded bar stock of PE was irradiated with a 50 kGy or 75 kGy dose of gamma rays in a N₂ gas and annealed at 120°C for 7.5 h. PMPC-grafting of CLPE was carried out using MPC aqueous solutions at a concentration of 0.50 M at 60°C for 90 min under UV light irradiation with an intensity of 5.0 mW/cm². Untreated and PMPC-grafted CLPE irradiated with 50 kGy were sterilized with 25 kGy dose of gamma rays in an N₂ gas atmosphere. Untreated and PMPC-grafted CLPE irradiated with 75 kGy were sterilized with a low-temperature H₂O₂ gas plasma system. As control specimens, 75 kGy irradiated CLPE

and PMPC-grafted CLPE without any sterilization were prepared.

The surface chemical properties of PMPC-grafted CLPE with various extra-irradiation methods were analyzed by Fourier transform infrared (FT-IR) spectroscopy and X-ray photoelectron spectrophotometer (XPS). Cross-section of PMPC-grafted CLPE was observed by a transmission electron microscope (TEM). The surface wettability and friction property were measured by water static contact angle measurement and the friction test using a pin-on-plate machine, respectively.

The hip simulator wear test for CLPE and PMPC-grafted CLPE liners with various extra-irradiation methods was performed using a 12-station hip simulator according to ISO standard 14242-3. A Co–Cr–Mo alloy ball was used as the femoral head. Gravimetric wear was determined by weighing the liners at intervals of 0.50 × 10⁶ cycles. Load-soak controls were used to compensate for fluid absorption according to ISO standard 14242-2. Volumetric wear of the liners after the test was measured using a three-dimensional coordinate measurement machine. Wear particles were isolated from the lubricant and observed by field emission scanning electron microscope analysis.

To evaluate the oxidation resistance of PMPC-grafted CLPE after extra-irradiation methods, the oxidative degradation (oxidation index) after accelerated aging was evaluated by microscopic FT-IR according to the ASTM F2102 standard.

Results: The peaks attributed to MPC were clearly observed in the FT-IR and XPS spectra of PMPC-grafted CLPE after extra irradiation. In TEM images, a uniform PMPC layer with a thickness of 100 to 150 nm was observed on the surface regardless of the extra irradiation. PMPC-grafted CLPE had a much lower water-static contact angle than CLPE. Moreover, the gamma-ray and plasma irradiated samples revealed a lower contact angle compared to the non-extra irradiated sample. There was no difference between gamma-ray and plasma irradiation for the wettability of PMPC-grafted CLPE (Fig. 1). The coefficient of dynamic friction of PMPC-grafted CLPE was less than half compared with those for CLPE for all extra irradiations. The coefficient of dynamic friction did not differ significantly between the three groups of PMPC-grafted CLPE.

During the hip simulator wear test, PMPC-grafted CLPE liners were found to undergo less gravimetric wear than untreated CLPE liners regardless of any extra irradiation (Fig. 2). In addition, PMPC-grafted CLPE liners showed a slight, gradual increase in weight during the hip simulator wear test. PMPC-grafted CLPE liners revealed extremely small-volumetric wear that was rarely detectable, although substantial volumetric wear was detected in the untreated CLPE. These volumetric wear results support the gravimetric wear results. Regardless of extra irradiation, wear particles generated from the PMPC-grafted CLPE liners were remarkably fewer than those from the CLPE liners.

As for the oxidation resistance measurement, the oxidation indices after accelerated aging of PMPC-grafted CLPE showed higher values in gamma-ray irradiation than those receiving non-extra or plasma irradiation.

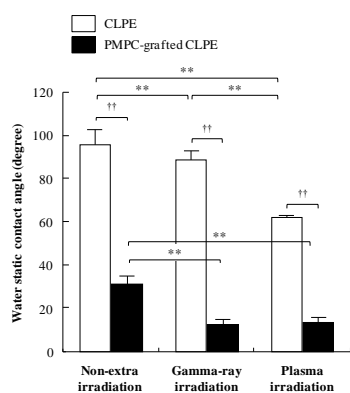


Fig. 1 Water static contact angle of CLPE and PMPC-grafted CLPE with various extra-irradiation during the hip simulator wear test. ** indicates $p < 0.01$ by Tukey Kramer's test and †† indicates $p < 0.01$ by student's t -test.

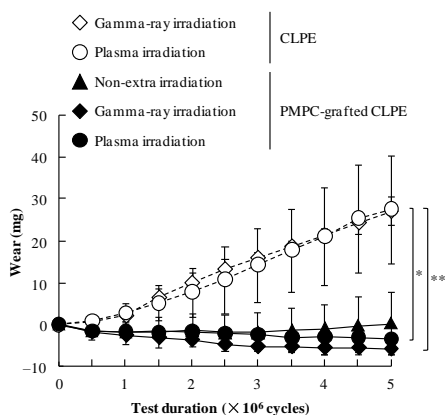


Fig. 2 Gravimetric wear of CLPE and PMPC-grafted CLPE with various extra-irradiation during the hip simulator wear test. * indicates $p < 0.05$ and ** indicates $p < 0.01$ by Tukey Kramer's test.

Discussion: Although we could not clearly observe changes in the chemical structure and morphology of the

PMPC surface, the PMPC-grafted CLPE receiving gamma-ray and plasma irradiation exhibited reduction of the coefficient of dynamic friction, improved surface wettability, and improved wear resistance compared to the non-extra irradiated PMPC surface. The effect of gamma-ray irradiation to these properties of PMPC-grafted CLPE may be attributed to the cross-linking of PMPC chains at the surface and interface of PMPC and CLPE substrate. On the other hand, it was assumed that the plasma itself affected within the very limited surface area of the PMPC layer which was highly hydrophilic and was consisted of low-energy chemical bonds such as C-H, C-N, and C-O. In addition, we thought that the UV light which secondary generated through plasma irradiation process would not influence the PMPC surface to the extent that it would affect the clinical benefits of PMPC, given UV light irradiation of a relatively low intensity was conducted for less than one hour.

In the hip simulator test, PMPC-grafted CLPE liners resulted in substantial improvements in wear resistance compared with untreated CLPE liners, regardless of extra-irradiation process. This is due to the significant differences observed in wettability and frictional properties. Fluid-film lubrication (or hydration lubrication) of the PMPC-grafted surface was therefore provided by the hydrated layer. Additionally, the PMPC-grafted CLPE with gamma-ray and plasma irradiations showed less gravimetric wear than samples without any extra irradiation. This result also supports the previous point that a portion of the wear-reduction effect is attributable to cross-linking of the PMPC layer by extra irradiation.

Oxidation degradation of CLPE induces the reduction of mechanical strength of CLPE substrate and finally leads to CLPE fracture or abrasive wear in clinical use. The oxidation indices of PMPC-grafted CLPE receiving plasma irradiation did not show any significant difference compared to those with non-extra irradiation. There were remarkably fewer residual free radicals in the CLPE substrate after extra irradiation, which prompted improved oxidation resistance of PMPC-grafted CLPE with plasma irradiation.

In conclusion, PMPC-grafted CLPE liner with plasma irradiation is expected to have high wear and oxidation resistance that does not induce severe abrasive wear or implant fracture during long-term clinical use.

References:

- [1] Moro T et al., Wear resistance of artificial hip joints with poly(2-methacryloyloxyethyl phosphorylcholine) grafted polyethylene: comparisons with the effect of polyethylene cross-linking and ceramic femoral heads. *Biomaterials* 2009;30:2995–3001.
- [2] Paul TJ et al., Gas-Plasma Sterilization. In: Roger LC et al., editors. *Irradiation of Polymers*. Washington DC: American Chemical Society; 1996. p 216–239.

Characterization of alginate modified UHMWPE; morphology and wear properties

Zsoldos, G.¹; Kollár, M.²; Szabo, T.³

^{1,2} University of Miskolc, Institute of Ceramics and Polymer Engineering

¹ femzsgab@uni-miskolc.hu

² femmaja@uni-miskolc.hu

³ polsztam@uni-miskolc.hu

Introduction: Previous research was carried out based on the work of Jian-Ping Wang, Xing-Xiang-Zhang, Xue-Chen Wang [Preparation, characterization and permeation of calcium alginate macro-capsules containing shape-stabilize phase change materials, Renewable Energy, vol.36 (2011)pp.2984-2991]. When we made basic experiments in GUR 4210 UHMWE powder to form an alginate layer which could hold calcium from calcium solution, we have determined the sequence of the treatments, and the necessity of etching the UHMWPE powder.

During the second series of experiments we used GUR 1020 UHMWE powder, and two types of modification carried out, to form insoluble alginate layers. After sample preparations, morphological examinations, Ca²⁺ ion extraction tests and wear tests were carried out.

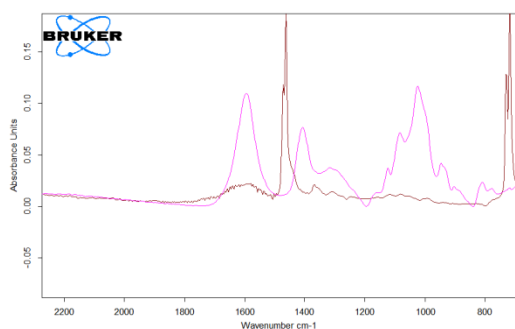
Methods and Materials: The used UHMWPE is GUR 1020 (Average molecular weight: 4×10⁶ g/mol (M_w)) powder.

First method: first the sodium alginate's (ISP Alginates) aqueous solution (1 wt% solution) then calcium chloride (2 wt% aqueous solution) was sprayed onto the polymer powder.

Second method: first the sodium alginate (ISP Alginates) solution (1 wt% aqueous solution) then calcium sulfate (2 wt% aqueous solution) was sprayed onto the polymer powder.

The methods were repeated in reverse order. First, the treatment with the Ca-salt solution then the alginate spraying.

The samples were heated at 50°C for 1 day. The treated and untreated UHMWPE powder was pressed into sheets at 175 ° C. After the forming, 20 kGy gamma irradiation followed, simulating sterilization of implant components.



D:\R\Alginate\algina.0 algina sample form 2013.06.13
D:\R\Alginate\Baklagar\be\ugazart\CaSO4_algin_UHMWPE.1 ugazart\CaSO4_algin_UHMWPE Instrument type and / or access 2015.04.28

Page 1/1
FTIR curve (alginate-magenta, UHMWPE-red)

FTIR (Bruker Tensor 27) tests were carried out to answer if the surface of the treated UHMWPE powder holds the alginate in different forms. From the results of the tests, we could to select the most optimal method of blending Ca on the surface of the UHMWPE powder.

If after the pressing and irradiation, the FTIR curves show the alginate absorption peaks, it also means that the calcium alginate is present on the polymer which was our intent, however the sodium alginate is water-soluble but calcium alginate is not.

Linear wear tests were carried out to determine the effect of alginate on the wear resistance of the UHMWPE material, the influence of alginate on the wear properties. Evaluation of wear resistance was executed, using a pin-on-disk tribometer.

Migration behavior of the Calcium (II) ions was evaluated using extraction method, where for 24 and 48 hours the samples were kept in distilled water and also in isotonic salt solutions. The change in Ca²⁺ content was detected using SF-ICP-MS method.



ICP spectrometer

Results:

The treatments which we have tried proved to be suitable for implantation of Calcium (II) ions on UHMWPE polymer surfaces. The polymer powder is capable of binding to the surface of the sodium alginate and is able to hold the created calcium alginate during processing and after the 20 kGy irradiation process. The presence of calcium alginate on the surface was proved with great confidence using FTIR measurements. The wear tests and the extraction experiments are still in progress.

Discussion: Our experiments were carried out on GUR 1020 UHMWPE powder. We would also like to carry out these tests on production UHMWPE hip joint cups too, to check that the alginate is able to adhere to the surface of a processed hip joint cup.